Study of Water Treatment Method with Nanosecond Pulsed Power System

March　　2017

森本　充

Index

1. Introduction

Environmental problems such as water pollution and atmospheric pollution constitute a serious threat to human health today, both locally and globally. The total volume of water on the Earth is about 1.35 billion km^3, 97% of which is seawater. Freshwater is about 2.5% of the total, and 70% of that is found as ice in the Antarctic and the Arctic. Drinking water is only 0.01% (0.1 million km^3) of the total [1.1]. On the other hand, approximately 70% of the human body is formed by moisture, which is supplied from drinking water and water contained in the food. Therefore, because the water pollution can affect the food, the water pollution also has a direct effect on the human body.

Naturally, plankton acts as a self-cleaning mechanism on seawater as well as freshwater, by consuming and decomposing pollutants. However, this self-cleaning mechanism does not work properly when the pollutants' concentration is too high. Furthermore, some chemical contaminants cannot be decomposed in the same manner. Red tide, blue tide, coral bleaching, and desertification are caused by water pollution. At present, because of the improvement of the living standards and the population growth (Fig. 1-1), domestic wastewater is also a major cause of water pollution.

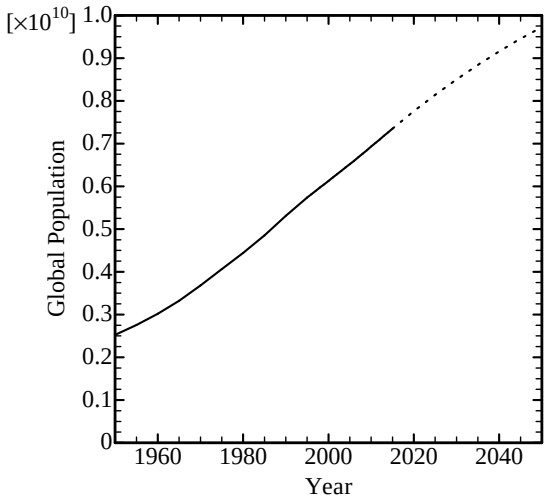

Fig. 1-1. Global population transition [1.2].

Above all, the largest volume of domestic wastewater comes from kitchen drainage. All leftovers and rice-washing water lead to water pollution. In addition, synthetic detergents used for dishwashing also cause water pollution. On the other hand, industrial wastewater discharged from factories and offices is also one of the causes of water pollution. In high economic growth periods, pollution is caused by harmful substances contained in industrial wastewater. Thereafter, the pollution is reduced by imposing regulations and improved maintenance of the sewers. However, at present, in areas where sewers are not popular, industrial wastewater is flowed to the river and the sea without treatment. Moreover, not only domestic and industrial wastewater but also illegal dumping may contribute to water pollution. When the soil is contaminated by hazardous substances (dioxins PCB, lead, and arsenic), they leach into the groundwater. By drinking the groundwater, these toxic substances affect the human body. Furthermore, the seawater pollution affects the reproduction,

growth, and mortality of marine organisms, therefore, indirectly, leading to food shortage in the future.

In order to solve the water pollution issue, measures, such as preparing legislation adopted against industrial wastewater, and water treatment technologies have been also studied around the world. As one of water treatment technologies, advanced oxidation processes (AOPs) and biological treatment with anaerobic and aerobic microorganisms improved sewage system. However, some problems remain, such as collecting activated carbon used in final process of AOPs and the burden on the microorganisms used in biological treatment. In order to generate ozone and treat wastewater more efficiently, water-treatment methods using electric discharges have been studied. In these treatments, streamer discharges can produce chemical active species such as ozone, hydroxyl radical (OH radical), hydroperoxyl radical (HO_2), and superoxide anion radical (O_2^-). The respective oxidation-reduction potential (ORP) values are shown in Table 1-1 [1.3]. As shown in Table 1-1, ozone and the OH radical have ORP values of 2.075 and 2.38 eV, respectively. In addition to the stronger ORP of the OH radical than ozone, the OH radical is able to react with organic compounds unselectively, whereas ozone reacts with organic compounds selectively. Furthermore, because treatment using the OH radical is faster, the OH radical has attracted attention. Moreover, physical phenomena such as UV and ion wind [1.4] generated by electric discharges can produce not only more ozone but also more OH radical, so that it is suggested that chemical reactions in gas and/or water for decomposition of organic compounds including persistent substances are promoted by electric discharges.

Table 1-1. Oxidation-reduction potential of chemically active species [1.3].

Material	Symbols for element	Potential (eV)
Fluorine	F_2	2.870
Hydroxyl radical	OH	2.380
Ozone	O_3	2.075
Hydrogen peroxide	H_2O_2	1.763
Chlorine	Cl_2	1.396
Oxygen	O_2	1.229

Atmosphere pollutants such as nitrogen oxides (NOx) and sulfur oxides (SOx) are released by liquefied natural gas, coal, and oil burning factories, power stations, diesel engines, and plants. These pollutants cause urban smog, acid rain, and so on. NOx removal technologies such as selective catalytic reduction, electron beam flue gas treatment technology, and dielectric barrier discharges (DBDs) have been studied. However, the gas treatment system requires large processors and has a high cost. Therefore, a compact NOx treatment system is needed at low cost. Moreover, oil and acid rain can also cause water pollution.

In order to solve the water pollution problem, the nanosecond pulsed power system has been

studied. When the nanosecond pulsed power system is used, the pulse width is very short with several nanoseconds, so that it can control the progress to arc discharges. By using the nanosecond pulsed power system, streamer discharges are stably generated. Moreover, the nanosecond pulsed power system has high electric power, high energy density, and very short rise time. These characteristics of the system are utilized for many application fields. For example, not only instantaneous high voltage, strong electric fields, and large currents but also electric discharges and plasma generated by nanosecond pulsed power system have been used for water treatment.

High ozone concentration can increase OH radical production [1.5]. Ozone can be produced efficiently using the nanosecond pulsed power system. Moreover, in order to investigate the structure of the coaxial reactor, this system has also been used for the treatment of nitrogen oxides (NOx).

References-1

[1.1] “The Present Situation of Japanese Aquatic Resources ~Water Environment and Installment Balance Situation of Water Resource~,” Ministry of Land, Infrastructure, Transport, and Tourism, no. 1, p. 1, 2015. (in Japanese)

[1.2] “World Statistics ~Pollution~,” Statistics Bureau, Ministry of Internal Affairs and Communications (Statistics Bureau, MIC), no. 2, p. 16, August, 2015. (in Japanese)

[1.3] Y. Iwasawa, “Chemical Handbook Fundamentals Revised 5th Edition,” The Chemical Society of Japan, vol. 2, pp. 580-583, February, 2004. (in Japanese)

[1.4] T. Sato, “Biological Interference Mechanism of an Atmospheric Plasma Flow,” Institute of Fluid Science, Tohoku University, pp. 61-65, February, 2012. (in Japanese)

[1.5] T. Iijima, R. Makise, and T. Murata, “OH Radical Generator for Waste Water Treatment Containing Recalcitrant Organic Matter,” TOSHIBA review, vol. 61, no. 8, pp. 40-43, 2006. (in Japanese)

2. Target Materials

The details of target materials such as indigo carmine, surfactant, ozone, and NOx are presented in this chapter.

2.1. Indigo Carmine [2.1]

Indigo carmine ($C_{16}H_8N_2Na_2O_8S_2$) is a dark blue, odorless, and neutral powder, which is dissolved easily by light, heat, nitric acid, bromine water, or chlorine water. Figs. 2-1(a) and 2-1(b) show the structural formula of indigo carmine (*trans* isomer) and decomposed indigo carmine (leuco indigo) [2.2]. Indigo carmine is a synthetic coloring agent, which gives a blue color tinged with purple, and it is classified under edible tar dyes. Indigo carmine is also found as a food additive, specified as blue no. 2 in the food hygiene law in Japan. After carbon-carbon double bond (C=C) of H-type chromophore was decomposed first of all as shown in Fig. 2-1(b) when indigo carmine was decomposed, C-C was formed. After that, carbon-carbon double bond (C-C) was decomposed, so that benzene rings could be opened.

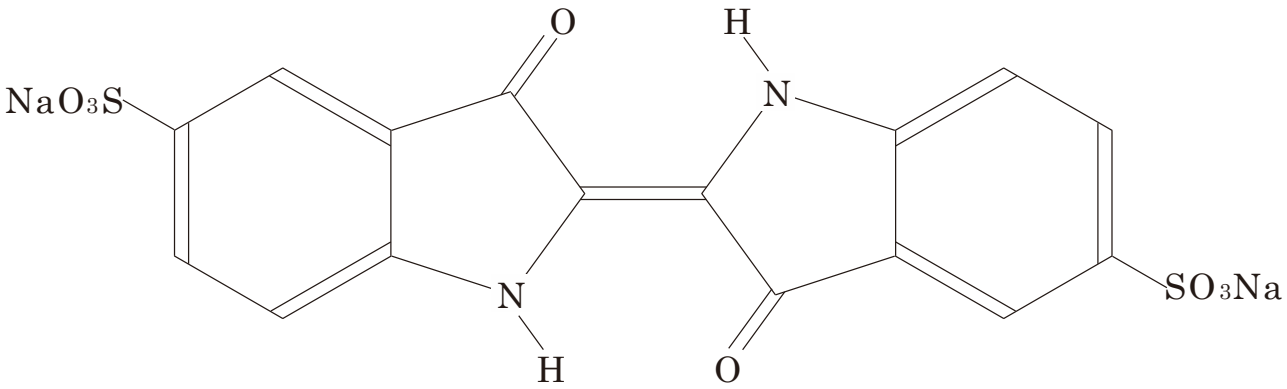

(a) Indigo carmine

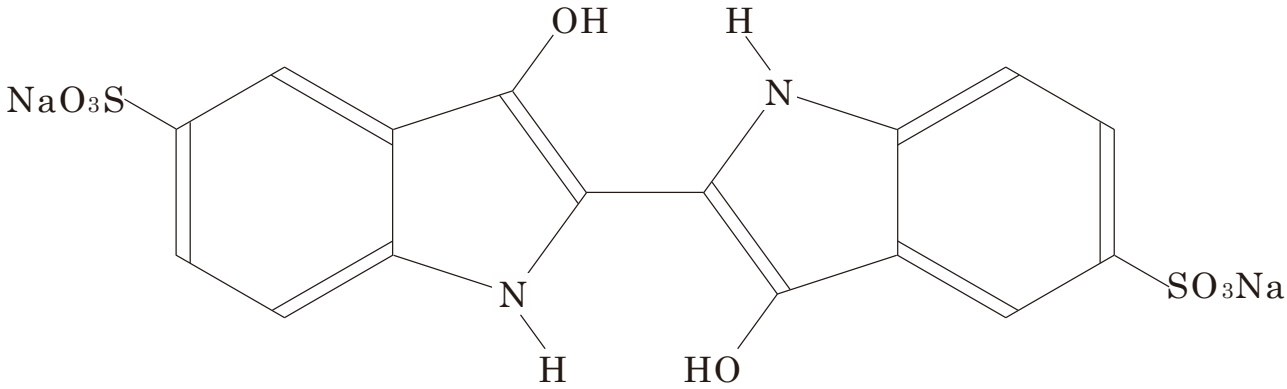

(b) Leuco indigo

Fig. 2-1. Structural formula of indigo carmine and decomposed indigo carmine (leuco indigo).

2.2. Surfactants [2.3, 2.4]

Surfactants are organic compounds that lower the surface tension (or interfacial tension) between a liquid and a solid or between two liquids. Fig. 2-2 presents the image of foam which is a characteristic of surfactants. As organic compounds, surfactants have been widely used not only for washing with foam as shown in Fig. 2-2, but also as emulsifiers in food manufacturing, for ice cream, mayonnaise, and so on. There are three kinds: natural surfactants such as lecithin or soybean saponin, soap, and synthetic surfactants. Moreover, ionic (anionic and cationic) surfactants are ionized in water, and nonionic surfactants are not ionized in water. Anionic surfactants whose hydrophilic group is ionized to an anion in water are often used as synthetic detergents, whereas cationic surfactants whose hydrophilic group is ionized to a cation in water are often used as softening finish agents, conditioner agents, and disinfectants. Nonionic surfactants whose hydrophilic group is not ionized in water are often used with all other surfactants. The ester type of nonionic surfactants, in particular, is used widely as an emulsifier for food-based cosmetics. Moreover, the ether type of nonionic surfactants is used as a washing agent. Fig. 2-3 shows the relationship between the surfactant concentration, micellar formation, and molecular structure of surfactant. Note that each position A, B, and C which indicates the surfactant concentration shown in Fig. 2-3(a) corresponds to a position shown in Fig. 2-3(b). As seen in Fig. 2-3(c), surfactant molecular has a hydrophobic group and a hydrophilic group. When the lower critical micelle concentration (CMC) of the surfactant aqueous solution appears in the positions A and B of Figs. 2-3(a) and 2-3(b), surfactant molecules are concentrated on the water surface, so that surface tension of water decreased. When the surfactant concentration is higher than CMC in the position C of Figs. 2-3(a) and 2-3(b), micelles which are composed of a hydrophilic outer layer and a hydrophobic inner layer are generated in the water. When surfactant concentration was higher than CMC, because surfactant molecules on water surface was not able to increase, surface tension was not decrease.

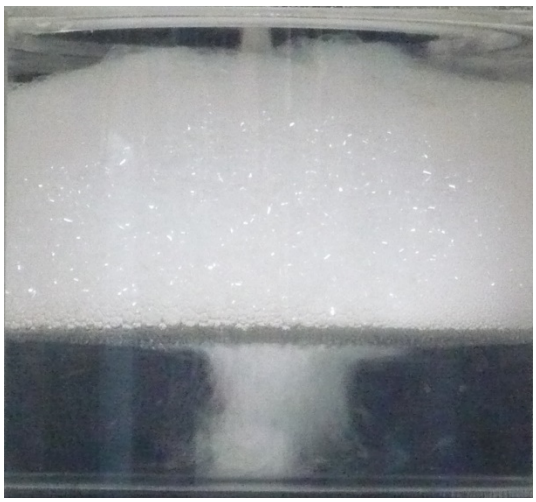

Fig. 2-2. Image of foam on surfactant solution.

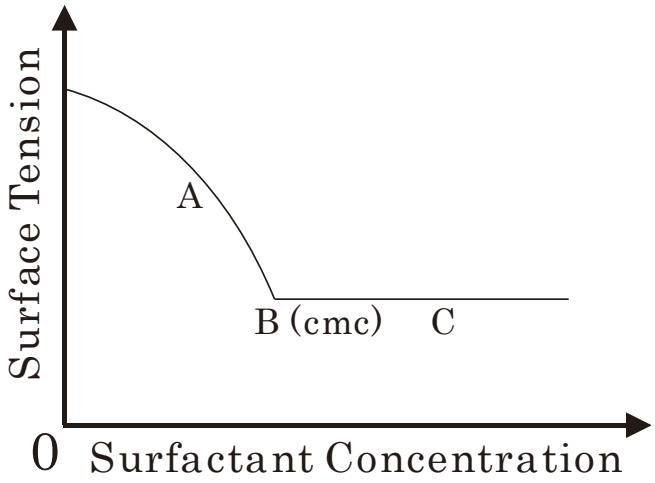

(a) Relationship between surfactant concentration and surface tension

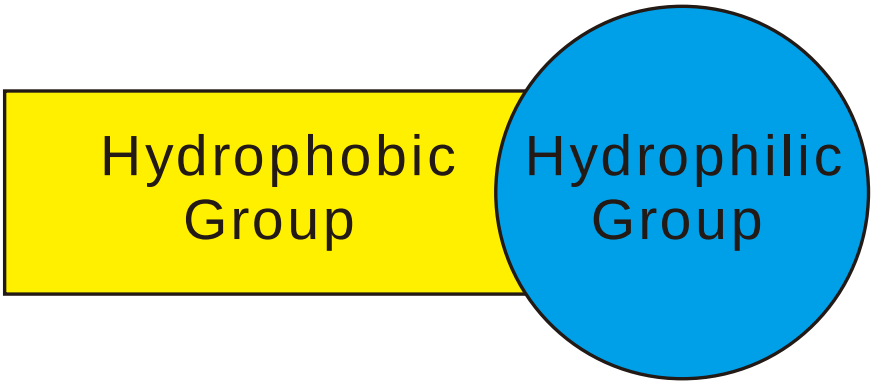

(b) Schematic diagram surfactant's molecular structure

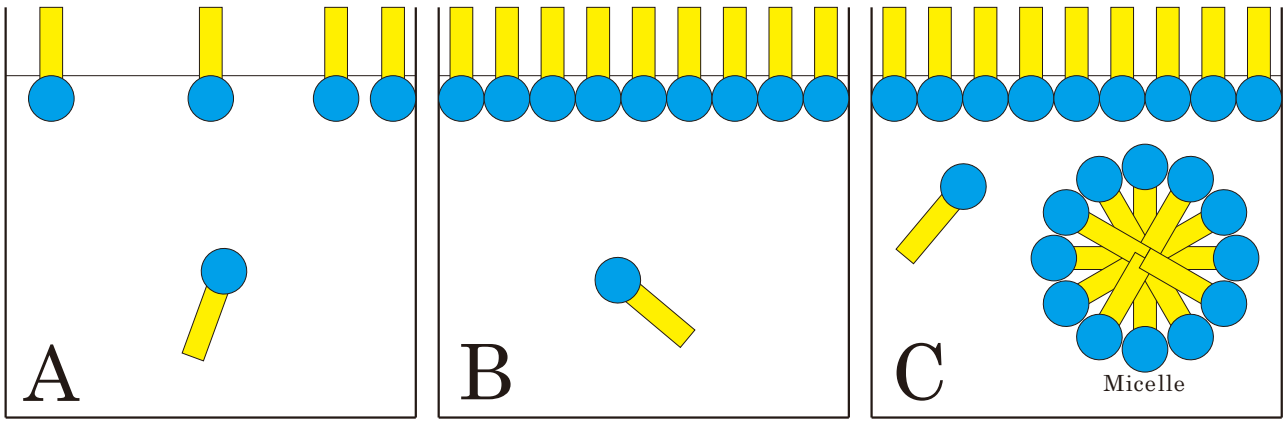

(c) Schematic representation of the micellar formation [2.5]

Fig. 2-3. Relationship between the surfactant concentration and micellar formation.

Because the micelle is formed with hydrophilic groups facing outward, it is considered that a hydrophilic group is decomposed firstly in surfactant treatment. Active species, whose oxidation-reduction potential was higher, such as OH radical could decompose a hydrophilic group of surfactant faster. Then, because surfactant concentration decreased, surface tension increase, so that foaming power of surfactant also became frailer.

2.3. Ozone and NOx [2.6–2.8]

Ozone is an inorganic molecule with the chemical formula shown in Fig. 2-4. Ozone is formed from oxygen molecule (O_2) by the action of UV rays and atmospheric electric-discharges, and it is present in low concentration throughout the Earth's atmosphere (stratosphere). In total, the ozone makes up only 0.6 ppm of the Earth's atmosphere. Ozone is a powerful oxidant (far more so than oxygen molecule (O_2)) and has many industrial and consumer applications related to oxidation. Moreover, ozone has characteristics of deodorization, decoloration, environmental improvement, and sterilization. As a deodorant component, ozone is used in raw sewage processing; bathroom, hospital, and old man facilities deodorants; stock raising; fisheries; and food processing. Deodorization with ozone is performed by the oxidative decomposition of the unwanted ingredient and neutralization of the ozone odor ingredient. Sterilization with ozone depends on the decomposition of the bacterial cell wall. Moreover, ozone does not produce toxic by-products.

Ozone is produced by electric discharges, as shown in Eqs. 2-1 and 2-2. Eq. 2-1 indicates that electrons released from electric discharges collide with stable oxygen molecules, so that oxygen atoms are formed. Moreover, in Eq. 2-2, ozone is generated by three collisions.

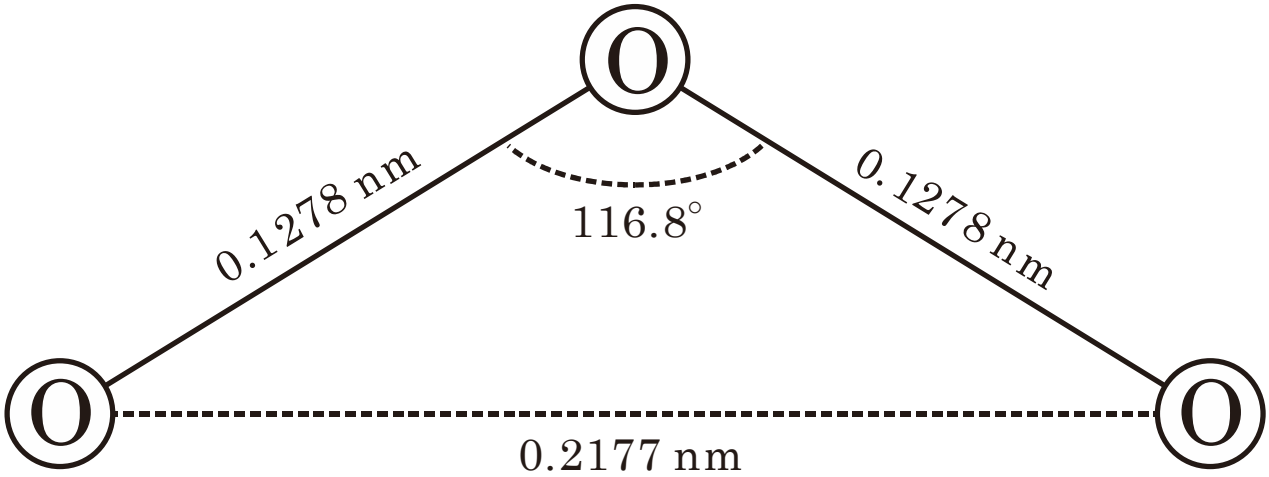

Fig. 2-4. Structural formula of ozone.

$$O_2 + e \rightarrow 2O + e \tag{2-1}$$

$$O + O_2 + M \rightarrow O_3 + M \tag{2-2}$$

NOx is a generic term for nitric oxide (NO) and nitrogen dioxide (NO_2). They are produced from the reaction of hydrocarbons during combustion, oxygen (O_2), and nitrogen (N_2), especially at high temperatures. The small particles of NOx are able to penetrate deeply into sensitive lung tissue, causing premature death in extreme cases. Inhalation of such small particles may cause or worsen respiratory diseases, such as emphysema or bronchitis, or it may aggravate an existing heart disease.

References-2

[2.1] M. Morimoto, K. Shimizu, K. Teranishi, and N. Shimomura, “Indigo Carmine Solution Treatment by Nanosecond Pulsed Power with a Dielectric Barrier Electrode,” IEEE Transactions on Dielectrics and Electrical Insulation, vol. 22, no. 4, pp. 1872-1878, August, 2015.

[2.2] T. Yano, N. Shimomura, I. Uchiyama, F. Fukawa and K. Teranishi, “Decolorization of Indigo Carmine Solution Using Nanosecond Pulsed Power,” IEEE Transactions on Dielectrics and Electrical Insulation, vol. 16, no. 4, pp. 1081-1087, August, 2009.

[2.3] M. Morimoto, K. Shimizu, K. Teranishi, and N. Shimomura, “Indigo Carmine Solution Treatment by Nanosecond Pulsed Power with a Dielectric Barrier Electrode,” IEEE Transactions on Dielectrics and Electrical Insulation, vol. 22, no. 4, pp. 1872-1878, August, 2015.

[2.4] M. Morimoto, K. Shimizu, K. Teranishi, and N. Shimomura, “Effect of the Number of Inner Wire Electrodes on Surfactant Treatment Using Nanosecond Pulsed Powers,” IEEE International Power Modulators and High Voltage Conference (IPMHVC2016), July, 2016.

[2.5] M. Tokita and S. Miyata, “The Structure of Liquid Crystal Formed by Surfactants,” The Chemical Society of Japan, vol. 47, no. 4, pp. 242-244, 1999.

[2.6] M. Morimoto, T. Ninomiya, T. Ikemoto, K. Teranishi, and N. Shimomura, “Ozone Production by Streamer Discharges Using Nanosecond Pulsed Powers and Coaxial Reactor with Tensioned Inner Electrode,” IEEE Transactions on Plasma Science, vol. 44, no. 10, pp. 2190-2195, October, 2016.

[2.7] M. Morimoto, R. Arai, K. Omatsu, K. Teranishi, and N. Shimomura, “Introduction of Tensioned Inner Wire Electrode for NOx Treatment with Nanosecond Pulsed Power System,” IEEE Transactions on Plasma Science, vol. 44, no. 11, pp. 2874-2879, November, 2016.

[2.8] T. Takeda, “Bases of Gas Discharges,” Tokyo Denki University Press, pp. 75-76, 1990. (in Japanese)

3. Nanosecond Pulsed Power System and Measurement Methods

A schematic diagram of the nanosecond pulsed power generator used in this study is shown in Fig. 3-1 [3.1-3.3]. The nanosecond high-voltage pulsed power generator consists of a Tesla transformer (Fig. 3-2), a short pulse-forming line, a highly pressurized gas gap switch, and a transmission line (Fig. 3-3). As shown in Fig. 3-2, the Tesla transformer consists of capacitor C_1 for initial energy storage and air-core coils with a coupling factor of approximately 0.6, which is adjusted to obtain the maximum transfer efficiency. The triggered spark gap switch of the Tesla transformer is controlled by Arduino Uno (Fig. 3-4). The pulse-forming line acts as capacitor C_2, which is also a component of the Tesla transformer. The highly pressurized gas gap switch with a short gap separation (0.43 MPa and 1.0 mm) is used in order to achieve extremely fast rise time of the output pulsed high voltage. Nanosecond high-voltage pulses are transmitted to load through the transmission line. The voltage and current waveforms in the nanosecond pulsed power system are shown in Fig. 3-5.

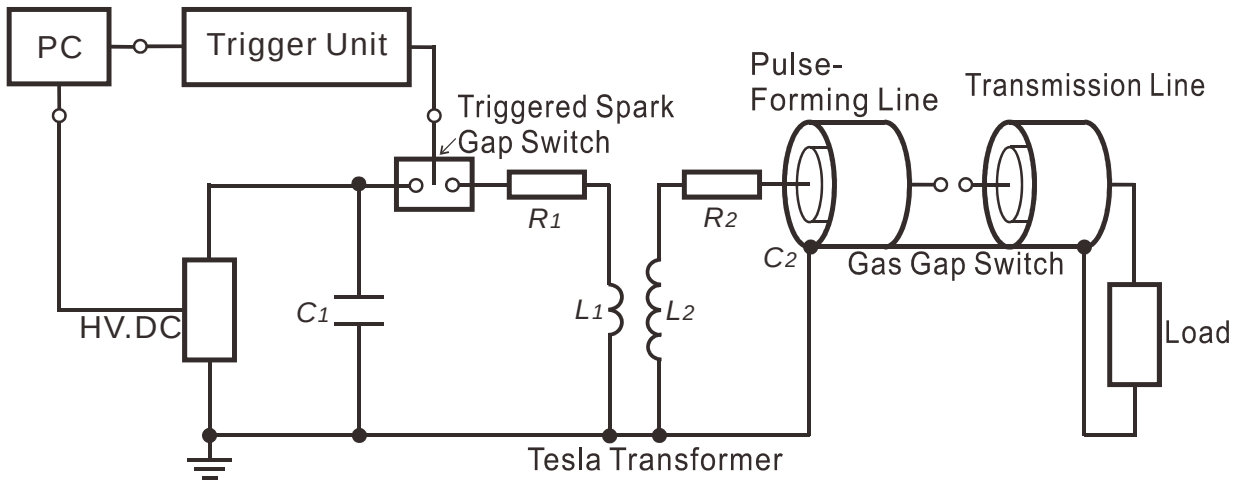

(C_1 = 25 nF, C_2 = 0.067 nF, L_1 = 0.35 μH, L_2 = 144.9 μH, R_1 = 0.56 Ω, R_2 = 0.29 Ω)

Fig. 3-1. Schematic diagram of the nanosecond pulsed power generator.

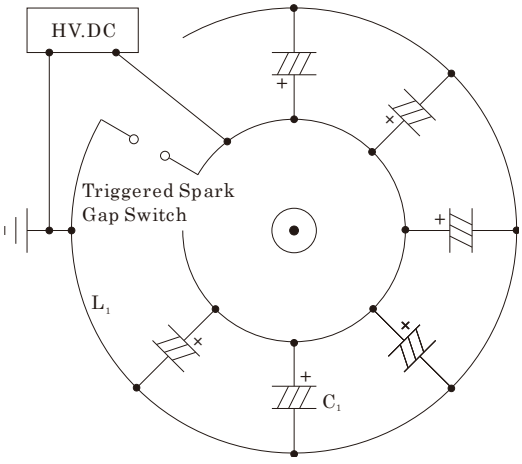

Fig. 3-2. Schematic diagram of the Tesla transformer in the pulsed power generator.

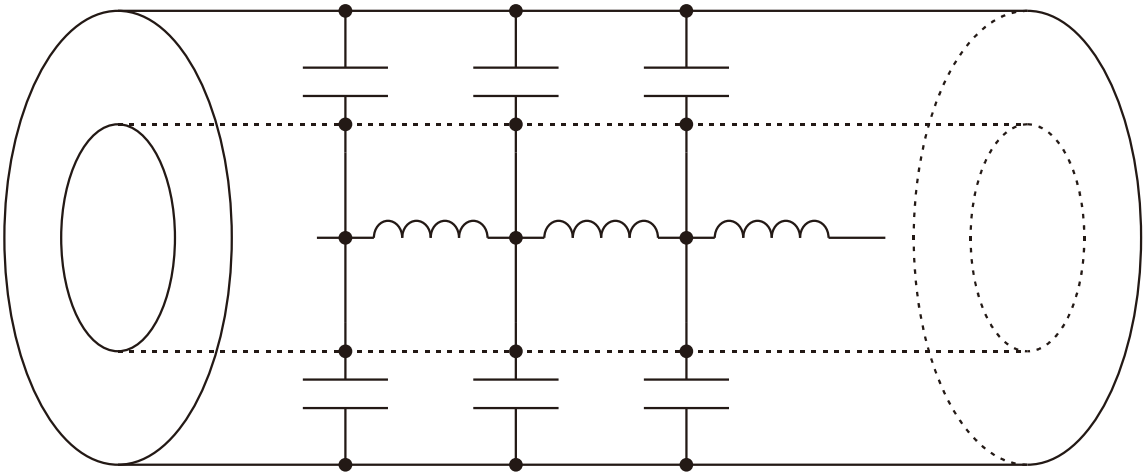

Fig. 3-3. Schematic diagram of the transmission line.

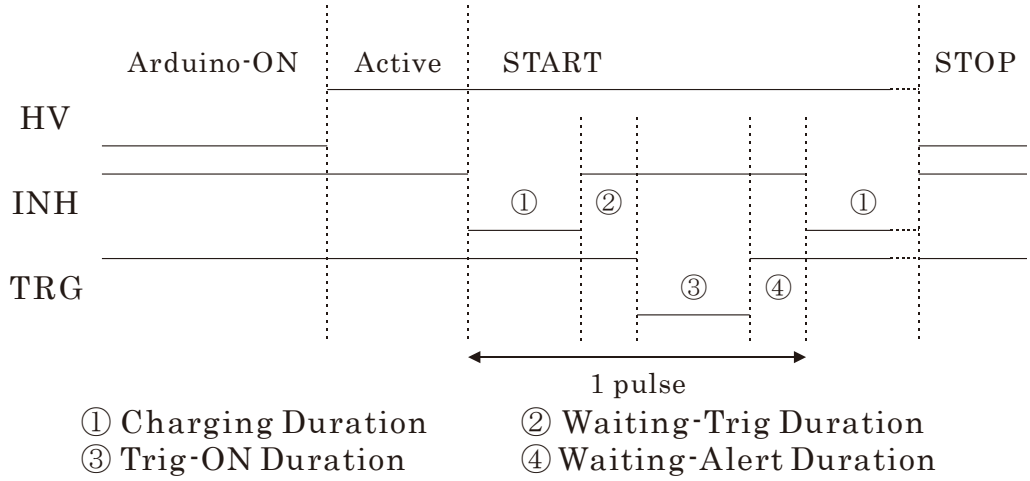

Fig. 3-4. Schematic diagram of Arduino Uno.

Fig. 3-6 shows the typical waveform of the output voltage at 86 Ω resistive load, when the initial charging voltage of C_1 is 3.0 kV [3.4]. The voltage and the current waveform were measured using a digital oscilloscope (Tektronix, DPO4104, 1 GHz) with a resistive voltage divider (1000:1) and a current viewing resister, as shown in Figs. 3-7 and 3-8. The full width at half maximum (FWHM) of the pulse and the peak voltage were 1.5 ns and approximately 38 kV, respectively. The current waveform was measured using a current viewing resister. Fig. 3-9 shows the interface used for experiments with pulse application. The pulse frequency (pps), pulse application time (s), charging duration of C_1, and so on were able to be changed by using the interface as shown in Fig. 3-9.

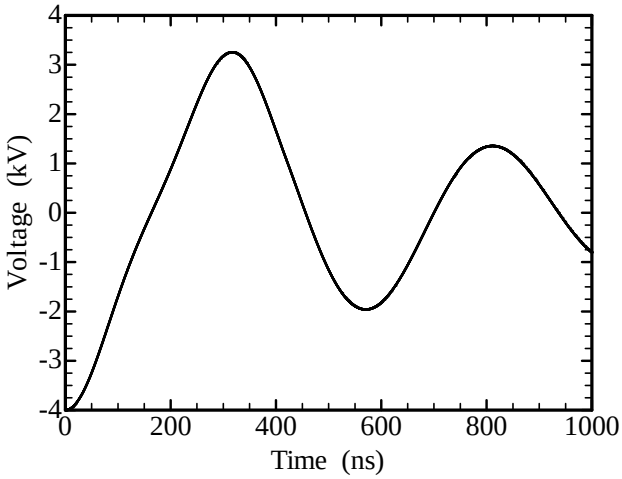

(a) End-to-end of C_1 voltage

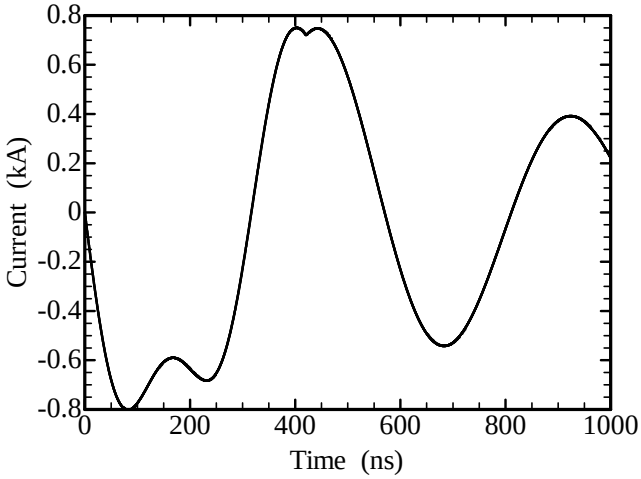

(b) C_1 Current

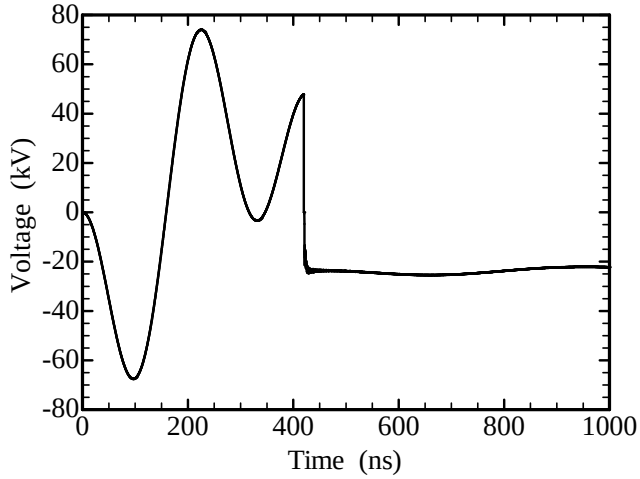

(c) Voltage at the end of the forming line

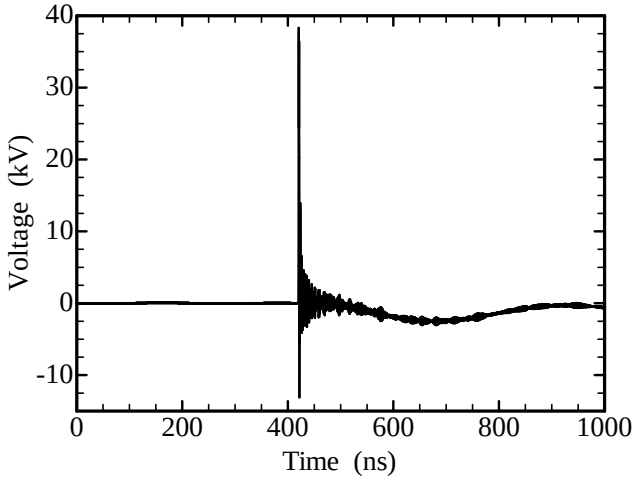

(d) Voltage at the end of the transmission line

Fig. 3-5. Typical waveforms of the voltage and the current in the pulsed power generator.

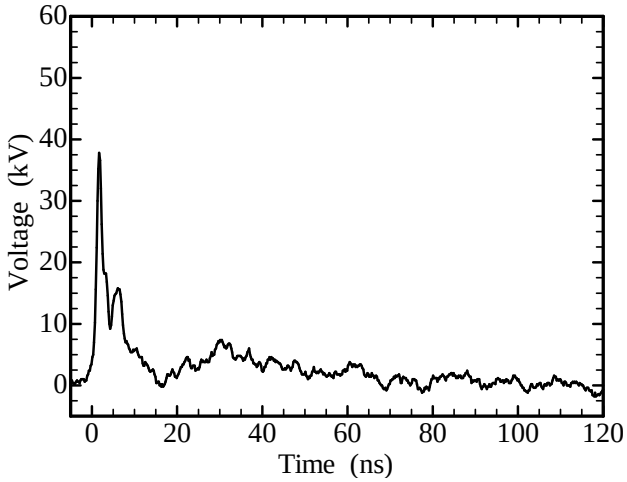

Fig. 3-6. Typical waveform of the output voltage at 86 Ω resistive load.

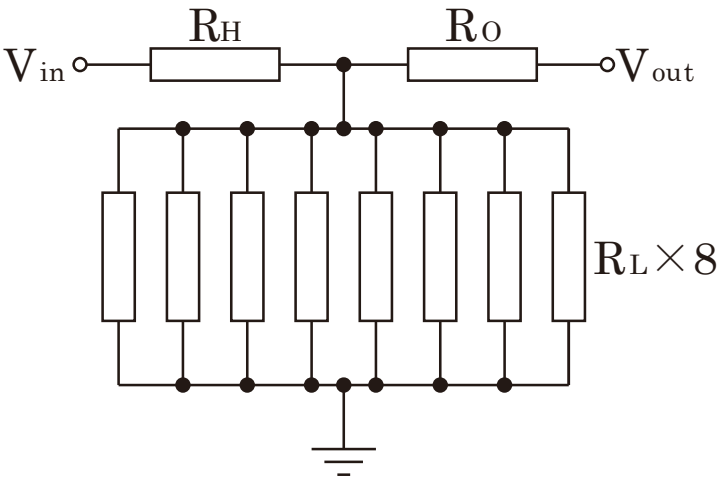

Fig. 3-7. Resistive voltage divider (1000:1): R_H = 1000 Ω, R_O = 50 Ω, R_I = 8 Ω.

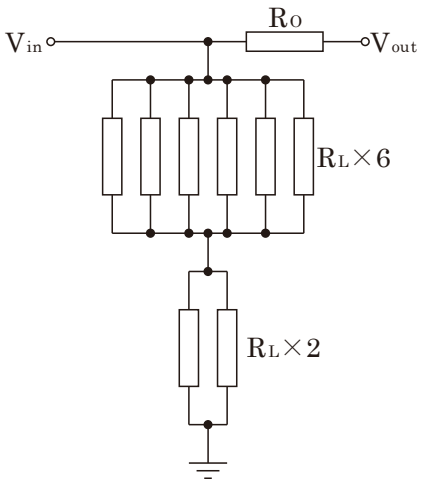

Fig. 3-8. Current viewing resistor: R_O = 50 Ω, R_L = 0.75 Ω.

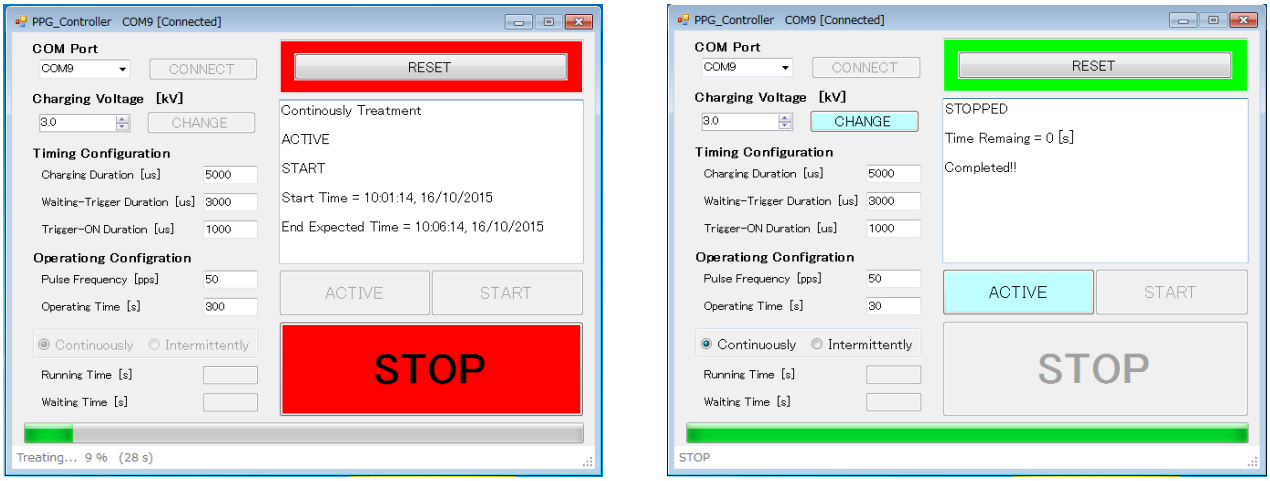

(a) During pulse application (b) After pulse application

Fig. 3-9. Interface for controlling pulse application.

The pulsed power is the pulse electric power consisting of very high voltage and a large current in very short domain from nanosecond to microsecond. Fig. 3-10 shows the temporal-compression state of the electric power [3.5]. The areas indicating electric energy in Fig. 3-11 are equal. The pulsed power could cause both short time and high voltage. There is an inverse relationship between the pulse rise time and the electric power, as shown in Fig. 3-11; the electric power increases with decreasing pulse rise time. Although the energy of every pulse was short, high electric power could have applied many times.

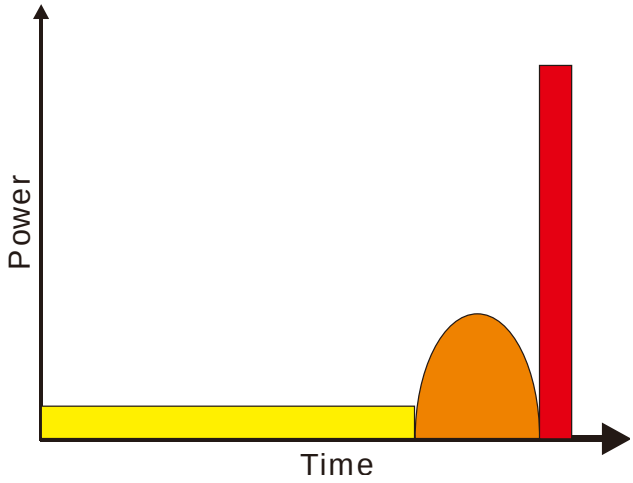

Fig. 3-10. State of the electric power time compression.

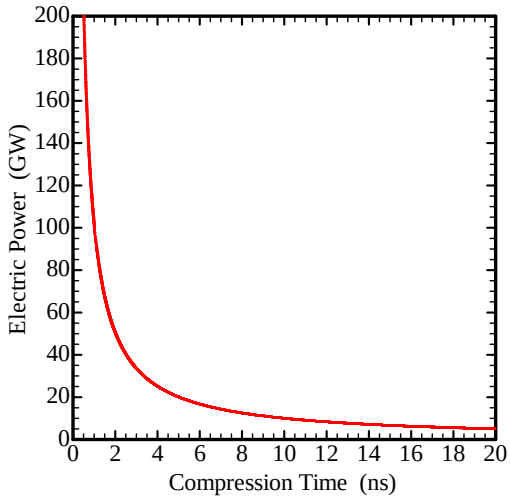

Fig. 3-11. Relationship between the pulse rise time and the electric power.

Fig. 3-12 shows the schematic diagram of progressing streamer discharges [3.6]. When pulse power was applied between electrodes, streamer discharges of non-thermal equilibrium were generated, where only electronic energy is high and the energy of the ion and the neutron is low. When high voltage was applied between electrodes, an electric field was generated between the electrodes, from the anode toward the cathode. At that time, because of the electric field between the electrodes, electrons in the gas moved from the cathode to the anode. When the electron moved,

ionization was caused through collision to the gas molecules. Then, the electrons moved because of the electric field, so that further ionization was caused. Because the number of electrons by the electronic collision ionization suddenly increased exponentially, an electron avalanche occurred. When the electron avalanche progressed, the first electronic avalanche progressed from the cathode to the anode with the speed of 2×10^7 cm/s. However, the cation produced by the collision ionization had a speed of 2×10^5 cm/s, which was lower than that of the electron, because the cation was heavier. Therefore, electrons accumulated on the tip of the electron avalanche, whereas the cations remained behind the electrons (Fig. 3-12(1)). When the electron avalanche arrived at the anode, an electron was absorbed by the anode, and the cation was left behind in the conic volume as space charge. The cation formed a strong electric field and strengthened the electric field with the cathode interval. As the electron avalanche progressed, an ionized photoelectron was generated by the electron avalanche because of the UV rays. A secondary electron avalanche was caused by the photoelectric movement (Fig. 3-12(2)). The electron avalanche formed plasma pillars (streamers) with both ions and electrons (Fig. 3-12(3)). When a streamer progressed from the anode to the cathode and arrived at the cathode, a large discharge current flowed as a conductive pillar of the streamer, causing electrical breakdown (Fig. 3-12(4)).

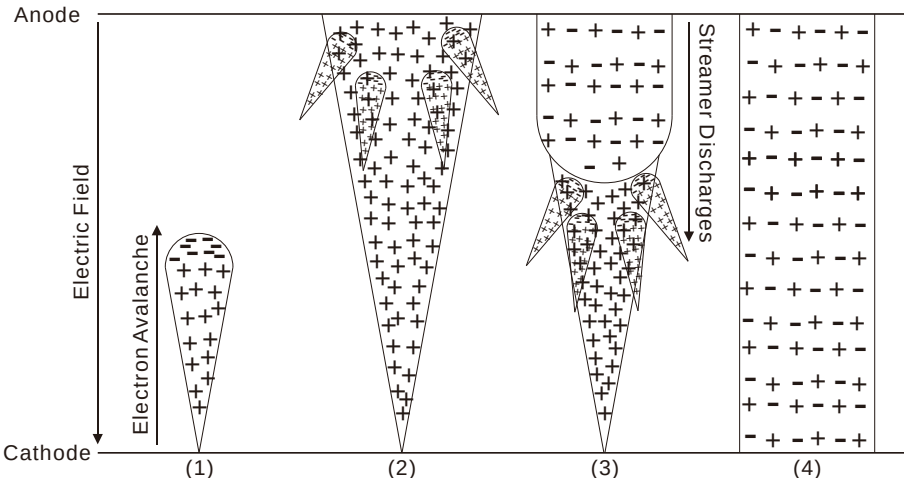

Fig. 3-12. Schematic diagram of progressing streamer discharges.

References-3

[3.1] M. Morimoto, K. Shimizu, K. Teranishi, and N. Shimomura, “Indigo Carmine Solution Treatment by Nanosecond Pulsed Power with a Dielectric Barrier Electrode,” IEEE Transactions on Dielectrics and Electrical Insulation, vol. 22, no. 4, pp. 1872-1878, August, 2015.

[3.2] M. Morimoto, T. Ninomiya, T. Ikemoto, K. Teranishi, and N. Shimomura, “Ozone Production by Streamer Discharges Using Nanosecond Pulsed Powers and Coaxial Reactor with Tensioned Inner Electrode,” IEEE Transactions on Plasma Science, vol. 44, no. 10, pp. 2190-2195, October, 2016.

[3.3] M. Morimoto, R. Arai, K. Omatsu, K. Teranishi, and N. Shimomura, “Introduction of Tensioned Inner Wire Electrode for NOx Treatment with Nanosecond Pulsed Power System,” IEEE Transactions on Plasma Science, vol. 44, no. 11, pp. 2874-2879, November, 2016.

[3.4] M. Morimoto, K. Shimizu, K. Teranishi, and N. Shimomura, “Surfactant Treatment Using Nanosecond Pulsed Powers and Action of Electric Discharges on Solution Liquid,” IEEE Transactions on Plasma Science, vol. 44, no. 10, pp. 2167-2172, October, 2016.

[3.5] H. Akiyama, “High Voltage Pulsed Power Engineering,” IEEJ Ohmsha, p. 1, 2003.

[3.6] T. Takeda, “Bases of Gas Discharges,” Tokyo Denki University Press, pp. 75-76, 1990. (in Japanese)

4. Water Treatment with Nanosecond Pulsed Power System

4.1. Introduction to the Water Treatment and Device [4.1, 4.2]

The pulsed power system is one of the water treatment methods using electric discharges. By using the nanosecond pulsed power system, high ozone-production efficiency was achieved. The ozone-production efficiency in commercial devices with dielectric barrier discharges (DBDs) is approximately 80 g/kWh [4.3], whereas that using the pulsed power system is over 120 g/kWh [4.4–4.6]. Moreover, the effects of the OH radical which has stronger ORP than ozone were also investigated. For ozone production experiment, a horizontal coaxial reactor was used, while a vertical reactor was used for water treatment experiment because it was easy to flow water thinly and control the water flow. For practical application of water treatment in the future, a horizontal reactor should be also used.

First, using a water treatment system using nanosecond pulsed power developed with a dielectric barrier between the electrodes [4.7–4.9], water treatment was evaluated by decoloration of an indigo carmine (H-type coloring system) solution. Such as a food additive and as a dye for industrial products, indigo carmine is used widely. A change in the color of an indigo carmine solution indicates a change in its chemical structure. Treatment systems with and without a dielectric barrier were compared. Moreover, the effect of the working gas (i.e., N_2 or O_2) on the electric discharge was investigated.

In addition, either purified water or tap water was used as solvents of surfactant aqueous solution containing persistent substance. Thus, the influence of the difference of both the pH and the electric conductivity of water on the generation of the OH radical was considered. Water treatment with an external ozonizer, instead of the nanosecond pulsed power system, was investigated in order to understand the effect of electric discharges. In organic compounds, surfactants have been widely used for synthetic detergents at home and for detergents, emulsifiers, and dispersants in industries. The surfactants have been widely used not only for washing, but also as emulsifiers in food manufacturing for mayonnaise, ice cream, and so on. There are three kinds of surfactants: natural surfactants, soap, and synthetic surfactants. In particular, because synthetic surfactants are hardly decomposed by microbes, the synthetic surfactants lead to pollution. Moreover, the available practical methods for surfactant treatment are few because synthetic surfactants are exhausted from home and factory with low concentration and large quantities.

Figs. 4-1(a) and 4-1(b) show a schematic diagram of the first water treatment device and the cross-sectional view of the device electrode. The voltage and current waveforms of this device are shown in Figs. 4-1(c) and 4-1(d). The inner electrode was stainless steel wire with 1 mm diameter, and the outer electrode was a stainless steel pipe whose length and inner diameter were 250 and 26 mm, respectively. This device is called the SS device.

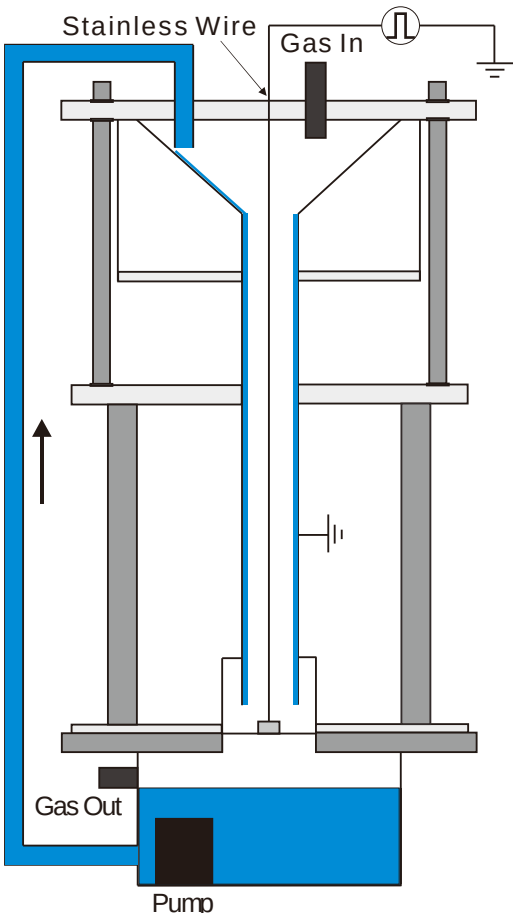

(a) Water treatment device

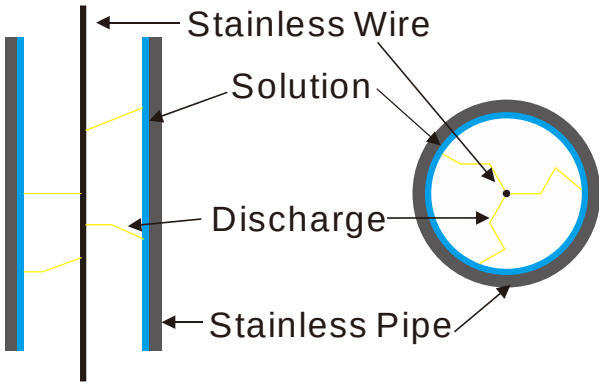

(b) Sectional views of the device electrode

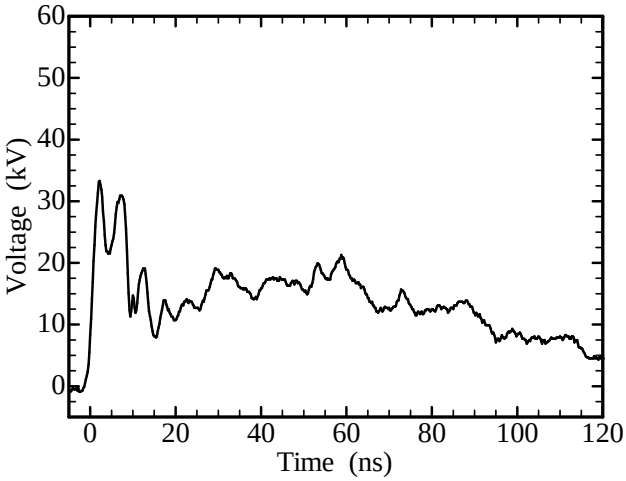

(c) Voltage waveform

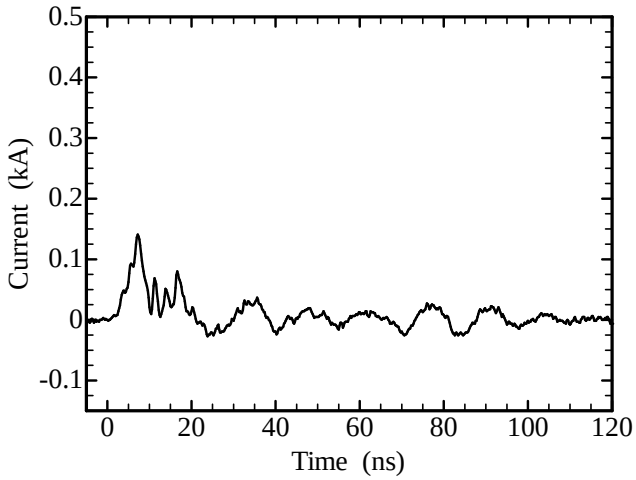

(d) Current waveform

Fig. 4-1. Water treatment device with a stainless steel pipe (SS device).

A water treatment device with a shorter separation of its electrodes was developed to produce dense plasma in the reactor. A glass pipe was adopted as a dielectric barrier to prevent spark discharges across the short electrode separation distance. Figs. 4-2(a) and 4-2(b) show a schematic diagram of the water treatment device using a glass pipe as the outer electrode and the cross-sectional view of the device electrode. The voltage and current waveforms of this device are shown in Figs. 4-

2(c) and 4-2(d). The inner electrode was a stainless steel wire with 1 mm diameter. The outer electrode was a glass pipe outer-wound with copper tape, and the length, inner diameter, and thickness of the glass pipe were 250, 10, and 1 mm, respectively. This device is called the SG device.

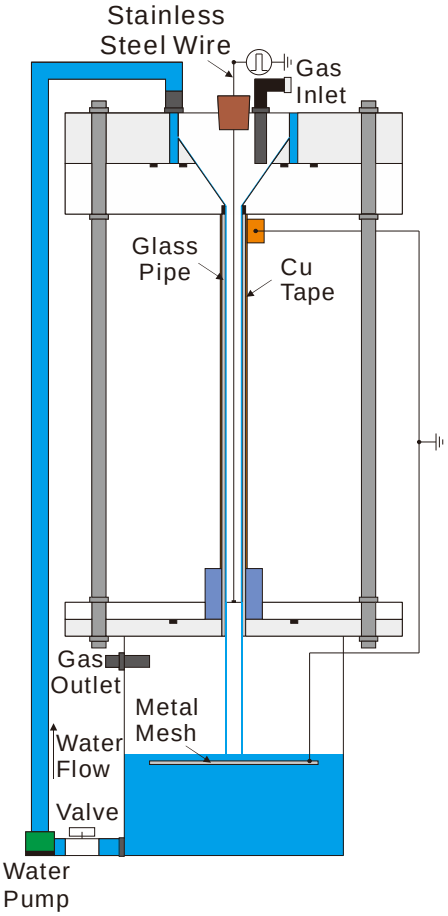

(a) Water treatment device

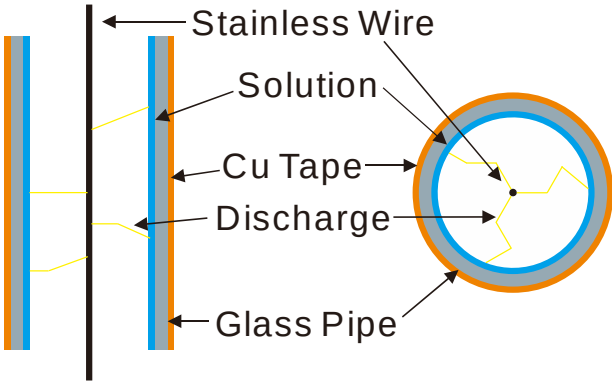

(b) Sectional views of the device electrode

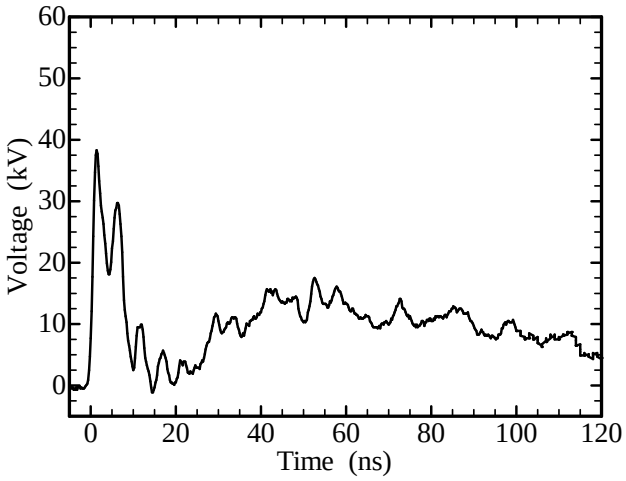

(c) Voltage waveform

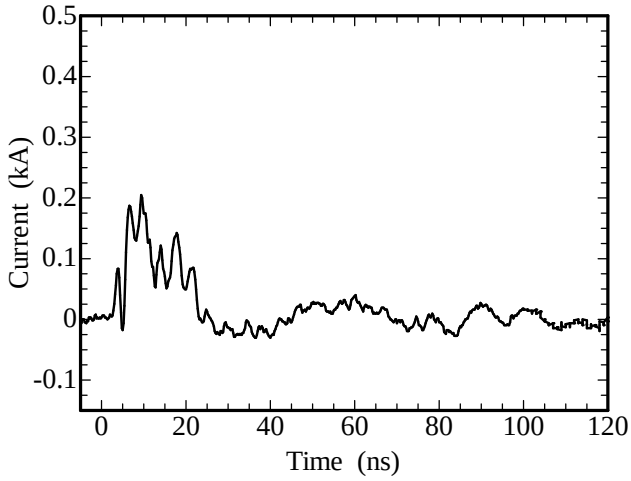

(d) Current waveform

Fig. 4-2. Water treatment device with a glass pipe (SG device).

The discharge plasma reactors of both devices consisted of vertical coaxial electrodes. The voltage pulse was applied on the inner wire electrode of the devices. The electric discharges occurred in the gas phase. Then, active species produced by electric discharges or UV irradiation could be pushed into the target aqueous solution by the ionic wind of the electric discharges and the impact of the streamer heads. The target solutions flowed on the inner surface of the outer pipe electrode, as shown schematically in Figs. 4-1(b) and 4-2(b). As shown in Figs. 4-1(c), 4-1(d), 4-2(c), and 4-2(d), the voltage and current waveforms of the SG device were similar to those of the SS device. When the solution was not being circulated in the reactors, the spark discharge occurred more frequently. The voltage and current waveforms changed when the spark discharge occurred, and the solution layer in the reactor prevented frequent spark discharges.

The target solution was placed in a water reservoir located under both electrodes and circulated in the system with a water pump. The flow rates of the water pump were 1.9 (SS) and 0.7 (SG) L/min. The ratio between the surface areas of the SS and the SG devices was 2.6. The gas surrounding the discharge (the working gas) was flowed through the reactor. During water treatment, the flow rate of the working gas was 1.5 (SS) and 0.1 (SG) L/min (selected based on preliminary experiments). The volume of the SS and SG devices were 133 and 20 cm^3, respectively. The ratio between the flow rates of the SS and the SG devices was 2.7. The ratio of the surface areas corresponded to that of the circumference of the pipes because both reactors of SS and SG devices had the same length. Because the falling velocity of water in the reactors should be the same, the thickness of the water layer in the reactors should also be the same when the ratio of water flow by the water pumps equaled the ratio of the surface areas.

4.2. Comparison of Indigo Carmine Treatments for Reactor Configuration [4.1]

An indigo carmine solution was chosen for treatment with these devices. The concentration (mol concentration) and volume of the indigo carmine aqueous solution were 20 mg/L (4.33×10^{-5} mol/L) and 1.0 L, respectively. The density and molecular weight of the indigo carmine were 1.01 g/cm^3 and 466.35 g/mol, respectively. The maximum absorption wavelengths of indigo carmine were both 288 and 610 nm. For measurement of the indigo carmine decoloration, two kinds of spectrophotometers were used. A spectrophotometer (SP-300, OPTIMA) was used in order to measure the solution transmittance. The spectral absorbance of the indigo carmine solution from 190 to 1100 nm was measured using an absorption ultraviolet-visible-near-infrared spectrometer (PD-3500UV, APEL). The relationship between the mol concentration of the indigo carmine solution and the absorbance at wavelength of 288 and 610 nm is shown in Fig. 4-3.

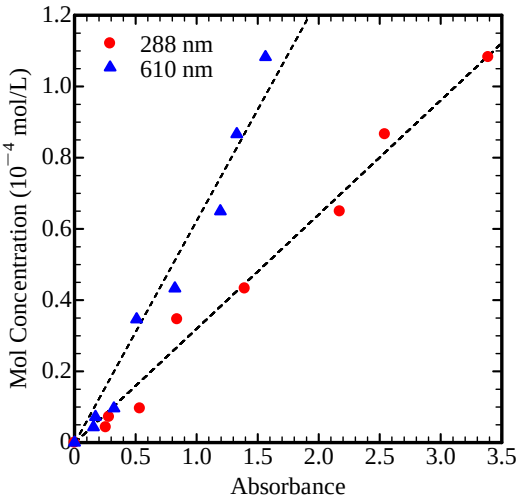

Fig. 4-3. Relationships between the mol concentration of the indigo carmine solution and the absorbance at wavelengths 288 and 610 nm.

According to Fig. 4-3, the relationships between the mol concentration and the absorbance at 288 and 610 nm are represented by

$$y = 3.21 \times 10^{-5} x \quad \text{(at 288 nm)}, \tag{3.1}$$

$$y = 6.25 \times 10^{-5} x \quad \text{(at 610 nm)}, \tag{3.2}$$

where y is the mol concentration (mol/L) and x is the absorbance. The mol concentration of indigo carmine in the treated solutions could be determined by each equation.

The decoloration ratio of indigo carmine increased with the initial charging voltage of C_1, as shown in Fig. 4-4(a). On the other hand, the treatment efficiency of indigo carmine decreased with increasing the initial charging voltage in both SS and SG devices. The treatment efficiency of indigo carmine could decrease when the untreated amount of indigo carmine in the solution is low. The

treatment efficiency of indigo carmine using the SS device was higher than that using the SG device for all initial charging voltages of C_1, as shown in Fig. 4-4(b). Because the discharge volume was restricted by the reactor volume, the energy deposited by the electric discharges in the SG device would be much smaller than that in the SS device. Moreover, the volume of the solution layer on the inner surface of the cylindrical electrode in the SG device was smaller than that in the SS device due to its smaller inner diameter. Similarly, the discharge plasma would have a lesser effect on the smaller solution surface area in the SG device.

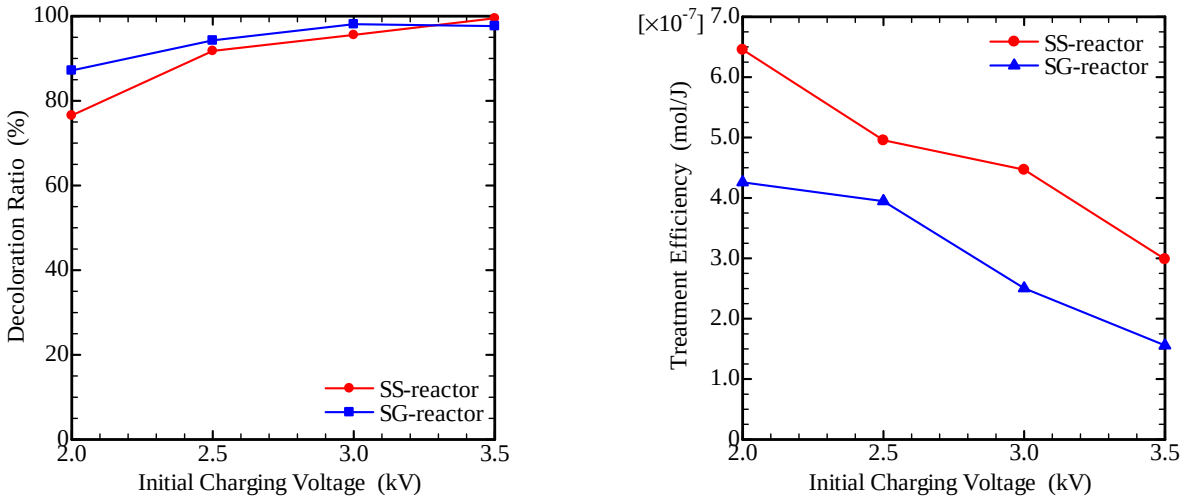

(a) Decoloration ratio of indigo carmine (b) Treatment efficiency

Fig. 4-4. Effects of the initial charging voltage on the indigo carmine solution treatment.

Figs. 4-5 and 4-6 show the spectral absorbance of the treated indigo carmine solution observed at each 2-min treatment time with pulse repetition ratios of 10 and 50 pps, respectively. It was determined that the indigo carmine solution was effectively treated, as evidenced by the decrease of absorbance at 288 nm with increasing treatment time. Considering Figs. 4-5(a) and 4-6(a), when nitrogen gas was used, nitric oxide ions, such as nitrate ions, nitric monoxide ions, and nitric dioxide ions, which have absorption wavelengths from 200 to 260 nm, were generated by the treatments with the pulsed power system. The oxygen required to generate nitric oxide ions would be supplied by the solution. However, in Figs. 4-5(b) and 4-6(b), when oxygen gas was used, absorbance from 200 to 260 nm decreased after increase. Then, it was found that the absorbance variation was caused by not nitric oxide ion but decomposition of indigo carmine. It would be considered that the absorbance from 200 to 260 nm decreased due to demolition of *trans*-isomer structure of indigo carmine [4.10].

Fig. 4-7 shows the changes in the mol concentration of the treated solutions obtained from the absorbance at 288 nm with increasing the treatment time at pulse repetition rates of 10 and 50 pps in Figs. 4-5 and 4-6, respectively. In Figs. 4-7(a) and 4-7(b), the mol concentration of the indigo carmine solution decreased with increasing the treatment time. The mol concentration of the indigo carmine solution with oxygen gas decreased more rapidly than that with nitrogen gas. When oxygen was used as the working gas in Figs. 4-5(b) and 4-6(b), ozone and active species such as OH radicals were

produced by electric discharge. Then, fast water treatment could be achieved due to high efficiency of ozone production. Moreover, decoloration treatment of indigo carmine with 50 pps was performed more rapidly than that with the 10-pps treatment. When the pulse repetition rate increased from 10 to 50 pps, the amount of removed indigo carmine increased by approximately five times with nitrogen as the working gas.

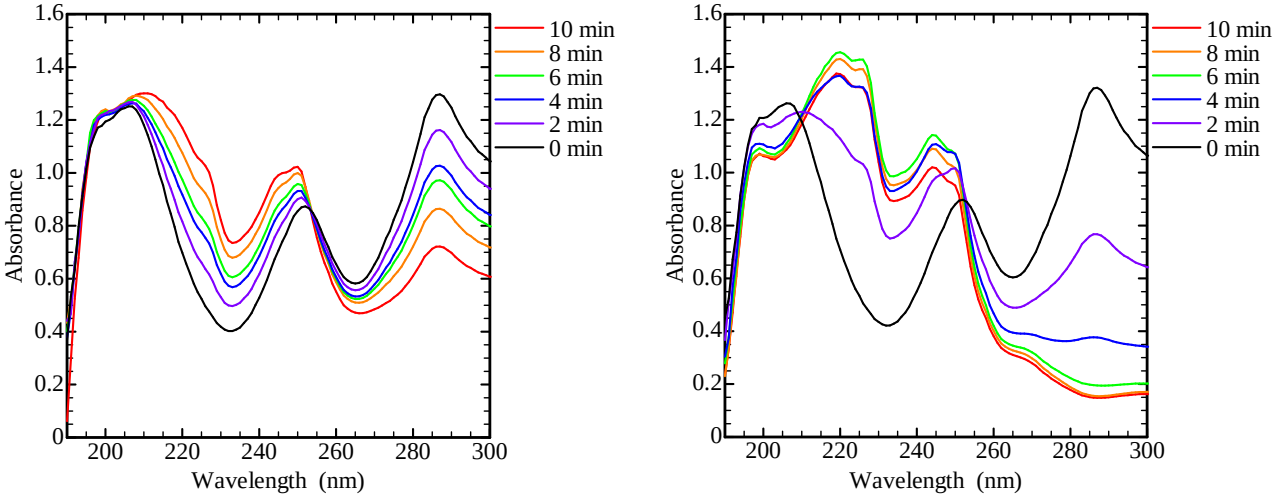

(a) Using nitrogen gas (b) Using oxygen gas

Fig. 4-5. Absorbance at wavelengths from 190 to 300 nm at 10 pps in the SG reactor.

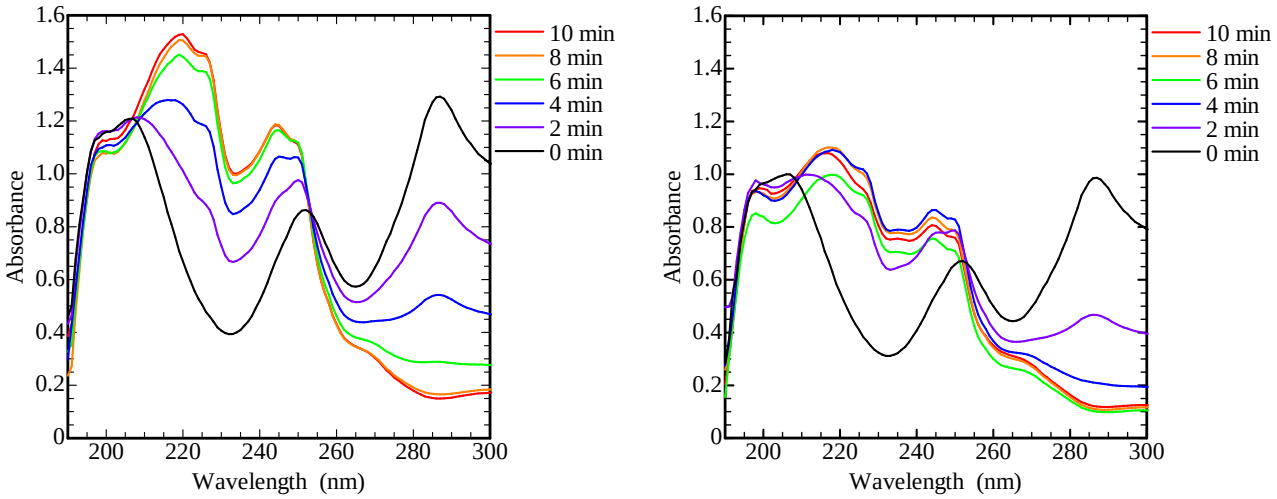

(a) Using nitrogen gas (b) Using oxygen gas

Fig. 4-6. Absorbance at wavelengths from 190 to 300 nm at 50 pps in the SG reactor.

On the other hand, the amount of removed indigo carmine increased only slightly with oxygen as the working gas; indeed, only a small amount of untreated indigo carmine remained, even with the 10-pps treatment. Because the decoloration efficiency is reduced when the concentration is low, the change in the mol concentration with increased pulse repetition rate was not noticeable. As shown in Fig. 4-7(b), the indigo carmine was decomposed well when nitrogen was supplied as the working gas.

This is because not only active species, such as nitric oxide ions and OH radicals, but also electric discharges induce the treatment of indigo carmine. In addition, using either gas as the working gas, the electric discharges provided the solutions with direct effects of the electric discharges such as UV rays, ion wind, and bombardment of streamer heads; the decoloration of indigo carmine thus proceeded. UV rays can cause the decomposition of indigo carmine; ion wind of electric discharges can help dissolve gas, including active species; and bombardment of streamer heads can affect the indigo carmine molecules.

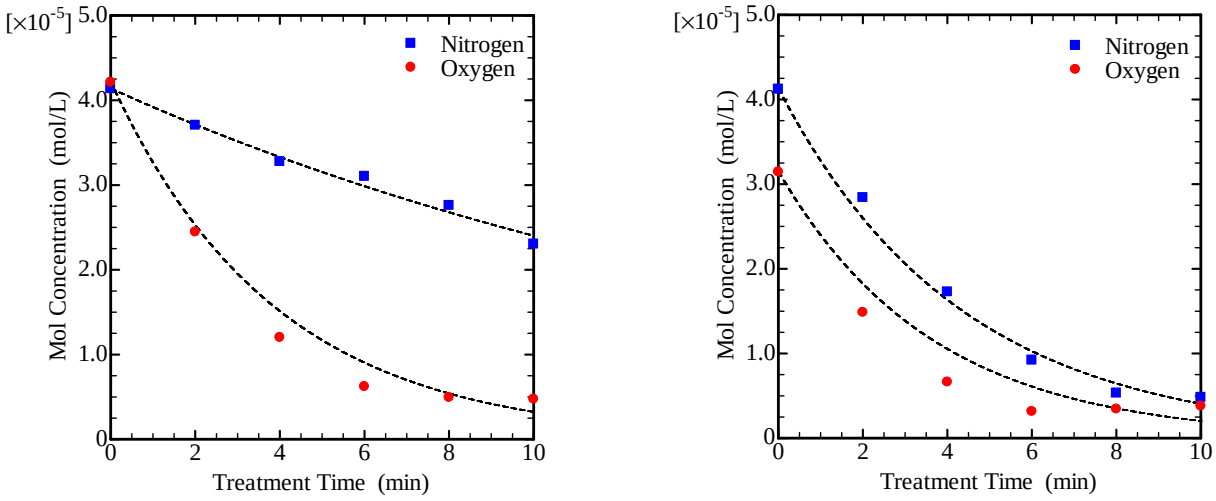

(a) 10 pps (b) 50 pps

Fig. 4-7. Variation in the mol concentration of indigo carmine observed after 2 minutes in the SG reactor.

4.3. Surfactant Treatment Using SG Reactor [4.2]

The mixture solution of lauryl alcohol ethoxylate (LAE) and nonylphenol ethoxylate (NPE), which is a typical surfactant, was chosen as a treatment target. The decomposition of LAE was easier than that of NPE. The surfactant solution of 400 ppm was made by mixing the product solution (200,000 ppm) with either purified water or tap water. In tap water, chlorine used for sterilization and impurities such as sodium ion, magnesium ion, potassium ion, calcium ion, and so on were included. Then, the absorbance around 200 nm of tap water including impurities was approximately 0.15 Abs larger than that of purified water. Moreover, the pH and the electric conductivity of the purified water and the tap water were 6.34 and 1.3 μS/cm, and 7.34 and 131.9 μS/cm, respectively. The initial surfactant concentration and the total volume of the surfactant solution were 400 ppm (0.04 %) and 500 mL, respectively. The surfactant solution was treated for 100 minutes with the nanosecond pulsed power system and was analyzed at every 20 minutes during treatment. The height of the foam, the absorbance, the pH, and the electric conductivity were measured for evaluation. The height of foam, which is characteristics of the surfactant, in the reservoir was gauged in the pictures of the reservoir. The absorbance of the surfactant solution from 190 to 300 nm was observed with an absorption ultraviolet-visible-near-infrared spectrometer (PD-3500UV, APEL), whose wavelength and photometric accuracy were 0.5 nm and 0.005 Abs at 1.000 Abs, respectively. Both the pH and the electric conductivity of the surfactant solution were measured using Waterproof Multiparameter (PCS Testr 35, OAKTON) before and after the treatment. The tap water and the purified water without the surfactant were treated in order to consider the phenomena in water treatment.

In order to evaluate the OH radical production during the treatment with the nanosecond pulsed power system, disodium terephthalate (NaTA) was added to the solutions. Disodium terephthalate (NaTA) reacts only with the OH radical [4.11]. When the hydrogen atom of the benzene ring in the NaTA was substituted by a hydroxyl group, 2-hydroxyterephthalic acid (HTA) was formed. The OH radical production during treatment was estimated by observing the absorption at 310 nm, which is absorption wavelength of HTA. 1.0 g NaTA was added to the solutions, and each solution was treated for 20 minutes. The absorbance of the solution was observed with the spectrometer from 190 to 400 nm at every 4-min treating time.

Moreover, in order to investigate the OH radical production by pulsed power discharges, the solutions were also treated with an external ozonizer instead of the nanosecond pulsed power system. The external ozonizer setup condition was adjusted to produce an equivalent ozone concentration using the nanosecond pulsed power system (12 g/Nm^3) at an oxygen flow rate of 0.1 L/min.

Figs. 4-8(a) and 4-8(b) show image of foam and temporal variations in the foam height in the reservoir. In Fig. 4-8(b), the error bars indicate the maximum and minimum heights of the foam in the reservoir. Note that the surfactant solution did not bubble at 0 minute because the solution circulation also started at that time. The foam heights at 40 ppm and 4 ppm of the solution in the reservoir were measured by only circulation with the pump without the nanosecond pulsed power system. Note that these heights (68 and 14 mm) are indicated as dash lines in Fig. 4-8(b).

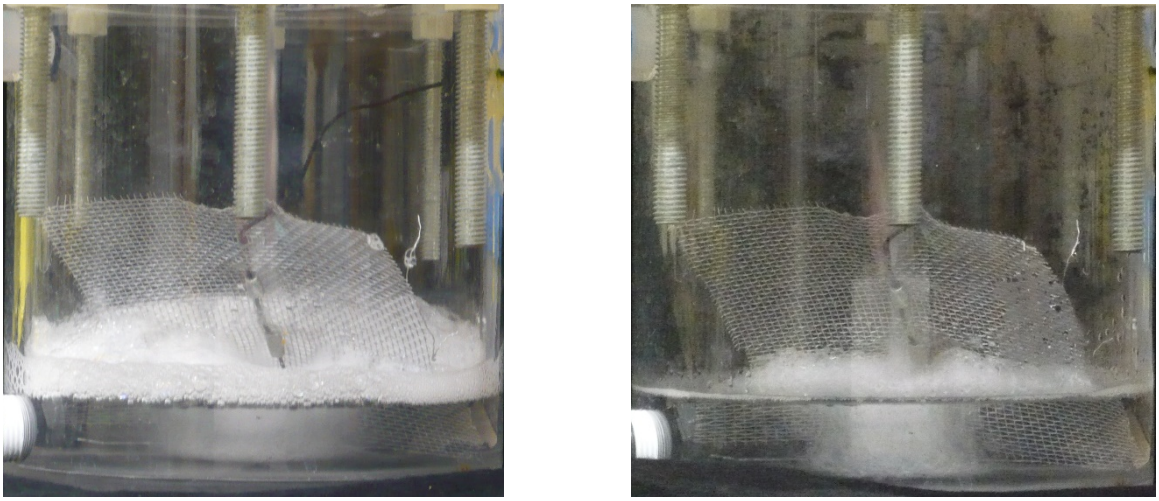

(L) Tap water (R) Purified water

(a) Image of foam in the reservoir after 100 minutes' treatment

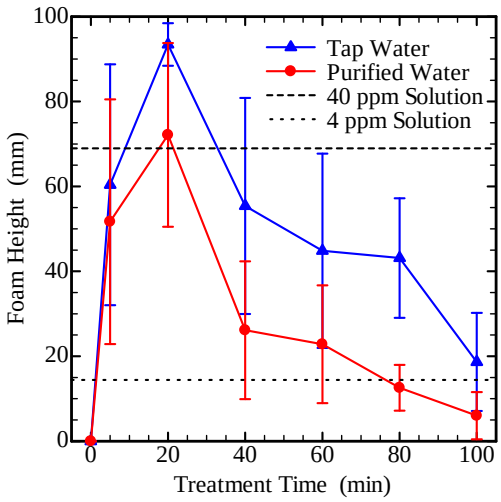

(b) Foaming height

Fig. 4-8. Temporal variation of the foam height in tap and purified water.

The foam height decreased with the surfactant concentration. The foam heights on the surfactant in purified and tap water increased until 20 minutes from the start of the pulse application and decreased after 20 minutes. The initial increase in the foam height arose with the start of the solution circulation owing to the foamability of the surfactant. When the concentration of the NPE solution was greater than 0.1 ppm, the surfactant showed foamability [4.12] because the hydrophobic groups and the hydrophilic groups of the surfactants formed micelles containing atmospheric (O_2) gas. After 20 minutes of treatment, the foamability of the surfactant would be lost because a hydrophilic group in the surfactant molecule was decomposed. This means that the surfactant in both waters was treated. The foam height of surfactant in purified water decreased faster than that in tap water. This suggested that because the surfactant was decomposed, the surfactant concentration in the solution decreased. Note that it was difficult to change this surfactant property with heat because the solution temperature

increased by 5 K for 100-minutes' treatment because of heat from a water pump.

Fig. 4-9 presents the variation of the absorbance spectrum at each treatment time. Fig. 4-10 shows the pH and electric conductivity measured before treatment (0 min) and after treatment (100 min). The results of the pH and electric conductivity would be considered with experiment of OH radical production.

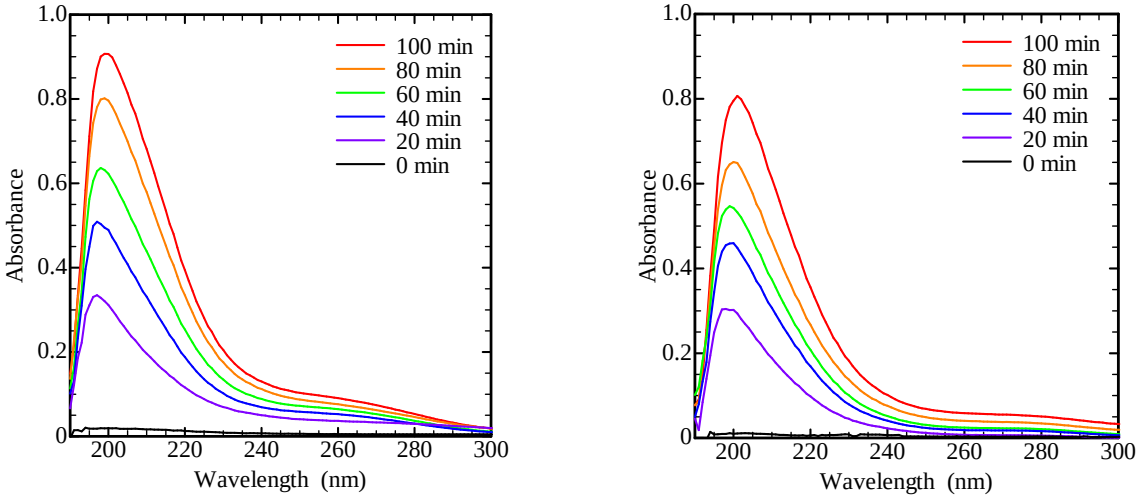

(a) Purified water (b) Tap water

Fig. 4-9. Variation of absorbance during treatment.

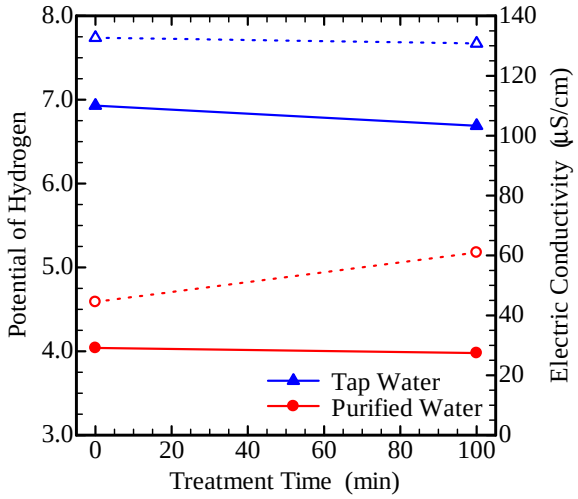

Fig. 4-10. Variation of pH (solid symbol) and conductivity (open symbol) of the surfactant solution.

The absorbance around wavelength of 200 nm increased with increasing the treatment time, possibly because 4-nonylphenol (NP) was being produced due to surfactant decomposition or hydrogen peroxides were produced during electric discharges. The absorbance difference between surfactants in purified water and in tap water at 0 minute would be attributed to an instrumental error in the spectrometer. After treatment for 100 minutes, the surfactant absorbance in purified water (0.91) was larger than that in tap water (0.80). It was suggested that surfactant treatment in purified water was

faster than in tap water, as well as decreasing foaming height. Because the surfactant could be effectively decomposed by active species such as the OH radical, possibly some active species reacted with impurities in tap water. Meanwhile, because the impurities affect water characteristics such as pH and electric conductivity, the pH and the electric conductivity of tap water were different from those of purified water.

The OH radical, as one of the active species that can be produced during water treatment, has the strongest ORP and is the most important agent for organic compounds degradation. Thus, we investigated the production of the OH radical in this treatment system. The disodium terephthalate (NaTA) added to purified and tap water reacted only with the OH radical to form 2-hydroxyterephthalic acid. Absorbance spectra of treated surfactant solution in purified water and tap water with NaTA are shown in Figs. 4-11(a) and 4-11(b). Figs. 4-12(a) and 4-12(b) show absorbance spectra of purified water and tap water with NaTA. The surfactant absorbance spectrum around 310 nm in purified water (Fig. 4-11(a)) was not different from that of the surfactant in tap water (Fig. 4-11(b)). On the other hand, as shown in Fig. 4-12, when the surfactant was not included, the absorbance spectrum around 310 nm of purified water was much higher than that of tap water. It was thought that the OH radical, which should react with disodium terephthalate, would react with more impurities in tap water. When the solutions included the surfactant, micelles were formed because of the structure of the surfactant molecules, so that impurities would be enfolded in the micelles' cores with surfactant molecules. Even when tap water including more or less impurities was used, the OH radical would react with not the impurities but both disodium terephthalate and the surfactant. Therefore, it is thought that the absorbance in Fig. 4-11(b) was not different from that in Fig. 4-11(a). That is to say, the amount of produced OH radical would be the same regardless of the type of solution used. However, the difference in the water quality, such as impurities in tap water, would affect the amount of produced OH radical with increasing treatment time. The water quality could be indicated by the pH value, the electric conductivity, and so on. As seen in Fig. 4-10, the pH value and the electric conductivity of the surfactant solution in purified water were lower than those in tap water. Water treatment using an acidic solution was faster than using neutral and alkaline solutions because the OH radical would react with the CO_3^{2-} formed during organic compounds degradation unselectively in the alkaline solution [4.13, 4.14]. Thus, the reaction between the OH radical and the target organic compounds in alkaline solution could be reduced. In addition, it was reported that less OH radical was produced in the higher electric conductivity solution [4.15]. As shown in Fig. 4-10, the electric conductivity of the surfactant in purified water increased after treatment for 100 minutes. Because of more ions and impurities in tap water, more surfactant in purified water could be decomposed by pulsed power system than surfactant in tap water. The pH value and the electric conductivity could also influence the amount of OH radical produced in this experiment.

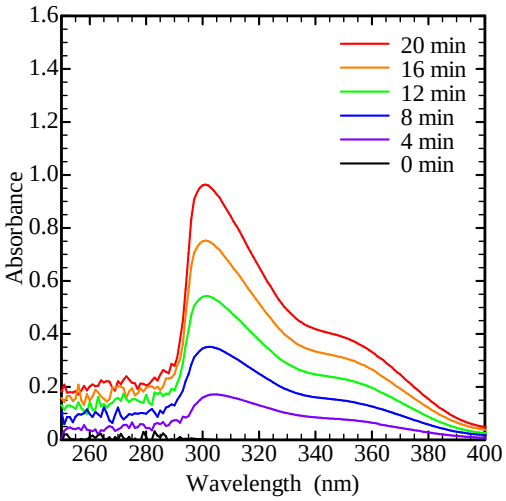

(a) Surfactant (Purified water)

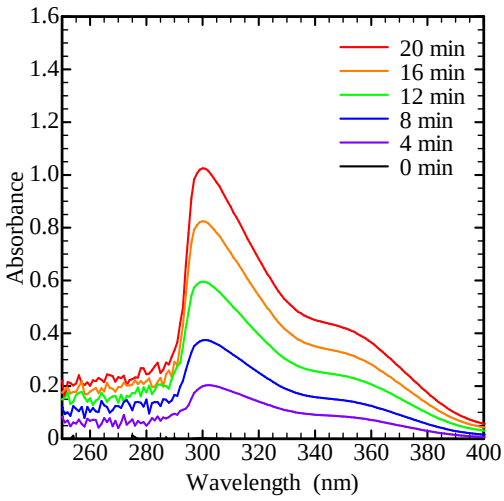

(b) Surfactant (Tap water)

Fig. 4-11. Variation in the absorbance of the surfactant, when disodium terephthalate is added, using the pulsed power system.

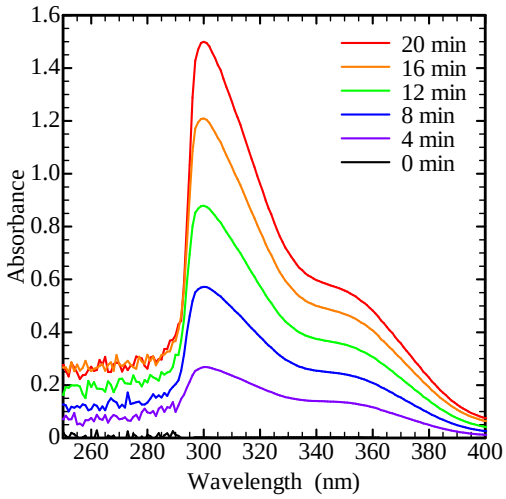

(a) Purified water

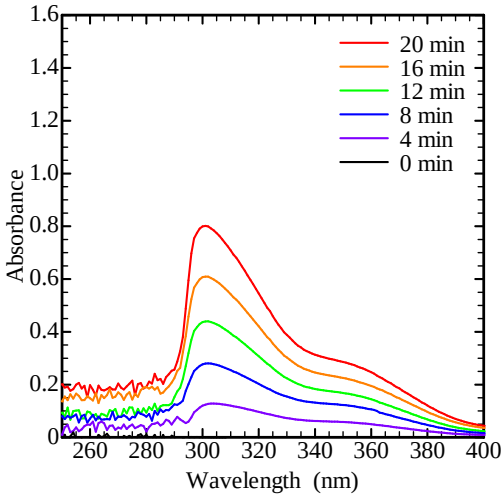

(b) Tap water

Fig. 4-12. Variation in the absorbance of water, when disodium terephthalate is added, using the pulsed power system.

The solutions were treated in the water treatment system with an externally connected ozonizer instead of the nanosecond pulsed power system. Fig. 4-13 shows absorbance spectra of purified water and tap water with NaTA added when the solutions did not include the surfactant.

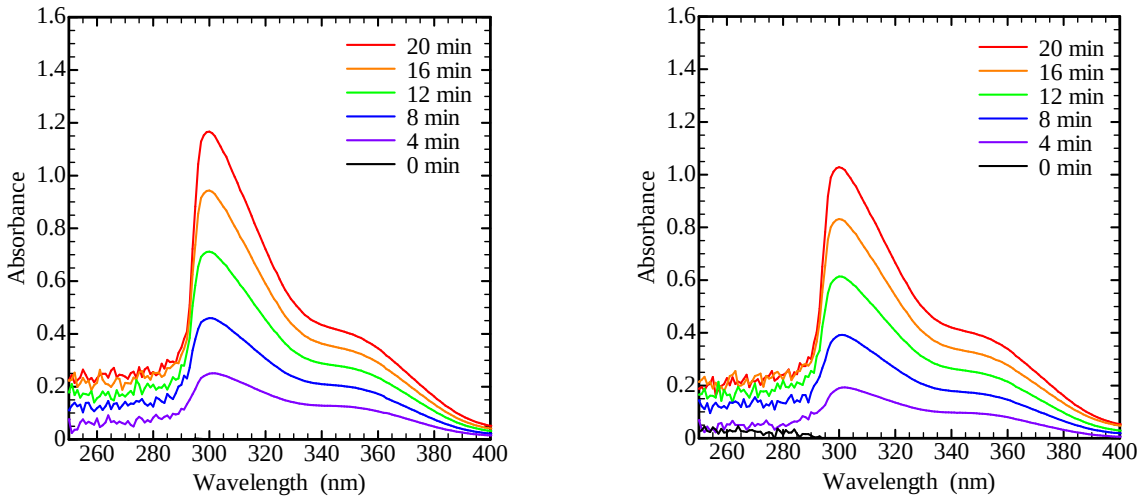

(a) Purified water (b) Tap water

Fig. 4-13. Variation in the absorbance of water, when disodium terephthalate is added, using an external ozonizer.

The absorbance spectrum using the ozonizer in Fig. 4-13(a) was lower than that with the nanosecond pulsed power system in Fig. 4-12(a). It was suggested that electric discharges had some direct effect on water, leading to the generation of more OH radical. On the other hand, using tap water as shown in Figs. 4-12(b) and 4-13(b), the absorbance spectrum with the external ozonizer was higher than that with the pulsed power system. When the pulsed power system was used for water treatment, electric discharges might be affected by impurities in the tap water.

The surfactant solutions were also treated using the external ozonizer. Although OH radical production with the pulsed power system was changed by water quality, the pulsed power system could have a capacity for more OH radical production. The image of foam and temporal variation of the foam height of the surfactant in purified water is shown in Figs. 4-14(a), 4-14(b). The foam was dissolved much slower using the external ozonizer than using the pulsed power system. The surfactant was not sufficiently treated with the ozonizer because less OH radical would be produced. Fig. 4-15 shows the variation in the absorbance spectrum of the surfactant solution in purified water during the ozonizer treatment. The absorbance spectrum during the ozonizer treatment was lower than that during pulsed power discharges treatment shown in Fig. 4-9(a). Because of the lower absorbance spectrum around 200 nm, which would indicate the existence of 4-nonylphenol generated by decomposition of the surfactants, ozonation using the external ozonizer could weakly decompose the surfactants. Moreover, the absorbance spectra at 80 and 120 minutes were approximately the same. It was suggested that there was a limitation in decomposing surfactants by simple ozonation. On the other hand, when the pulsed power system was used for surfactant treatment, ozone could be pushed into the surfactant solution by the ion wind of the electric discharges and bombardment of the streamer heads. More active species such as the OH radical could be generated from ozone in the solution. It would be considered that the electric discharges improved production and reactivity of active species due to UV from electric discharges [4.16], as shown in Eqs. (4.3)–(4.5) [4.17], and electrons formed

by streamer heads, as shown in Eqs. (4.6)–(4.8) [4.18], so that decomposition of organic compounds such as surfactants was promoted.

$$H_2O + h\nu \rightarrow * OH + * H \quad (4.3)$$
$$O_3 + H_2O + h\nu \longrightarrow H_2O_2 + O_2 \quad (4.4)$$
$$H_2O_2 \longrightarrow * OH + * OH \quad (4.5)$$

$$e + H_2O \longrightarrow e + * OH + * H \quad (4.6)$$
$$e + O_2 \longrightarrow e + * O + * O \quad (4.7)$$
$$* O + H_2O \longrightarrow * OH + * OH \quad (4.8)$$

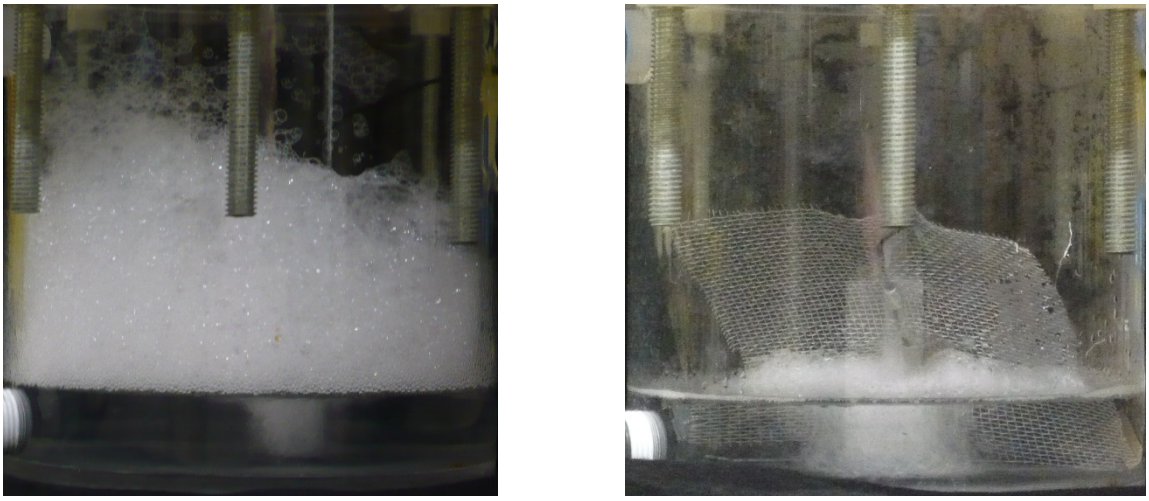

(L) External Ozonizer (R) Pulsed Discharge

(a) Image of foam in the reservoir after 100 minutes' treatment

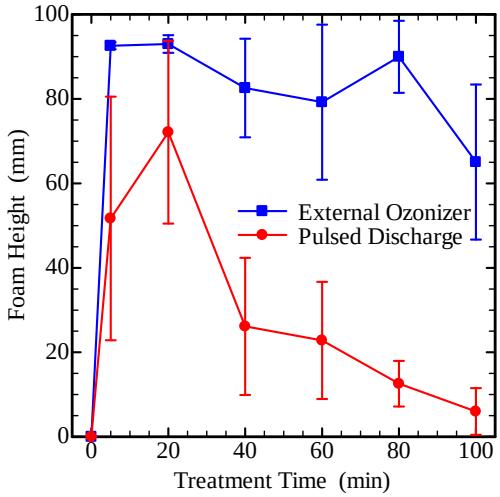

(b) Foaming height

Fig. 4-14. Comparison of foam-height variation of the surfactant in purified water.

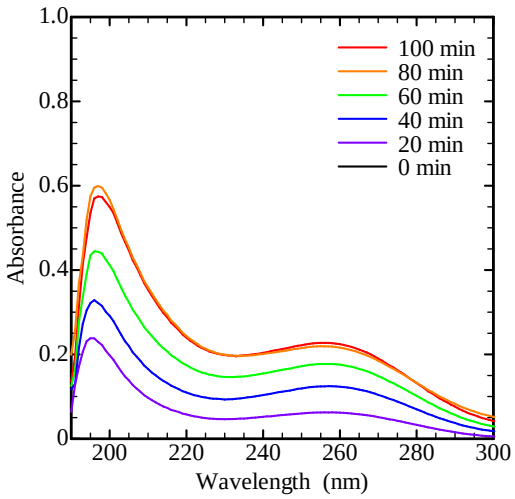

Fig. 4-15. Variation in the absorbance of surfactant treatment with external ozonizer.

4.4. Conclusion of Water Treatment

Indigo carmine in an aqueous solution was treated by the nanosecond pulsed power system. The treatment using oxygen as the working gas was faster than that using nitrogen. It was suggested that active species generated from oxygen such as ozone and OH radical caused stronger decomposition of indigo carmine than those generated from nitrogen such as nitrogen dioxide and nitric acid. Surfactant treatment with nanosecond pulsed power system was also investigated. The surfactant solution in purified water was treated faster than solution in tap water including impurities because the difference in the pH value and the electric conductivity of the solutions could affect the OH radical production. It was suggested that water quality of target solution could not a little influence water treatment. Moreover, the surfactant treatment using nanosecond pulsed power system was compared with using an external ozonizer. The foaming height using the pulsed power system was lower than that using the ozonizer. Then, it would be indicated that the surfactant could not be decomposed sufficiently by only ozone. Although OH radical that is higher oxidation-reduction potential (ORP) than ozone caused stronger decomposition of surfactant, OH radical production using the nanosecond pulsed power system was almost the same as that using the ozonizer. For water treatment with the pulsed power system, when electric discharges were used, the electric discharges would promote chemical reactions between ozone or OH radical and surfactants. In order to promote chemical reactions between more OH radical and target compounds efficiently, the nanosecond pulsed power system should be applied in water treatment.

References-4

[4.1] M. Morimoto, K. Shimizu, K. Teranishi, and N. Shimomura, “Indigo Carmine Solution Treatment by Nanosecond Pulsed Power with a Dielectric Barrier Electrode,” IEEE Transactions on Dielectrics and Electrical Insulation, vol. 22, no. 4, pp. 1872-1878, August, 2015.

[4.2] M. Morimoto, K. Shimizu, K. Teranishi, and N. Shimomura, “Surfactant Treatment Using Nanosecond Pulsed Powers and Action of Electric Discharges on Solution Liquid,” IEEE Transactions on Plasma Science, vol. 44, no. 10, pp. 2167-2172, October, 2016.

[4.3] N. Tabata, “Ozone Generation and Generation Efficiency,” Journal of Plasma and Fusion Research, vol. 74, no. 10, pp. 1119-1126, 1998.

[4.4] F. Fukawa, N. Shimomura, T. Yano, S. Yamanaka, K. Teranishi and H. Akiyama, “Application of Nanosecond Pulsed Power to Ozone Production by Streamer Corona,” IEEE Transactions on Plasma Science, vol. 36, no. 5, pp. 2592-2597, October, 2008.

[4.5] W. J. M. Samaranayake, T. Namihira, S. Katsuki, Y. Miyahara, T. Sakugawa, R. Hackam, and H. Akiyama, “Pulsed Power Production of Ozone Using Nonthermal Gas Discharges,” IEEE electrical insulation magazine, vol. 17, no. 4, pp. 17-25, August, 2001.

[4.6] N. Takamura, T. Matsumoto, D. Wang, T. Namihira, and H. Akiyama, “Ozone Generation Using Positive- and Negative- Nano-Seconds Pulsed Discharges,” IEEE Pulsed Power Conference, pp. 1300-1303, June, 2011.

[4.7] M. Morimoto, K. Kusunoki, H. Nakai, K. Teranishi, and N. Shimomura, “Development of Water Treatment System Using Nanosecond Pulsed Powers to Treat Surfactant,” IEEE Pulsed Power & Plasma Science Conference (PPPS2013), pp. 1765-1769, June, 2013.

[4.8] M. Morimoto, K. Kusunoki, K. Teranishi, and N. Shimomura, “Effect of the Surfactant Treatment Using Nanosecond Pulsed Powers,” IEEE International Power Modulator and High Voltage Conference (IPMHVC2014), pp. 411-414, June, 2014.

[4.9] M. Morimoto, K. Shimizu, K. Teranishi, and N. Shimomura, “Effect of Addition of Hydrogen Peroxide on Surfactant Treatment Using Nanosecond Pulsed Powers,” Euro-Asian Pulsed Power Conference (EAPPC2014), pp. 403-406, September, 2014.

[4.10] V. O.Ajibola, “Recovery of Indigo from a Textile Effluent in Nigeria,” Journal of Scientific & Industrial Research, vol. 60, pp. 735-737, September, 2001.

[4.11] S. Kanazawa, H. Kawano, S. Watanabe, T. Furuki, S. Akamine, R. Ichiki, T. Okubo, M. Kocik, and J. Mizeraczyk, “Observation of OH Radicals Produced by Pulsed Discharges on the Surface of a Liquid,” Plasma Sources Science and Technology, vol. 20, no. 3, April, 2003.

[4.12] K. Matsumoto, M. Ueno, I. Nakanishi, and K. Anzai, “Density of Hydroxyl Radicals Generated in an Aqueous Solution by Irradiating Carbon-Ion Beam,” Chemical and Pharmaceutical Bulletin, vol. 63, no. 3, pp. 195-199, January, 2015.

[4.13] H. Wang and X. Chen, “Kinetic Analysis and Energy Efficiency of Phenol Degradation in a Plasma-Photocatalysis System,” Journal of Hazardous Materials, vol. 186, no. 2-3, pp. 1888-1892, February, 2011.

[4.14] A. T. Sugiarto, T. Ohshima, and M. Sato, “Advanced Oxidation Processes Using Pulsed Streamer Corona Discharge in Water,” Thin Solid Films, vol. 407, no. 1-2, pp. 174-178, March, 2002.

[4.15] B. Sun, N. N. Aye, Z. Gao, D. Lv, X. Zhu, and M. Sato, “Characteristics of Gas-Liquid Pulsed Discharge Plasma Reactor and Dye Decoloration Efficiency,” Journal of Environmental Sciences, vol. 24, no. 5, pp. 840-845, May, 2012.

[4.16] R. Andreozzi, V. Caprio, A. Insola, and R. Marotta, “Advanced Oxidation Processes (AOP) for Water Purification and Recovery,” Catalysis Today, vol. 53, no. 1, pp. 51-59, October, 1999.

[4.17] H. Okabe, “Photochemistry of Small Molecules New York,” NY, USA: Wiley, p. 202, 1978.

[4.18] T. Iijima, R. Makise, and T. Murata, “OH Radical Generator for Waste Water Treatment Containing Recalcitrant Organic Matter,” TOSHIBA review, vol. 61, no. 8, pp. 40-43, 2006. (in Japanese)

5. Ozone Production with Nanosecond Pulsed Power System

5.1. Introduction to the Ozone Production and Reactor [5.1]

In order to carry out water treatment more efficiently, it is important to produce more ozone and OH radical. Because more ozone can result in more OH radical [5.2], ozone production with the nanosecond pulsed power system has also been investigated in recent years. High ozone production efficiency with the nanosecond pulsed power system was obtained because of non-thermal equilibrium plasmas caused by electric discharges, even if a dielectric barrier was not used [5.3–5.5]. Comparing the ozone production efficiency using the different methods, the characteristics map of air-fed ozonizers was presented [5.5].

In a previous study, streamer discharges generated by the nanosecond pulsed power system realized high ozone production efficiency. In order to generate streamer discharges efficiently, a coaxial reactor in experiments was used due to electric field enhancement. However, high ozone concentration was not obtained. This was because ozone concentration decreased after it increased up to the peak concentration. Then, frequent occurrence of spark discharges was observed. In order to clarify this phenomenon, ozone production experiments used a stud bolt and stainless steel wires wound around the glass rod as an inner electrode of the coaxial reactor were performed in order to obtain high density ozone with preventing spark discharges. In these experiments, a stable ozone concentration was obtained, which increased inconsiderably.

In this chapter 5, when a stainless steel wire electrode was used as an inner electrode of the coaxial reactor, the appearances of the inner wire electrode and electric discharges in the coaxial reactor were confirmed using a coaxial reactor which had an aperture on the outer electrode. Moreover, we introduced the coaxial reactor whose inner wire electrode could be tensed. The ozone concentration and the state of electric discharges in the coaxial reactor were also investigated.

Fig. 5-1 shows a schematic diagram of the ozone production system. Nanosecond high-voltage pulses were applied to inner wire electrode of the coaxial reactor.

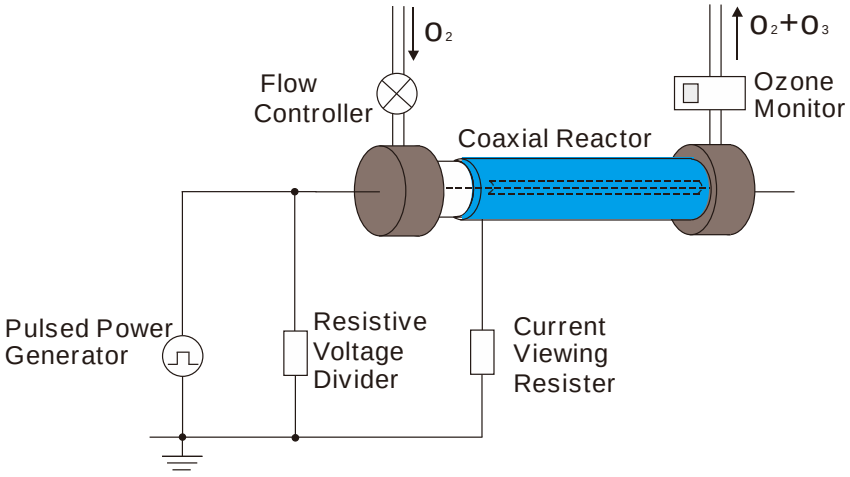

Fig. 5-1. Schematic diagram of the ozone production experiment.

The voltage and current waveforms were measured with a digital oscilloscope (Tektronix, DPO4104, 1 GHz) through a resistive voltage divider (1000:1) in Fig. 3-7 and a current viewing resistor in Fig. 3-8. Oxygen gas (99.95%) was flowed in the reactor at a flow rate of 1.0 L/min. The ozone concentration caused in the coaxial reactor was measured using an ozone monitor with ultraviolet absorption (PG-320A, Ebara, Japan). The charged voltage of the nanosecond pulsed power generator was 3.1 kV. As a pulse repetition rate, 10, 50, and 80 pps (pulses per second) were chosen.

Fig. 5-2 shows a cross-section view of the coaxial reactor. The inner electrode of the coaxial reactor was a stainless steel wire (SUS304) with 1.0 mm diameter. As the outer electrode of the coaxial reactor, a stainless steel pipe was used, whose length and inner diameter were 500 mm and 20 mm, respectively. In order to observe electric discharges occurring inside the coaxial reactor, the reactor had an aperture. The stainless steel pipe had a slit, whose width and height were 450 and 5 mm, respectively. In order to prevent gas leaks, this slit was covered with an acrylic pipe.

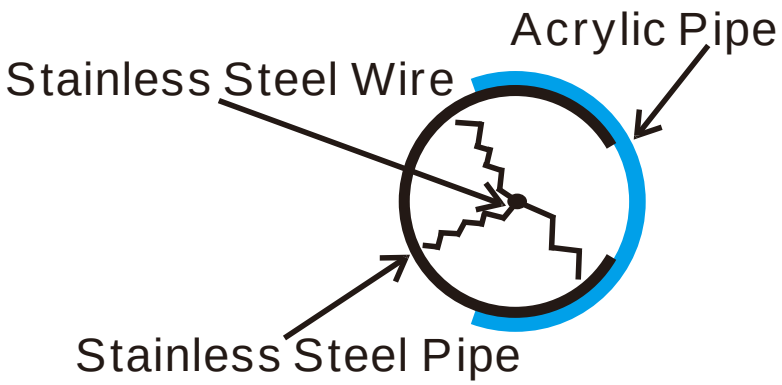

Fig. 5-2. Cross-section view of a reactor with an aperture.

The end cap of the coaxial reactor (Fig. 5-3) was designed and manufactured in order to change the tension of the inner wire electrode. By rotation of a cap part, the inner wire electrode of the coaxial reactor was tensed. When nanosecond high-voltage pulses were applied to the coaxial reactor, streamer discharges occurred and developed from the inner wire electrode to the outer pipe electrode. Ozone molecules were mainly produced by the streamer discharges.

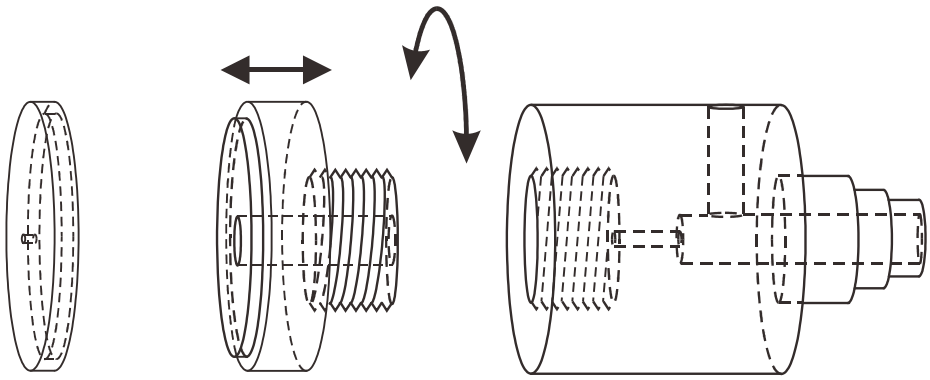

Fig. 5-3. Schematic of the cap unit of the reactor.

5.2. Ozone Production with Coaxial Reactor

Ozone was produced when the cap was adjusted so as not to tense the inner wire electrode. Temporal variations in the ozone concentration at 10, 50, and 80 pps are shown in Fig. 5-4. The ozone concentrations increased from 10 s pulse application. The ozone concentration at 10 pps became constant at 1.0 g/Nm^3 after the initial rising. On the other hand, ozone concentration at 50 and 80 pps reached peak values of 5.2 and 8.3 g/Nm^3, respectively. After the peaking, these ozone concentrations decreased and became approximately constant after 100 s.

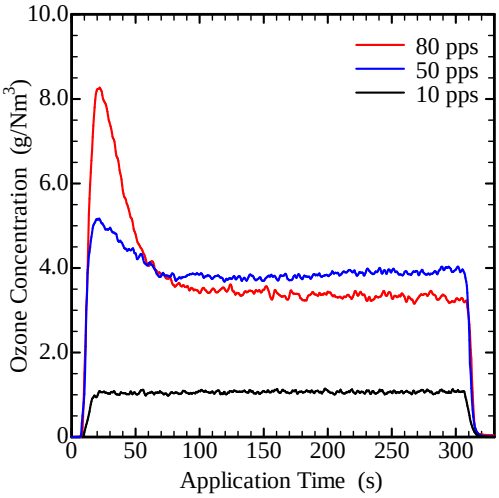

Fig. 5-4. Temporal variations in ozone concentration with non-tensioned inner wire electrode.

Fig. 5-5 shows the voltage and current waveforms observed on the reactor until 20 s from the start of pulse application. Fig. 5-6 shows the voltage and current waveforms measured after 150 s from start of pulse application. As shown in Fig. 5-5(a), the voltage waveform fell down from about 40 ns at 50 pps and from 30 ns at 80 pps.

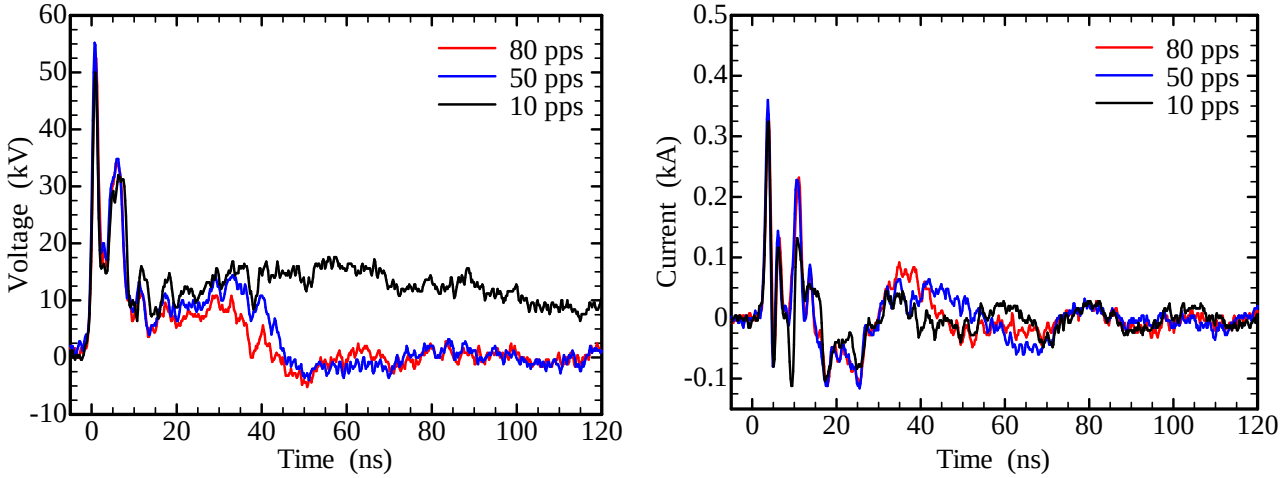

(a) Voltage waveform (b) Current waveform

Fig. 5-5. Voltage and current waveforms before 20 s with non-tensioned inner wire electrode.

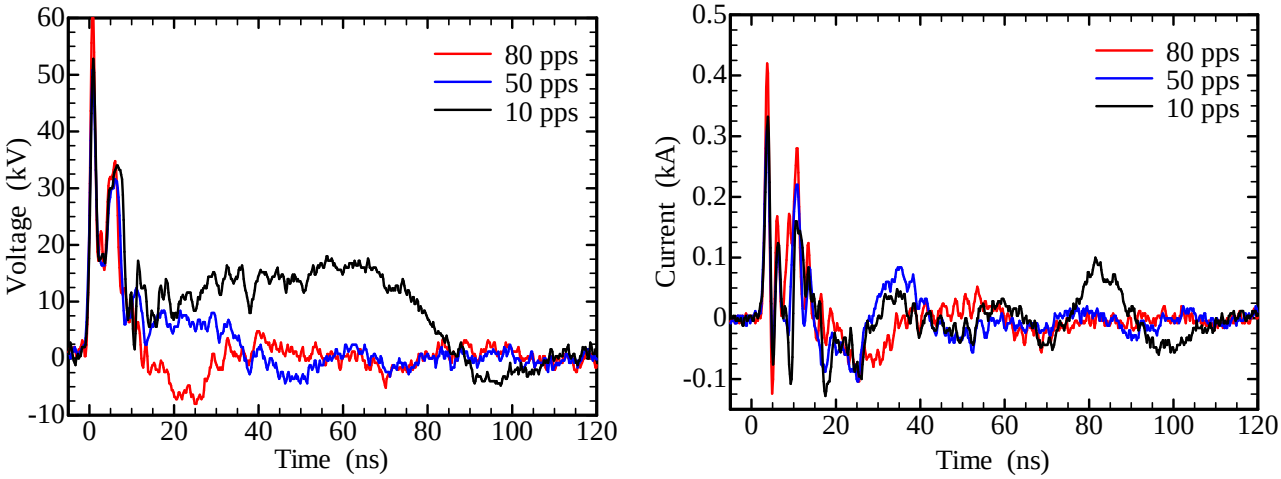

(a) Voltage waveform (b) Current waveform

Fig. 5-6. Voltage and current waveforms after 150 s with non-tensioned inner wire electrode.

The voltage waveforms in Fig. 5-6(a) became different from those in Fig. 5-5(a). In Fig. 5-6(a), the voltage fell to around 75 ns at 10 pps. At 50 and 80 pps, the fall came earlier in comparison with Fig. 5-5(a). In the current waveforms, related symptoms were similarly observed as seen in Figs. 5-5(b) and 5-6(b). It was suggested that spark discharges occurred earlier with increasing pulse repetition rate and duration time of pulses application.

Fig. 5-7 shows photographs of the inside of the coaxial reactor with electric discharge using a non-tensioned inner wire electrode, when the pulse repetition rate was 10, 50, and 80 pps. All photographs were taken around the center of the reactor and after 150 s from the start of the pulse application. Note that a broken line was drawn on the inner wire electrode to distinguish its position. With increasing pulse repetition rate, the incidence of the spark discharges increased and the locations where spark discharges occurred moved toward the center of the coaxial reactor. At the same time, the center of the inner wire electrode moved to the lower side of the reactor (Fig. 5-7). Because the wire was fixed at both end caps of the coaxial reactor, the inner wire electrode was curved at 50 and 80 pps. In the photographs, spark discharges occurred in the lower side of the inner wire electrode. The wire would be attracted to the lower side with spark discharges, and the separation between inner and outer electrodes around the area became shorter because of the curving of the inner wire electrode. These phenomena were more obvious at higher pulse repetition rates. At the center of the coaxial reactor, the downward displacement of the stainless steel wire used as an inner wire electrode from the initial position was estimated at 2.72 mm in Fig. 5-7(c). The stainless steel wire gradually returned with time after the end of the pulse application.

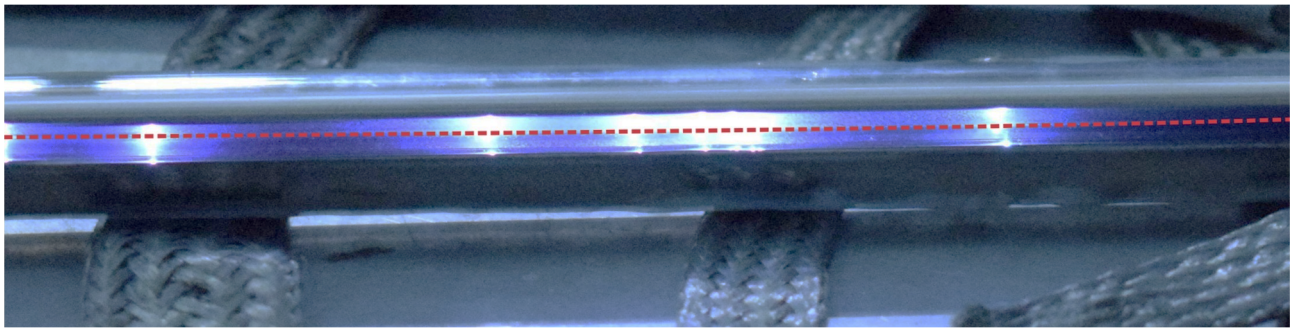

(a) 10 pps

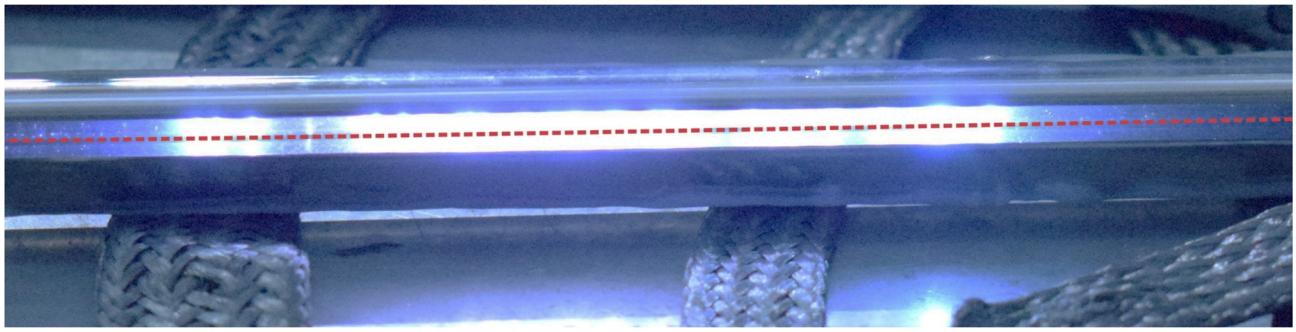

(b) 50 pps

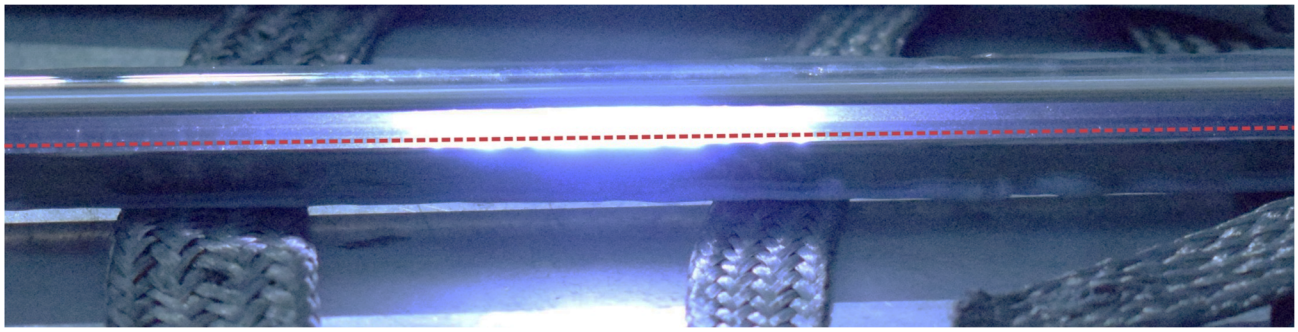

(c) 80 pps

Fig. 5-7. Photographs of the electric discharges with non-tensioned inner wire electrode.

Although the temperature of the inner wire electrode was measured using a radiation thermometer, it could not be measured exactly because the wire electrode was thin and the temperature elevation was slight. A gas temperature measurement at the inside of the reactor showed an increasing temperature from 296 to 298 K during pulse application. Here the stainless steel wire temperature was assumed the same as the gas temperature. The average thermal expansion coefficient of SUS304 used in the wire was 17.3×10^{-6} /K at 273–373 K. The 2 K temperature rise of the 500-mm stainless steel wire lengthens the stainless steel wire by 0.0173 mm. When the stainless steel wire was elongated to become an obtuse isosceles triangle, since the wire was fixated at both ends on the reactor caps, the displacement of the wire center was evaluated at 2.08 mm. The calculated displacement (2.08 mm) of the wire roughly corresponded to the downward displacement (2.72 mm) estimated in Fig. 5-7(c). The center would move to the lower side by gravity and several electric forces caused by

spark discharges. At that time, spark discharges occurred more frequently around where the distance between the inner and outer electrodes became smaller. Thus, the reduction of ozone concentration after 20 s was caused by temporal and spatial restriction of both the spark-discharge occurrence and the inner wire curving. Moreover, when the frequency of the spark discharges increased with increasing the pulse repetition rate, the temperature of the stainless steel wire would increase higher. Then, because the wire moved further down, the distance between the inner and outer electrodes was smaller. Therefore, because formation of spark discharges would require less time for the distance to become smaller, the spark discharges occurred earlier. As shown in Figs. 5-5 and 5-6, these phenomena changed the voltage and current waveforms. The propagation velocity of the streamer discharge was roughly 1 mm/ns, when the voltage was 40 kV [5.6]. In this experiment, although streamer discharges would propagate at 1 mm/ns for a 1.5 ns pulse, the propagation velocity would be less than 1.0 mm/ns for sustaining 10 kV after the pulse. Thus, it would take much more than 10 ns until the streamer discharges reached the outer electrode from the inner electrode because the between the electrodes was 9.5 mm. Although ozone would be produced when the streamer discharges were propagating, the occurrence of spark discharges stopped the propagation of the streamer discharges and the increase of ozone production. Therefore, as seen in Fig. 5-4, the earlier occurrence of spark discharges reduced the ozone concentration. In addition, ozone could be pyrolyzed by the spark discharges. Accordingly, it would be suggested that stable ozone concentration using coaxial reactor could be obtained by preventing occurrence of the spark discharge caused by the curving of the inner wire electrode. Next, ozone production with a tensed inner wire electrode of the same reactor was tested.

5.3. Ozone Production Using Tensed Inner Wire Electrode

A certain degree of tension was given to the inner wire electrode by adjusting the cap unit (Fig. 5-3). Fig. 5-8 shows the temporal variations in the ozone concentration at 10, 50, and 80 pps using a tensed inner wire electrode. The ozone concentrations were approximately constant at 1.0, 4.6, and 7.9 g/ Nm^3 for 10, 50, and 80 pps, respectively. The peaking and decrease of the ozone concentration as shown in Fig. 5-4 were not observed in Fig. 5-8.

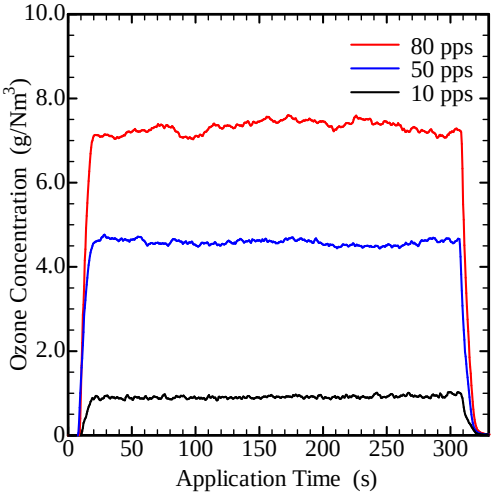

Fig. 5-8. Temporal changes in the ozone concentration using a tensed inner wire electrode.

Fig. 5-9 shows the voltage and current waveforms observed until 20 s from the start of the pulse application. Fig. 5-10 also shows the voltage and current waveforms measured after 150 s from the start of the pulse application.

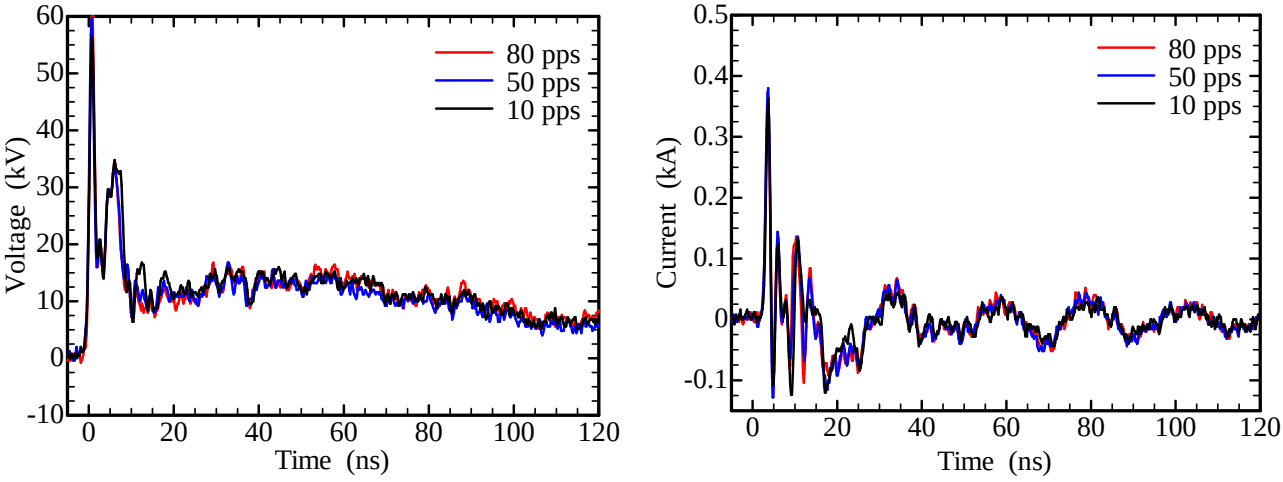

(a) Voltage waveform (b) Current waveform

Fig. 5-9. Voltage and current waveforms before 20 s using a tensioned inner wire electrode.

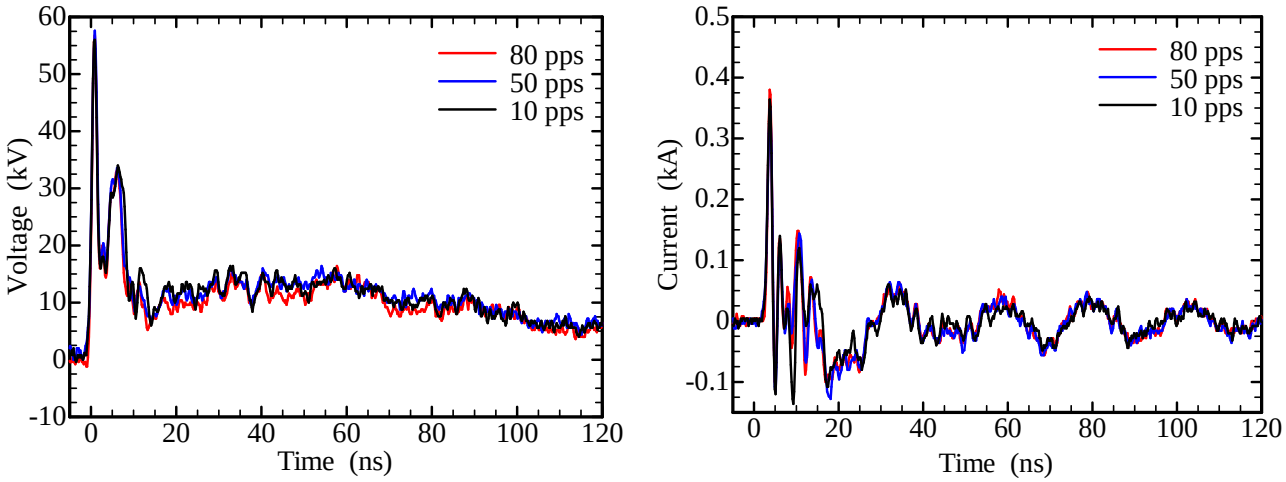

(a) Voltage waveform (b) Current waveform

Fig. 5-10. Voltage and current waveforms after 150 s using a tensioned inner wire electrode.

The voltage abrupt drops as seen in Figs. 5-5(a) and 5-6(a) were not observed regardless of the pulse repetition rate in Figs. 5-9(a) and 5-10(a). All voltage waveforms in Figs. 5-9(a) and 5-10(a) nearly corresponded to each other. The current waveforms were the same way as the voltage waveforms. That is to say, using the tensed inner wire electrode, the voltage and current waveforms were independent of the pulse repetition rate and the duration of pulse application under these experimental conditions. Moreover, these voltage and current waveforms were similar to those at 10 pps using a non-tensioned inner wire electrode (Fig. 5-5).

Fig. 5-11 shows photographs of the electric discharges in the coaxial reactor at 10, 50, and 80 pps using a tensioned inner wire electrode. The position of the window edges and the inner wire electrode was described by solid lines and a broken line, respectively.

Not the spark discharges but the streamer discharges were observed in all photographs. In the photographs at 10 pps (Fig. 5-11(a)), the streamer discharges were difficult to be distinguished owing to weak emission, even after image processing. Because a stainless steel wire was approximately parallel to the window edge and did not move up and down in Fig. 5-11, adoption of the tensioned inner wire electrode prevented the curving of the inner wire electrode and controlled the spark discharges. As a result, the ozone concentration did not drop during pulse application regardless of the pulse repetition rate and the duration of the pulse application.

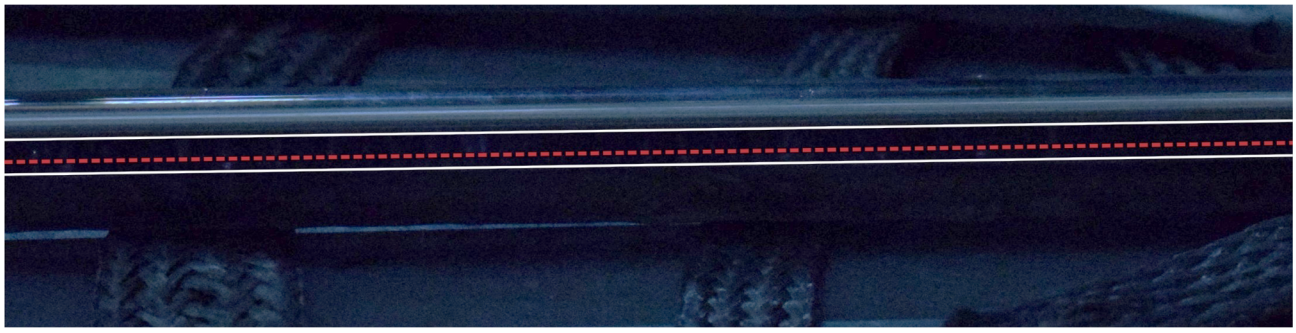

(a) 10 pps

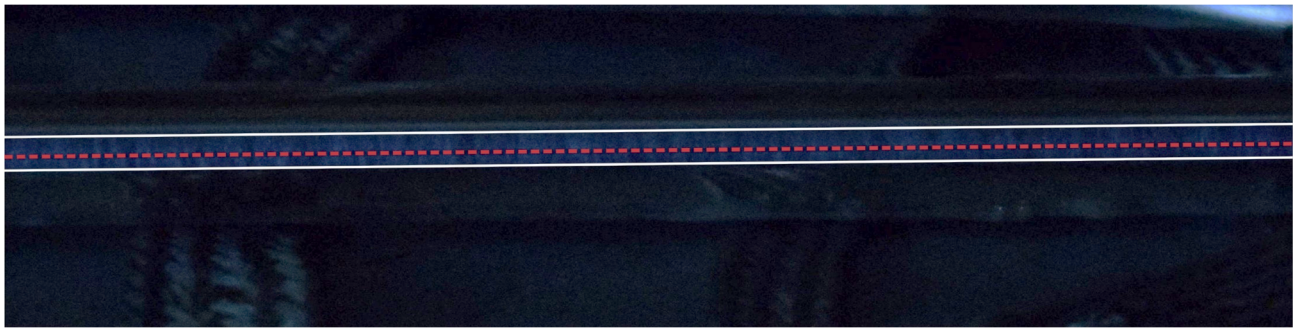

(b) 50 pps

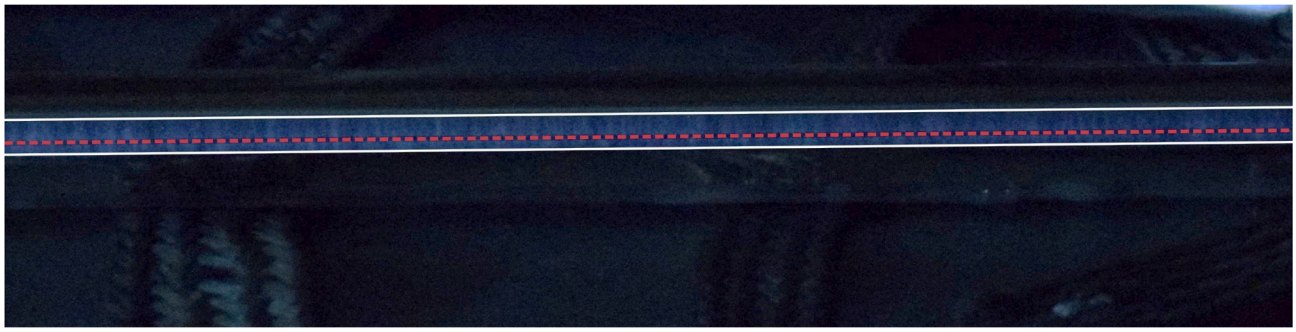

(c) 80 pps

Fig. 5-11. Photograph of the electric discharges using a tensioned inner wire electrode.

Figs. 5-12 and 5-13 show the ozone concentration and the ozone production efficiencies using the coaxial reactor with and without tension on the inner wire electrode, respectively. For the average ozone concentrations, constant ozone concentrations after 150 s in Figs. 5-4 and 5-8 were used. The ozone production efficiency was calculated based on the average ozone concentration and not the discharge energy but the system energy as the charging energy in the initial storage capacitor. Using a non-tensed-wire reactor, the ozone concentration decreased after increasing, as the pulse repetition rate increased. On the other hand, using a tensed-wire reactor, the ozone concentration increased linearly with increasing pulse repetition rate. As a result of using a tensed wire electrode, it was considered that the temporal decrease in the ozone concentration was prevented because the spark discharges were controlled. This had been predicted in a previous work [5.7, 5.8]. Interestingly, the peak ozone concentrations using the no-tensed reactor (Fig. 5-4) were higher than the steady ozone

concentrations using the tensed-wire reactor (Fig. 5-8) but the reason for this remains unclear. Using the no-tensed-wire reactor, the ozone production efficiency decreased with increasing pulse repetition rate; the ozone production efficiency decreased with increasing ozone concentration. This trade-off is a usual trend in ozone production. On the other hand, using the tensed-wire reactor, the production efficiency was roughly constant regardless of the pulse repetition rate and the produced ozone concentration. Therefore, it became clear that occurrence of spark discharges degraded the potential of the coaxial reactor. In addition, the existence of an aperture also degraded the potential for ozone production of the coaxial reactor in this experiment.

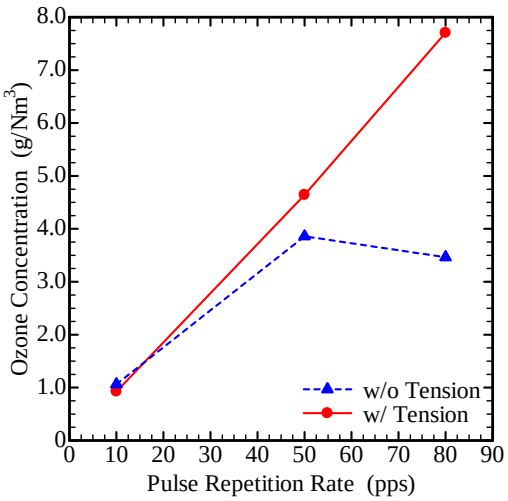

Fig. 5-12. Ozone concentration when tension was applied and not applied on the inner wire electrode.

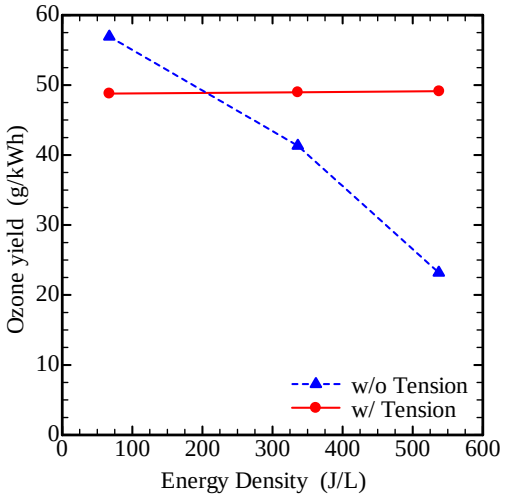

Fig. 5-13. Ozone production efficiency (system efficiency).

5.4. Conclusion of Ozone Production

In order to produce more ozone in the coaxial reactor, the nanosecond pulsed power system was used. However, spark discharges occurred in the coaxial reactor because the separation between inner and outer electrodes became shorter due to the presence of a curving inner wire electrode. Especially, inner wire electrode of the coaxial reactor was curving at high pulse repetition rate. In order to prevent the curving of the inner wire electrode, tensing the inner wire electrode using the structure of the coaxial reactor was proposed. As a result, the ozone concentration was not reduced and became approximately steady after increasing, since curving the inner wire electrode resulted in restraining of the spark discharges. Moreover, the ozone production efficiencies were constant regardless of the increasing pulse repetition rate. It was found that a high ozone concentration could be obtained using a stable streamer discharge.

References-5

[5.1] M. Morimoto, T. Ninomiya, T. Ikemoto, K. Teranishi, and N. Shimomura, “Ozone Production by Streamer Discharges Using Nanosecond Pulsed Powers and Coaxial Reactor with Tensioned Inner Electrode,” IEEE Transactions on Plasma Science, vol. 44, no. 10, pp. 2190-2195, October, 2016.

[5.2] T. Iijima, R. Makise, and T. Murata, “OH Radical Generator for Waste Water Treatment Containing Recalcitrant Organic Matter,” TOSHIBA review, vol. 61, no. 8, pp. 40-43, 2006. (in Japanese)

[5.3] H. Akiyama, T. Sakugawa, T. Namihira, K. Takaki, Y. Minamitani, and N. Shimomura, “Industrial Applications of Pulsed Power Technology,” IEEE Transactions on Dielectrics and Electrical Insulation, vol. 14, no. 5, pp. 1051-1064, October, 2007.

[5.4] N. Takamura, T. Matsumoto, D. Wang, T. Namihira, and H. Akiyama, “Ozone Generation Using Positive- and Negative- Nanosecond Pulsed Discharges,” IEEE Pulsed Power Conference, pp. 1300-1303, June, 2011.

[5.5] D. Wang, T. Namihira, and H. Akiyama, “Pulsed Discharge Plasma Generated by Nano-Seconds Pulsed Power in Atmospheric Air,” IEEE Pulsed Power Conference, pp. 1046-1049, July, 2009.

[5.6] D. Wang, M. Jikuya, S. Yoshida, and T. Namihira, “Positive- Negative-Pulsed Streamer Discharges Generated by a 100-ns Pulsed-Power in Atmospheric Air,” IEEE Transactions on Plasma Science, vol. 35, no. 4, pp. 1091-1094, August, 2007.

[5.7] Y. Nakata, R. Mabuchi, K. Teranishi, and N. Shimomura, “Investigation of Spark Discharge Control in Coaxial Reactors to Dense Ozone Using Nanosecond Pulsed Powers,” IEEE Pulsed Power Conference, pp. 1760-1764, June, 2013.

[5.8] Y. Nakata, R. Mabuchi, K. Teranishi, and N. Shimomura, “Effect of Small-Diameter Coaxial Reactors on Ozone Production Using Nanosecond Pulsed Power,” IEEE Transactions on Dielectrics and Electrical Insulation, vol. 20, no. 4, pp. 1146-1152, August, 2013.

6. NOx Treatment with Nanosecond Pulsed Power System

6.1. Introduction to the NOx Treatment and Reactor [6.1]

In chapter 5, the ozone concentration could be stabilized by applying tension to the inner wire electrode of the coaxial reactor. In the treatment of NOx which are atmosphere pollutants, it was suggested that increase of the NOx removal ratio was expected using the tensed inner wire electrode. As an effective method of NOx decomposition, the pulsed power technologies have also been used [6.2–6.4]. In order to induce a plasma chemical reaction that would lead to the effective NOx decomposition, electric discharges such as streamer discharges were needed. In order to achieve high NOx removal efficiency, the nanosecond pulsed power system has been applied to the NOx treatment using a coaxial reactor [6.5, 6.6]. Although NOx treatment with the pulsed power system was studied, high density of streamer discharges was rarely used. In order to obtain high density of the streamer discharges, the nanosecond pulsed power system with a thin coaxial reactor was applied for NOx treatment [6.7, 6.8]. However, during NOx treatment, occurrence of spark discharges was also observed frequently with the curving inner wire electrode in the coaxial reactor [6.8]. The dependence of the curving inner wire electrode on NOx removal ratio was discussed. Moreover, in order to prevent curving stainless steel wire used as the inner wire electrode of the coaxial reactor, an inner wire electrode tensed by a spring was introduced into the coaxial reactor for NOx treatment with the nanosecond pulsed power system. At that time, the phenomena in the reactor and their effects on the NOx removal ratio were also considered.

Fig. 6-1 shows a schematic of a coaxial reactor, which has an aperture for NOx treatment.

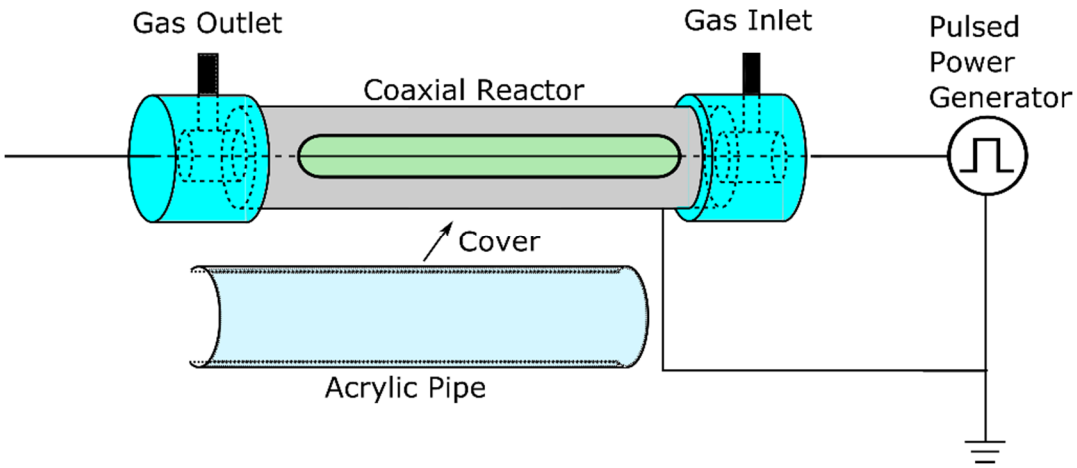

Fig. 6-1. Schematic of a coaxial reactor with an aperture for NOx treatment.

The coaxial reactor was connected to the nanosecond pulsed power generator as shown in Fig. 2-1. Nanosecond voltage pulses were applied on inner wire electrode of the coaxial reactor. A 1-mm diameter stainless steel wire was used as the inner wire electrode of the coaxial reactor. A stainless steel pipe, whose inner diameter and length were 14 and 500 mm, respectively, was used as the outer electrode of the coaxial reactor.

Fig. 6-2 shows a cross-section view of the coaxial reactor. The stainless steel pipe has an aperture

for observing the inside of the coaxial reactor. The aperture was covered with a partly cut-out acrylic pipe in order to prevent leakage of gases such as NO and NO_2 gases.

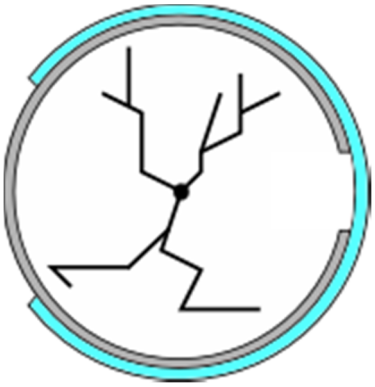

Fig. 6-2. Cross-sectional view of the coaxial reactor.

In order to tense the inner wire electrode of coaxial reactor, another coaxial reactor was prepared. The coaxial reactor configuration, apart from the end cap of the one side, was same as that of the reactor shown in Fig. 6-1. The end-cap structure of the coaxial reactor is shown in Fig. 6-3. When the end cap of the coaxial reactor as shown in Fig. 5-3 was used, because the end-cap part had to be turned before pulsed application, the end cap could not respond to thermal expansion of inner wire electrode during pulsed application, so that there would be a possibility that the curving inner wire electrode of coaxial reactor was obtained. The inner wire electrode of the coaxial reactor was tensed by using a spring made of stainless steel in the end cap, and the elastic force of the spring could be adjusted by inserting spacers. The constant and natural length of the spring were 0.833 N/mm and 17 mm, respectively.

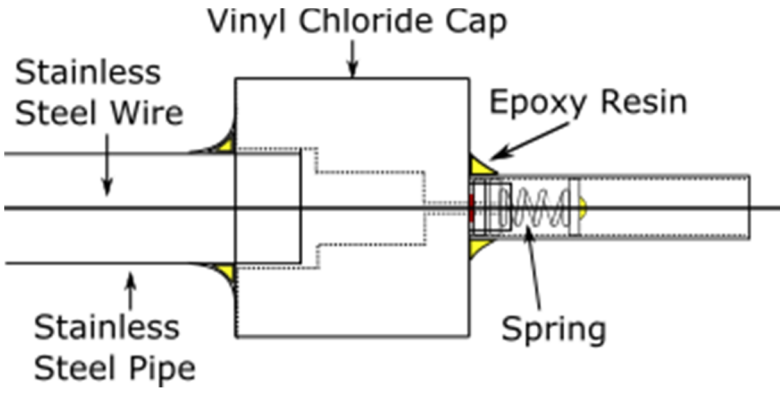

Fig. 6-3. End-cap structure of the reactor.

When nanosecond high-voltage pulses were applied to inner wire electrode of the coaxial reactors, streamer discharges occurred in the coaxial reactor and developed from the inner wire electrode to the outer electrode. The initial charging voltage of C_1 in Fig. 2-1 was 3.1 kV. The voltage and current waveforms were measured by using a digital oscilloscope (Tektronix, DPO4104, 1 GHz) through a resistive voltage divider (1000:1) in Fig. 3-7 and a current viewing resistor in Fig. 3-8. The pulse

repetition rate was changed between 10 and 50 pps (pulses per second) and the pulse application time was 300 seconds (5 min). A simulated gas compound of NO and N_2 was flowed in the coaxial reactor at a flow rate of 2.0 L/min and in 100 ppm. The concentrations of NO and NOx in the treated gas through the coaxial reactor were measured with a flue gas analyzer (HT-2300, HODAKA). The concentration of NOx was calculated as the sum of the NO and NO_2 concentrations.

6.2. NOx Removal and Electric Discharges inside the Coaxial Reactor

Figs. 6-4(a) and 6-4(b) show the temporal variations of the NO and NOx removal ratios during NOx treatment. Note that the NO and NOx removal ratios were somewhat decreased because the coaxial-reactor potential was lowered due to the presence of the acrylic aperture used in order to observe inside the coaxial reactor. The both NO and NOx removal ratios increased from 10 s and reached a peak around 30 s. Afterward, they decreased slightly at 10 pps. After 80 s, they became constant.

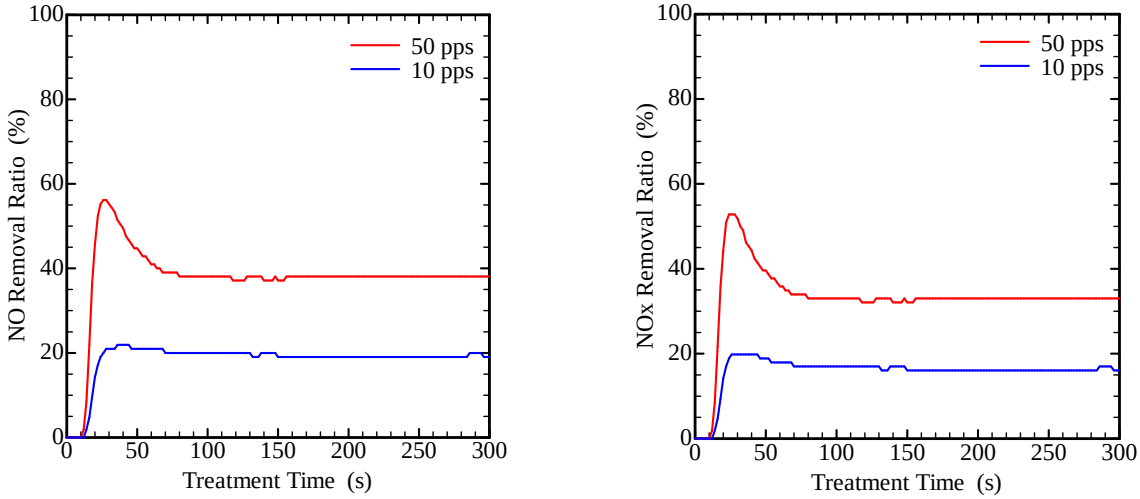

(a) NO (b) NOx

Fig. 6-4. Temporal variation of the NO and NOx removal ratios during NOx treatment.

The coaxial reactor voltage and current waveforms before 20 s and after 150 s from the start of the pulse application at 10 and 50 pps are shown in Figs. 6-5 and 6-6, respectively.

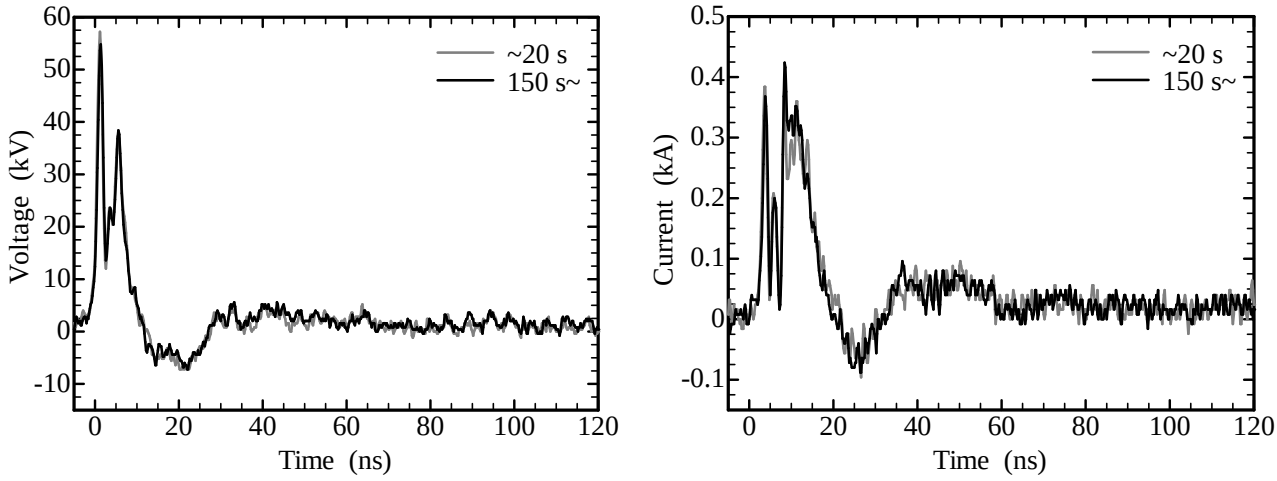

(a) Voltage waveform (b) Current waveform

Fig. 6-5. Typical voltage and current waveforms at 10 pps.

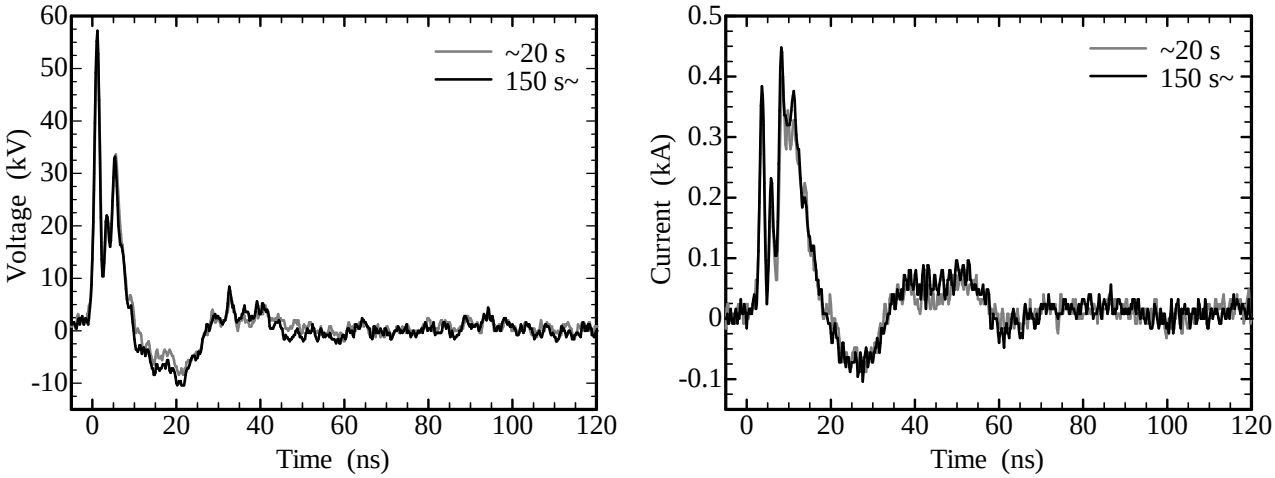

(a) Voltage waveform (b) Current waveform

Fig. 6-6. Typical voltage and current waveforms at 50 pps.

All waveforms were roughly the same. However, the second peak of the current waveforms before 20 s in Fig. 6-5(b) was smaller than those after 150 s in Fig. 6-6(b). Although the second peak of the current waveforms should be affected by spark discharges, other electric discharges such as glow-like discharges might affect it as well.

In order to investigate those phenomena, electric discharges in coaxial reactor were considered based on photographs taken during NOx treatment. At 10 and 50 pps, Figs. 6-7 and 6-8 show images of the inside of the coaxial reactor. The position of the window edges and the inner wire electrode were described by solid lines and a broken line, respectively. The coaxial reactors in the photographs corresponded to 5 cm of the reactor center. Intense spark discharges and weak streamer discharges in the coaxial reactor were observed. The spark discharges occurred around the center of the coaxial reactor. Using the position of the inner wire electrode at 0 s (Figs. 6-7(a) and 6-8(a)) as the initially fixed position, the inner wire electrode of the coaxial reactor moved from the initially fixed position to the outer electrode with increasing NOx treatment time. It seems that the observed spark discharges attracted the inner wire electrode. When the curving inner wire electrode occurred, the distance between inner and outer electrodes was shorter, so that occurrence of spark discharges would be more frequent. In Figs. 6-7 and 6-8, the distance between the electrodes at 120 s and 50 pps was the smallest. Then, streamer discharges between the electrodes were distributed lopsidedly.

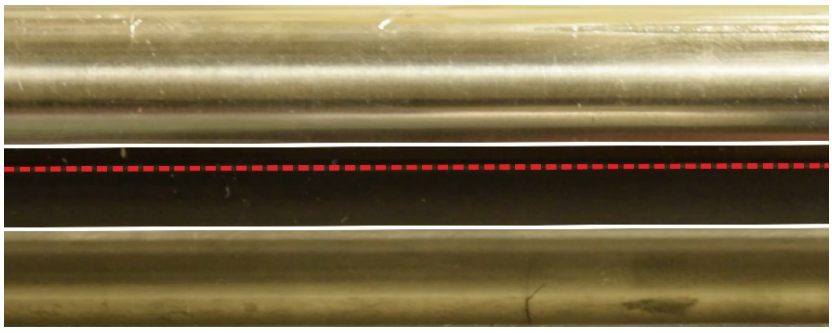

(a) 0 s

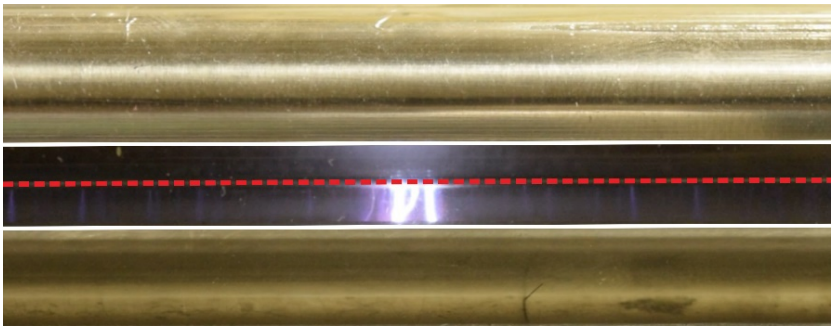

(b) 30 s

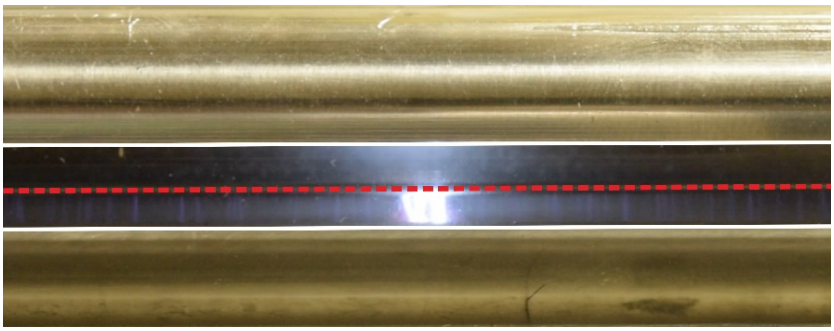

(c) 60 s

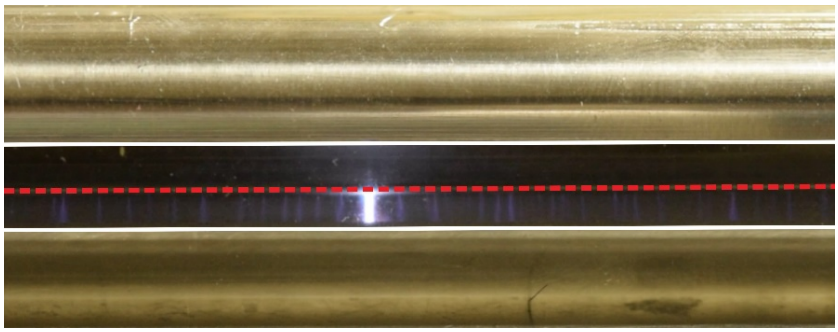

(d) 120 s

Fig. 6-7. Images of the inside of the coaxial reactor at 10 pps.

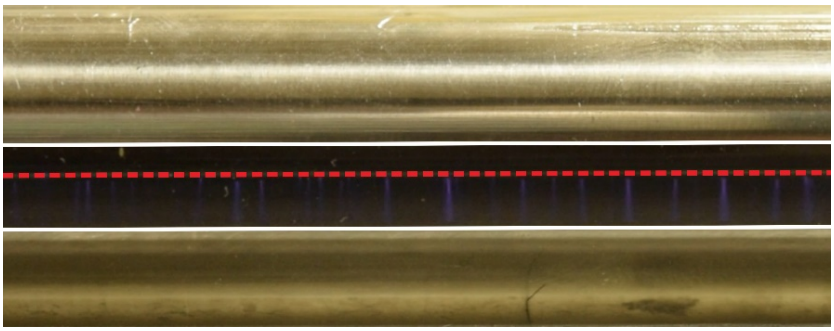

(a) 0 s

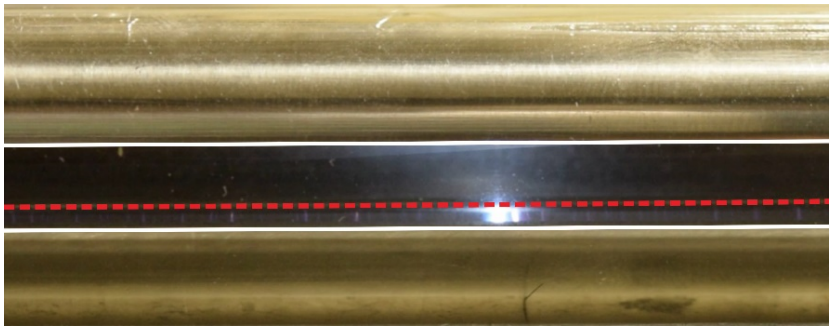

(b) 30 s

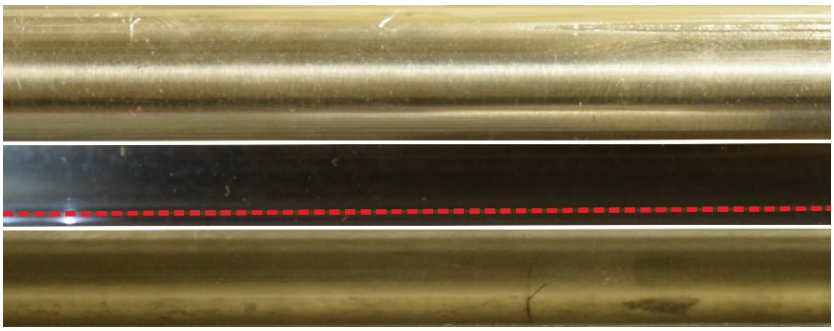

(c) 60 s

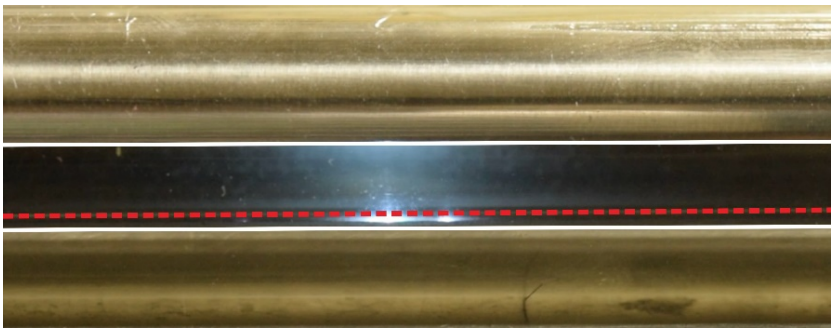

(d) 120 s

Fig. 6-8. Images of the inside of the coaxial reactor at 50 pps.

In addition, it was also thought that the stainless-steel-wire temperature rose because of the occurrence of spark discharges. In an ozone production experiment, 2 K of gas temperature rise was observed during pulse application with experimental setup and a similar coaxial reactor. It was supposed that the temperature of the inner wire electrode rose to 2 K or higher in experiment of NOx treatment. If the stainless-steel-wire temperature increased by 2 K, the length of the 500-mm stainless steel wire should increase for approximately 0.02 mm due to thermal expansion. Then, the displacement of the inner wire electrode from the center position of the coaxial reactor could be roughly evaluated at 2.1 mm, which almost corresponded to the photograph in Fig. 6-8(d). The center of the coaxial reactor would move to the lower side due to gravity and several electric forces of the spark discharges. Then, the spark discharges occurred more frequently where the distance between inner and outer electrodes decreased. Moreover, when the occurrence of the spark discharges increased with increasing pulse repetition rate, the stainless-steel-wire temperature increased further, and the center of the wire shifted toward the outer pipe electrode. Therefore, because spark discharges would spend less time for the smaller distance between the inner and outer electrodes, the spark discharges occurred earlier, so that the volume of the streamer discharges, which could decompose NO and NOx, was decreased. In order to understand these phenomena, time-resolved photographs and optical signal from the spark discharges should be measured.

6.3. NOx Removal Using Reactor Tensed Inner Wire Electrode

In order to prevent the curving inner wire electrode of coaxial reactor, it was tensed by the spring as shown in Fig. 6-3. Figs. 6-9(a) and 6-9(b) show the temporal variations in the NO and NOx removal ratios with increasing NOx treatment time. The NO removal ratio was stable after the introductory increase for both pulse repetition rates. The NOx removal ratio at 50 pps slightly decreased after it increased. Incidentally, when the coaxial reactor using the spring was used but the spring was a natural length at the beginning of NOx treatment, apparent temporal decrease of removal ratio, as shown in Figs. 6-4(a) and 6-4(b), was not observed even at 50 pps. However, the steady NO removal ratio was lower by 4% on 10 pps and 8% on 50 pps than that tensed by a spring. The NO and NO_2 decomposition rate were 3.1×10^{-17} and 9.0×10^{-44} s^{-1}, respectively [6.2]. Therefore, it was assumed that NO_2 was generated after NO decomposition. Then, the NOx removal ratio decreased after increase. By comparing Figs. 6-4(a) and 6-4(b), steadier and higher NO and NOx removal ratios were measured. The NO removal efficiencies on electric-discharge energy were calculated from voltage and current waveforms. When no-tensed inner wire electrode was used for NOx treatment, the NO removal efficiency at 10 and 50 pps was 0.20 (from 100 to 80 ppm of the NO concentration in Fig. 6-4(a)) and 0.10 mol/kWh (from 100 to 62 ppm of NO concentration in Fig. 6-4(a)), respectively. On the other hand, when inner wire electrode tensed by the spring was used, at 10 and 50 pps, the NO removal efficiency was 0.35 (from 100 to 75 ppm of NO concentration in Fig. 6-9(a)) and 0.20 mol/kWh (from 100 to 25 ppm of NO concentration in Fig. 6-9(a)), respectively. Moreover, when the inner wire electrode tensed without an aperture was used for NOx treatment, at 50 pps, the NO removal efficiency was 0.39 mol/kWh (from 100 to 5 ppm of the NO concentration). Although the aperture was used for observing the phenomena inside the coaxial reactor, it decreased the coaxial reactor's performance.

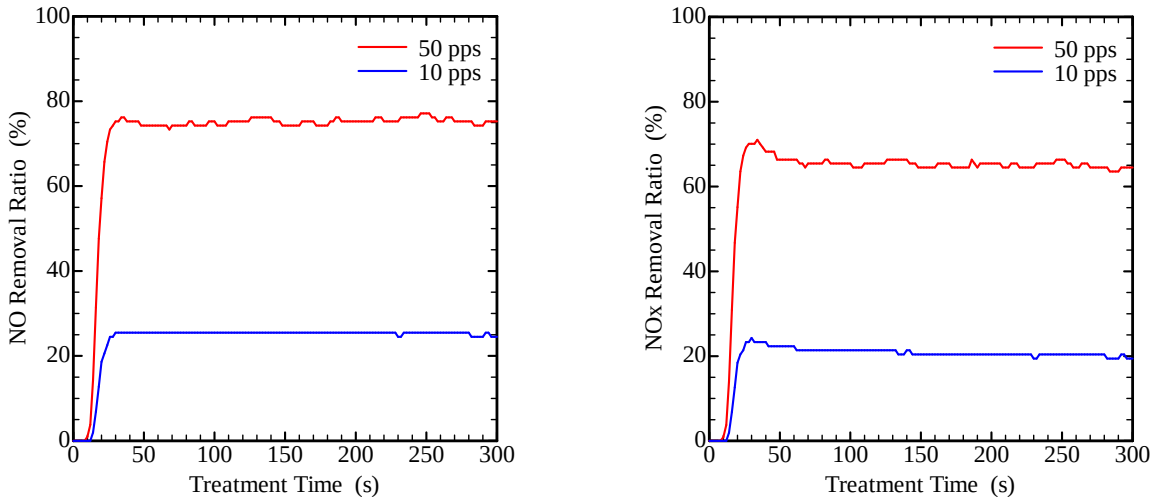

(a) NO (b) NOx

Fig. 6-9. Temporal variations in the NO and NOx removal ratios during NOx treatment.

Using inner wire electrode of the coaxial reactor tensed by a spring, Figs. 6-10(a) and 6-10(b) shows the voltage and current waveforms of the coaxial reactor observed after 150 s. The voltage waveforms were almost the same as those in Figs. 6-5(a) and 6-6(a). However, the second peaks of the current waveforms were smaller than those in Figs. 6-5(b) and 6-6(b). It was suggested that because the inner wire electrode was tensed by using the spring in order to prevent occurrence of spark discharges, the current flowed by only streamer discharges.

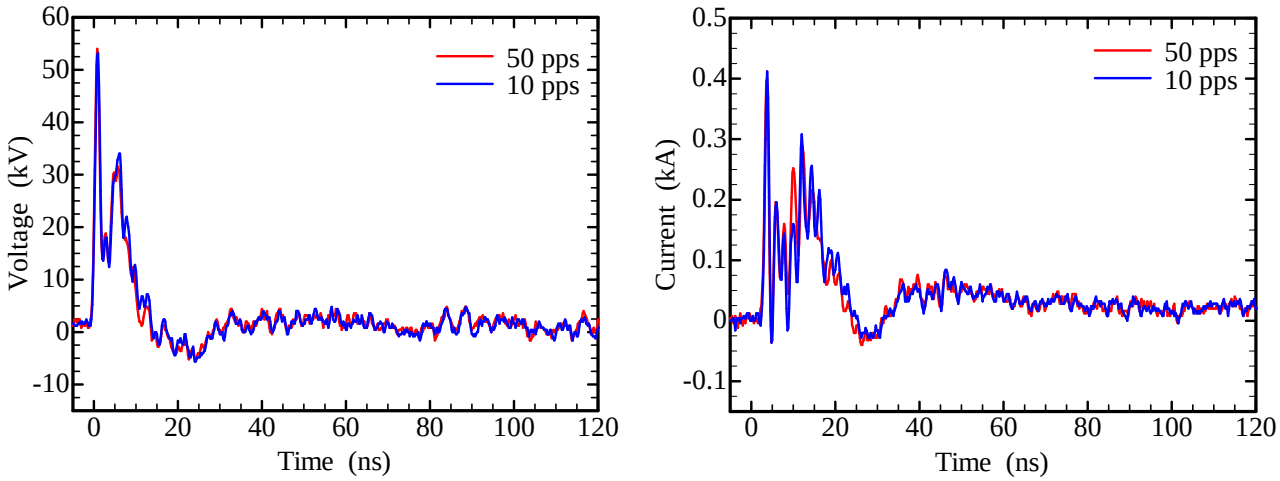

(a) Voltage Waveform (b) Current waveform

Fig. 6-10. Typical voltage and current waveforms after 150 s.

The appearance of electric discharges inside the coaxial reactor using the tensed inner wire electrode at 50 pps is shown in Fig. 6-11. Spark discharges were not observed in this photograph. Then, the inner wire electrode was not curved. Moreover, streamer discharges were observed in the entire observational area of the coaxial reactor. It was thought that the second peaks of the current waveforms were caused by the occurrence of spark discharges because the second peak of the current waveform as shown in Fig. 6-10(b) decreased preventing the spark-discharges occurrence. By the spark discharges, streamer discharges could be affected. It was considered that the decrease of the NO removal ratio with increasing NOx treatment time as shown in Fig. 6-4(a) was caused by decreasing the volume of streamer discharges. Consequently, using the nanosecond pulsed power system, in order to achieve high NOx removal ratio and removal efficiency, the introduction of the tensed inner wire electrode inside the coaxial reactor effectively prevents spark discharges.

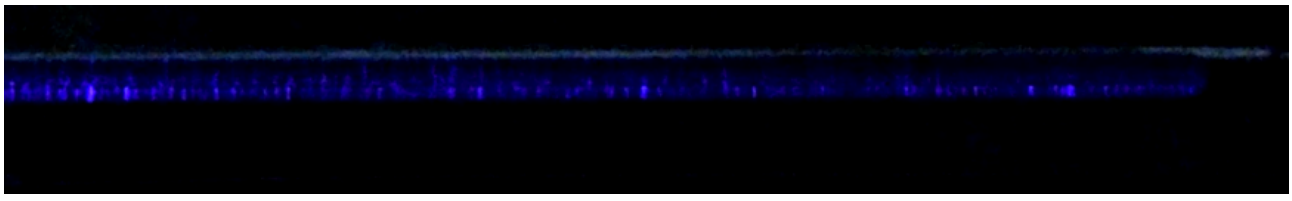

Fig. 6-11. Appearance of electric discharges using the tensioned inner wire electrode at 50 pps.

6.4 Conclusion of NOx Treatment

The tensed inner wire electrode of the coaxial reactor was also applied to NOx treatment in the coaxial reactor using nanosecond pulsed power system. When the inner wire electrode of coaxial reactor was not tensed, it was attracted and curved to the outer electrode, so that spark discharges occurred. Then, as well as experiment of ozone production, the NO and NOx removal ratios decreased. In NOx treatment, when the inner wire electrode in the coaxial reactor was tensed by a spring, the occurrence of spark discharge was suppressed, so that the NO and NOx removal ratios increased without decreasing because a large volume of streamer discharges was obtained. In order to achieve higher NOx removal ratios and removal efficiency, a tensed inner wire electrode to be able to control the occurrence of the spark discharges should be introduced in the coaxial reactor.

References-6

[6.1] M. Morimoto, R. Arai, K. Omatsu, K. Teranishi, and N. Shimomura, “Introduction of Tensioned Inner Wire Electrode for NOx Treatment with Nanosecond Pulsed Power System,” IEEE Transactions on Plasma Science, vol. 44, no. 11, pp. 2874-2879, November, 2016.

[6.2] A. Mizuno, J. S. Clements, and R. H. Davis, “A Method for the Removal of Sulfur Dioxide from Exhaust Gas Utilizing Pulsed Streamer Corona for Electron Energization,” IEEE Transactions on Industry Applications, vol. IA-22, no. 3, pp. 516-522, May, 1986.

[6.3] H. Akiyama, T. Sakugawa, T. Namihira, K. Takashi, Y. Minamitani, and N. Shimomura, “Industrial Applications of Pulsed Power Technology,” IEEE Transactions on Dielectrics and Electrical Insulation, vol. 14, no. 5, October, 2007.

[6.4] T. Namihira, S. Tsukamoto, D. Wang, S. Katsuki, and R. Hackam, “Improvement of NOx Removal Efficiency Using Short-Width Pulsed Power,” IEEE Transactions on Plasma Science, vol. 28, no. 2, pp. 434-442, April, 2000.

[6.5] N. Shimomura, K. Nakano, H. Nakajima, T. Kageyama, F. Fukawa, K. Teranishi, and H. Akiyama, “Nanosecond Pulsed Power Application to Nitrogen Oxides Treatment with Coaxial Reactors,” IEEE Transactions on Dielectrics and Electrical Insulation, vol. 18, no. 4, pp. 1274-1280, August, 2011.

[6.6] N. Shimomura, T. Kageyama, R. Mabuchi, K. Teranishi, and H. Akiyama, “Observational Study of Appearance of Streamer and Spark Discharges to Design Chemical Reactor Using Nanosecond Pulsed Power,” IEEE Transactions on Plasma Science,” vol. 39, no. 11, pp. 2270-2271, November, 2011.

[6.7] Y. Nakata, R. Mabuchi, K. Teranishi, and N. Shimomura, “Effect of small-diameter coaxial reactors on ozone production using nanosecond pulsed power,” IEEE Transactions on Dielectrics and Electrical Insulation, vol. 20, no. 4, pp. 1146-1152, August, 2013.

[6.8] R. Arai, N. Kaneda, T. Ikemoto, T. Ninomiya, K. Teranishi, and N. Shimomura, “Investigation of Discharge Appearance in Reactor and Removal Ratio on NOx Treatment Using Nanosecond Pulsed Powers,” Pulsed Power Conference (PPC2015), pp. 72-76, June, 2015.

7. Improved Water Treatment with Nanosecond Pulsed Power System

7.1. Introduction of Improved Water Treatment Device [7.1]

The coaxial reactor was improved for ozone production and NOx treatment in the chapters 5 and 6. In order to prevent spark discharge by curving of the inner wire electrode, the inner wire electrode of the coaxial reactor was tensed. Then, in order to prevent the curving of the inner wire electrodes, in a new water treatment device, not both ends but the tops of the inner wire electrodes were fixed. Moreover, in order to increase the treatment volume of the water treatment device, the inner diameter of a glass pipe that was used as the outer electrode was altered from 10 mm of SG device to 29 mm and the number of the inner wire electrodes was changed from 1 to 8, with 4.0 mm distance between outer and inner electrodes. In chapter 7, in order to evaluate the influence of discharge area magnitude on the surfactant treatment, the number of stainless steel wires was changed. In addition, the surfactant treatment using the nanosecond pulsed power system was compared with water treatment using an external ozonizer instead. A schematic diagram and sectional views of the new water treatment device are shown in Figs. 7-1(a) and 7-1(b).

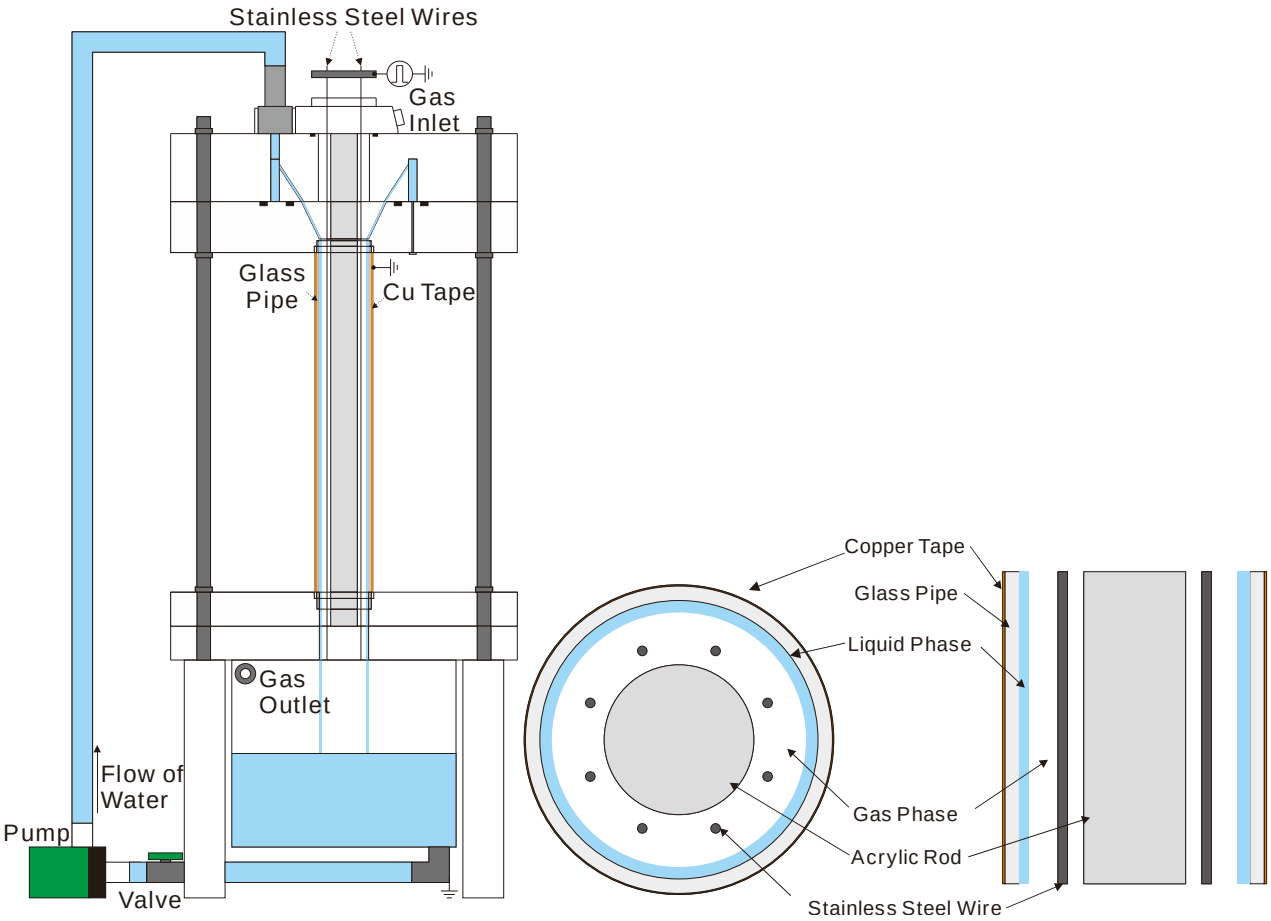

(a) Water treatment device (b) Sectional views of reactor

Fig. 7-1. Schematic of the new water treatment device.

Figs. 7-2(a) and 7-2(b) indicate the cross-sectional view of the reactor electrode when eight and two stainless steel wires (SUS304) were used, respectively, as the inner wire electrodes of the reactor.

The 1.0-mm diameter stainless steel wires were located at the vertex of a regular octagon. As the outer electrode, a coaxial glass pipe outer-wound with copper (Cu) tape was used. The length of the glass pipe, inner diameter, and thickness of the reactor were 380, 29, and 2.0 mm, respectively.

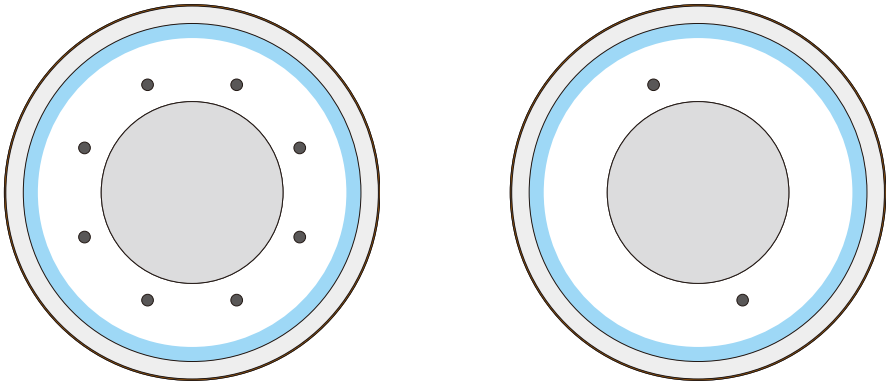

(a) Eight stainless steel wires (b) Two stainless steel wires

Fig. 7-2. Sectional views of the reactor and electrodes.

The target solution was placed in a water reservoir located under the inner wire electrodes. The solution was circulated by a water pump (MD-15R-N, IWAKI) and was flowed on the inner surface of the glass pipe in the reactor. The flow rate of the water pump was 3.6 L/min. Then, liquid layer was formed from the flowing solution on the glass pipe as shown in Figs. 7-1(b) and 7-2. The glass pipe used as a dielectric barrier was inserted to prevent spark discharges bridging electrodes across the short electrode separation distance. Moreover, an insulation rod was inserted in the center of the glass pipe in order to cover the residence space of gas. The nanosecond high-voltage pulses were applied on the eight inner wire electrodes and streamer discharges developed from the eight inner wire electrodes to the surface of the flowing solution on the outer electrode. The solution passed through the plasma as streamer discharges between the electrodes. During pulse application, the electric charges accumulated on the inner surface of the glass pipe were carried away with the flowing solution. When the nanosecond pulsed power system was used, the initial charging voltage of C_1 and pulse repetition rate were 3.1 kV and 50 pps, respectively.

In order to consider the effect of the discharge plasma on the surfactant, an external ozonizer was used for ozonation of the surfactant. The applied voltages of the external ozonizer were configured at 60.0 and 75.0 V. When the applied voltage was 60.0 V, the ozone concentration exhausted from the water treatment device was adjusted to that during pulse application after 20 minutes. The effect of using a different ozone concentration on the surfactant treatment was investigated using a higher ozone concentration produced by applying a voltage of 75.0 V. Ozone exhausted from the water treatment device was measured using an ozone monitor (PG-320A, EBARA) through handmade dehumidifier during surfactant treatment. Note that the measurement limit of the ozone monitor was up to 21.5 g/m^3 ozone concentration.

7.2. Surfactant Treatment with Nanosecond Pulsed Power System

Figs. 7-3(a) and 7-3(b) show the image of foam and the temporal variations in the foam height on the solution in the reservoir of the water treatment device. The error bars in Fig. 7-3(b) indicate the maximum and minimum foam height in the reservoir. After surfactant treatment for 80 minutes, because the foam height decreased, surfactant was decomposed during pulse application. The foam height using eight wire electrodes decreased slightly faster than using two wire electrodes. This was attributed to differences in the ozone concentration and the exposed area for discharges between eight and two inner wire electrodes.

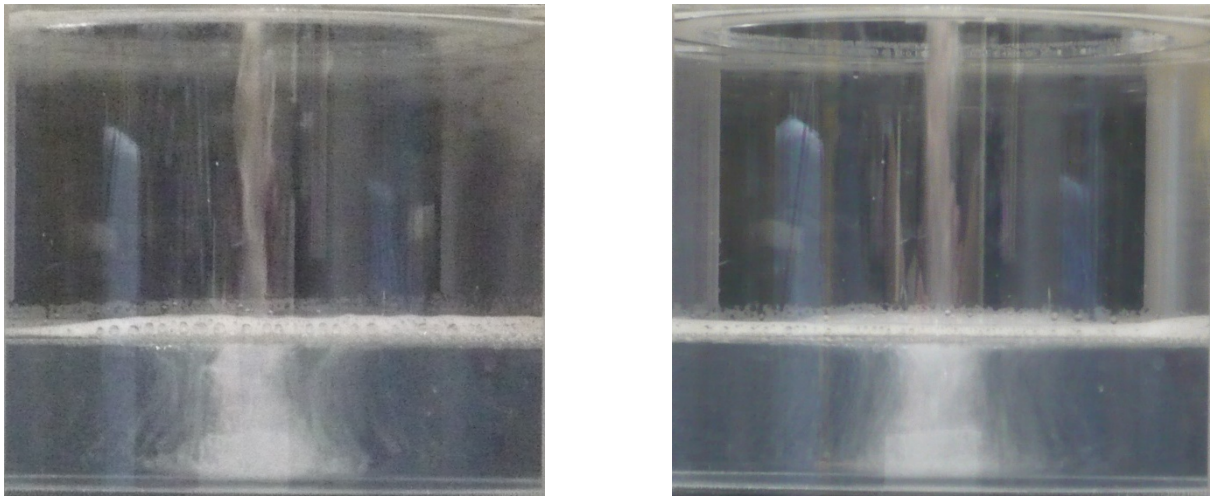

(L) Eight stainless steel wires (R) Two stainless steel wires

(a) Image of foam in the reservoir after 80 minutes' treatment

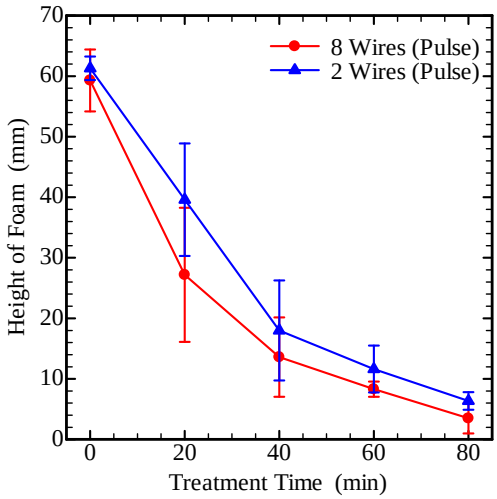

(b) Foaming height

Fig. 7-3. Variation in the foam height during pulse application.

Figs. 7-4 and 7-5 show typical voltage and current waveforms after 150 s from start of pulse application. The voltage waveform using eight stainless steel wires was almost the same as that using

two stainless steel wires. If anything, the voltage waveform using eight stainless steel wires after 40 ns was lower than that using two stainless steel wires. Moreover, the current waveform using eight stainless steel wires around 10 ns was larger than that using two stainless steel wires. Then, discharge energy using eight stainless steel wires was larger than that using two stainless steel wires. When eight stainless steel wires were used, the energy supplied from the nanosecond pulsed power generator could be consumed more efficiently. Because the initial charging voltage of C_1 was 3.1 kV, it was suggested that system efficiency increased with increasing the number of stainless steel wires.

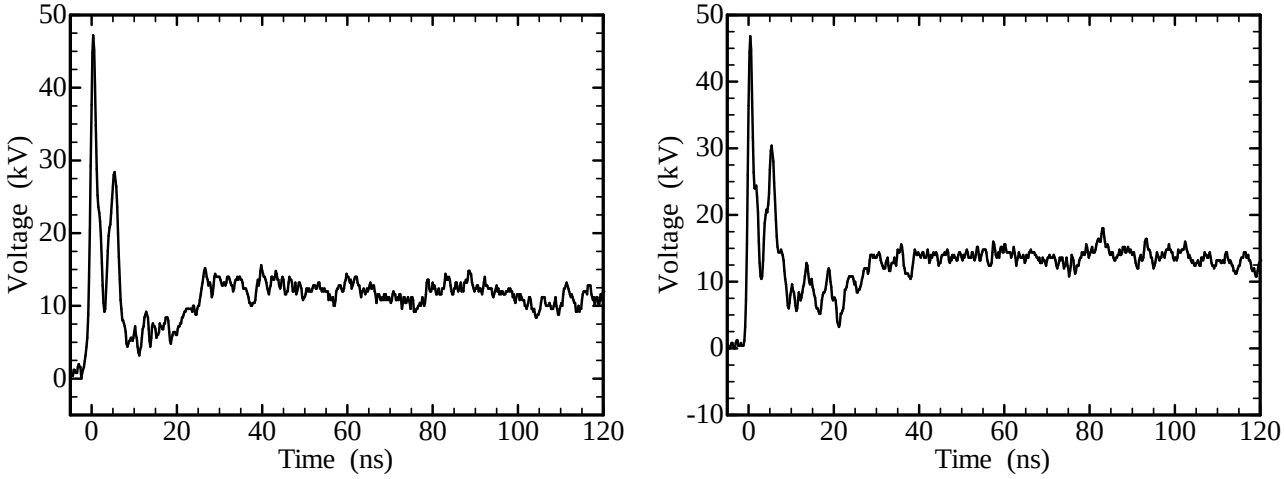

(a) Eight stainless steel wires (b) Two stainless steel wires

Fig. 7-4. Typical voltage waveforms after 150 s from start of pulse application.

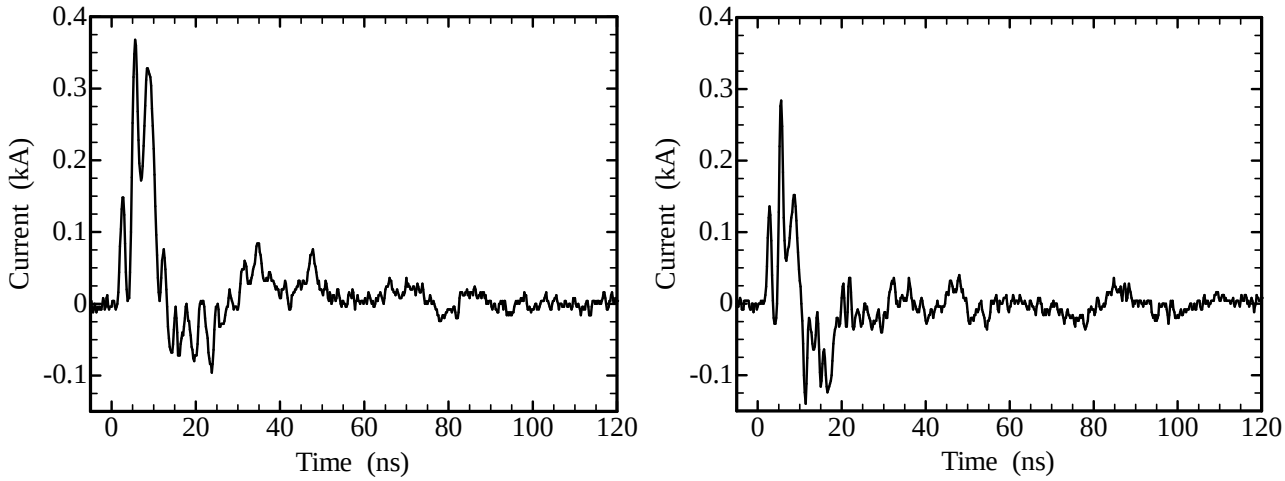

(a) Eight stainless steel wires (b) Two stainless steel wires

Fig. 7-5. Typical current waveforms after 150 s from start of pulse application.

The ozone concentration exhausted from the water treatment device during the treatment of the purified water or the surfactant solution is shown in Fig. 7-6. The exhausted ozone could be regarded as residual ozone for treatment. At the start of pulse application, the device was filled with oxygen gas. Then, the ozone concentration exhausted from the water treatment device was zero. Ozone concentration in the water treatment device and exhausted from the device temporally increased with

treatment. For surfactant treatment, the ozone concentration using eight inner wire electrodes was higher than that using two inner wire electrodes. The ozone concentration in case of eight inner wire electrodes approximated that for purified water. This could indicate that the surfactants' structures were decomposed after 80-minutes' pulse application. Moreover, the surfactant decomposition with eight inner wire electrodes was faster than that with two inner wire electrodes.

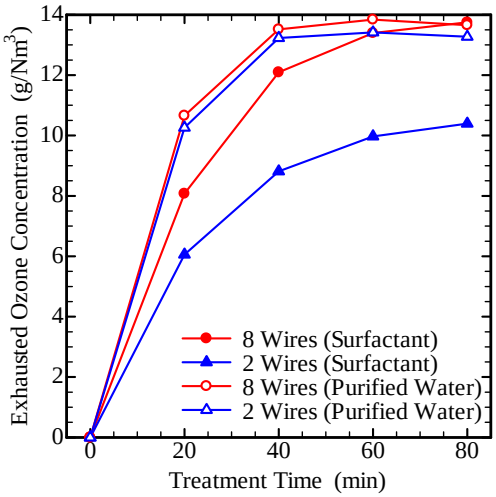

Fig. 7-6. Variation in the ozone concentration exhausted from the water treatment device during pulse application.

Fig. 7-7 shows the variation in the absorbance spectrum at each 20 minutes during surfactant treatment. The absorbance spectrum increased with the treatment time in the entire spectrum. The absorbance spectrum using eight wires increased faster than using two wires. This could indicate that more surfactant was decomposed and more active species, such as dissolved ozone, hydrogen peroxide, and so on, were dissolved in the solution using eight inner wire electrodes for 80-minutes' treatment. Using eight inner wires, not only a larger discharge area (Fig. 7-7) but also a stronger direct effect of the electric discharges such as UV and ion wind [7.2] was obtained. The UV promoted production of ozone and OH radical in gas and liquid phase. The ion wind and streamer heads struck the solution, so that chemical reactions of gas phase on the solution would be promoted. Therefore, because more ozone and more active species reacted with the surfactant, the surfactant was decomposed more quickly. Consequently, in order to carry out faster wastewater treatment, because more ozone and active species should be produced and react with organic compounds, a larger discharge area would be required.

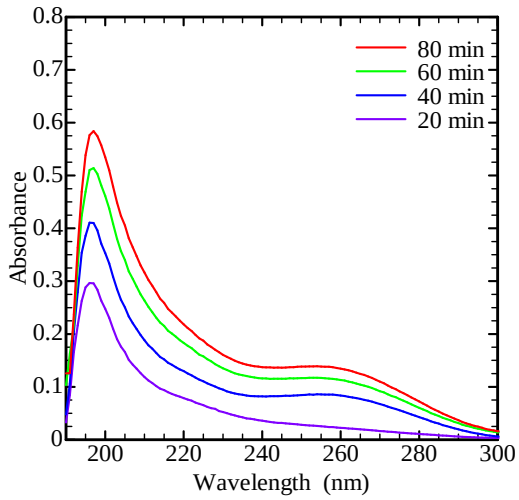

(a) Eight stainless steel wires

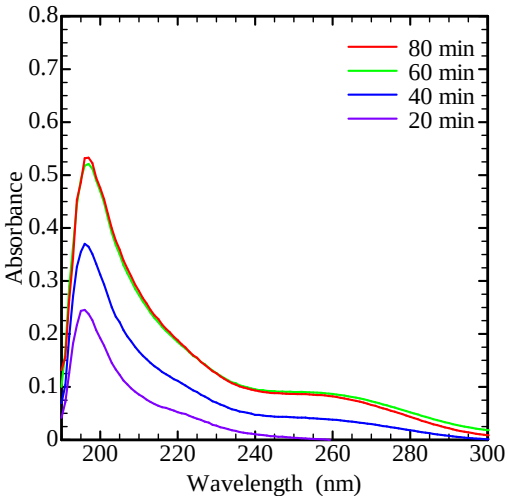

(b) Two stainless steel wires

Fig. 7-7. Variation in the absorbance at each 20 minutes during pulse application for surfactant treatment.

7.3. Surfactant Treatment with an External Ozonizer

In order to investigate the effect of electric discharges on the surfactant solution, an external ozonizer instead of the nanosecond pulsed power system was used for surfactant treatment. Fig. 7-8 presents the ozone concentration exhausted from the water treatment device using an external ozonizer or pulse application. When ozone concentration exceeded the maximum measurable ozone concentration of the ozone monitor, the concentration measurement was stopped but the treatment experiment was continued. A higher applied voltage of the external ozonizer resulted in a higher ozone concentration.

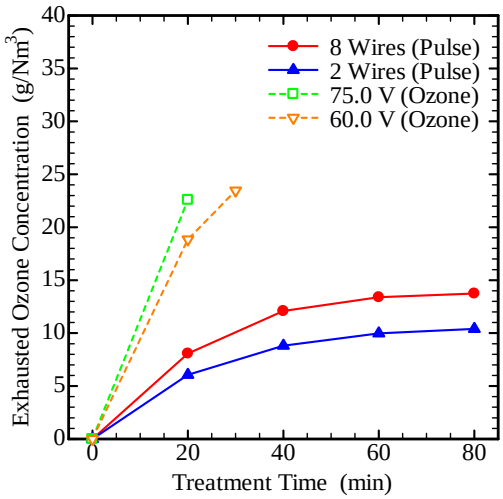

Fig. 7-8. Variation in the ozone concentration exhausted from the water treatment device during surfactant treatment.

Figs. 7-9(a) and 7-9(b) presents the image of foam and the temporal variation in the foam height in the reservoir of the water treatment device using the nanosecond pulsed power system or the external ozonizer. Because ozone concentrations during ozonation were different based on the ozone concentration of Fig. 7-8, changes of foaming height on the solution using treatment with ozonation were approximately same. However, when ozone concentration during ozonation was higher than that using the nanosecond pulsed power system, the foam height during pulse application decreased faster than that during ozonation. Thus, it was suggested that ozonation using the external ozonizer was not efficient for surfactant decomposition.

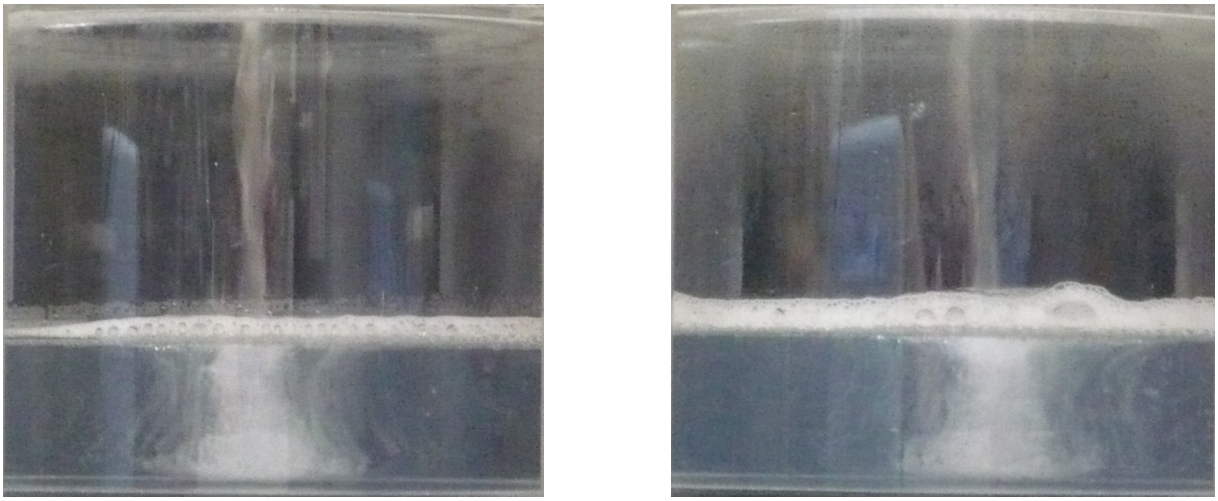

(L) Pulsed Discharge (8 wires) (R) External Ozonizer (75.0 V)

(a) Image of foam in the reservoir after 80 minutes' treatment

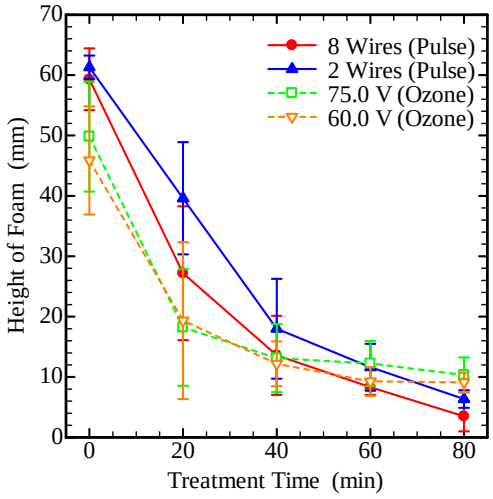

(b) Foaming height

Fig. 7-9. Variation in the foam height during ozonation or pulse application.

As seen in the absorbance spectrum around 260 nm in Fig. 7-10, the dissolved ozone during ozonation was larger than that during pulse application (Fig. 7-8) due to the higher ozone concentration with ozonation. Moreover, around 200 nm, active species such as hydrogen peroxide during ozonation were also more than those during pulse application. Although more ozone and active species in the solution were produced under higher ozone concentration, the foaming height by treatment using the ozonizer decreased lower than that using the pulsed power system. In treatment using the ozonizer, no discharges occurred near the target solution. Moreover, because of the lower ORP of ozone or hydrogen peroxide than that of the OH radical [7.3], ozone and hydrogen peroxide hardly reacted with target organic compounds including persistent substance. It was suggested that active species remained in the solution without reacting with the surfactant. When the surfactant treatment using the pulsed power system was performed, electric discharges near the solution could

promote chemical reactions between active species and surfactants. The direct effects of electric discharges such as UV rays and ion wind might also promote the treatment. Then, the absorbance spectrum using the external ozonizer was higher than that using the nanosecond pulsed power system. For faster wastewater treatment, it was suggested that electric discharges near the target solution which promote chemical reactions between active species, such as ozone and OH radical, and organic compounds such as surfactants were needed.

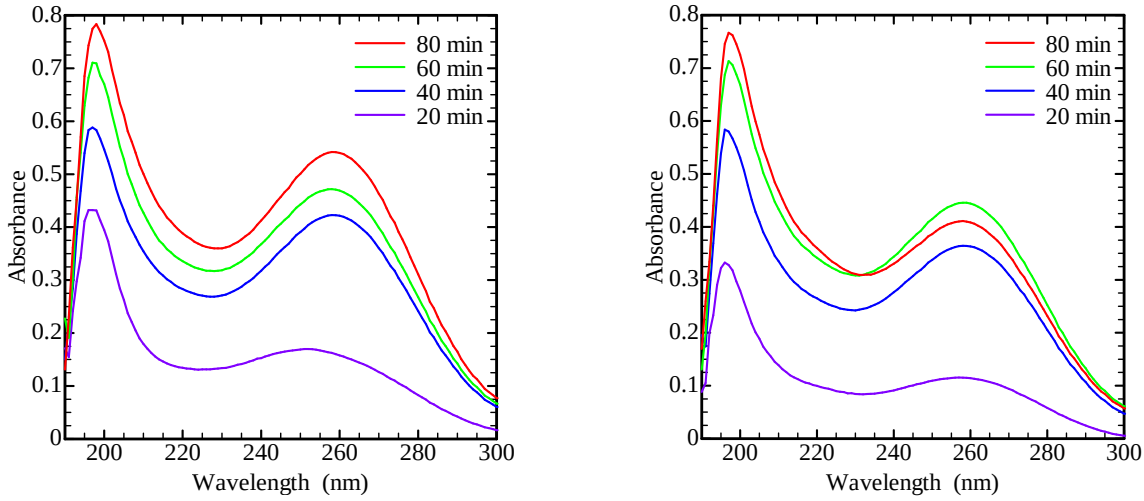

(a) 75.0 V of applied voltage (b) 60.0 V of applied voltage

Fig. 7-10. Variation in the absorbance spectrum at each 20 minutes during ozonation for surfactant treatment.

7.4. Surfactant Treatment with Combination of the Pulsed Power and the Ozonizer [7.4]

In previous experiment of ozone production, the result that ozone production increased using electric discharges in oxygen and ozone gas had been obtained [7.5]. In water treatment experiments, the results of the treatment using the pulsed power system and using the external ozonizer indicated that electric discharges near the target solution was able to improve reactivity of active species and more ozone was able to produce more active species, respectively. Then, surfactant treatment with combination of the nanosecond pulsed power system and the external ozonizer (75.0 V) was performed. In order to measure more than 21.5 g/Nm^3 of ozone concentration, another ozone monitor (EG-600, EBARA) was used. Figs. 7-11(a) and 7-11(b) present the image of foam after surfactant treatment with the combination system and the temporal variation in the foam heights in the reservoir of the water treatment device with each treatment method, respectively.

(a) Image of foam after 80 minutes' treatment with the combination system

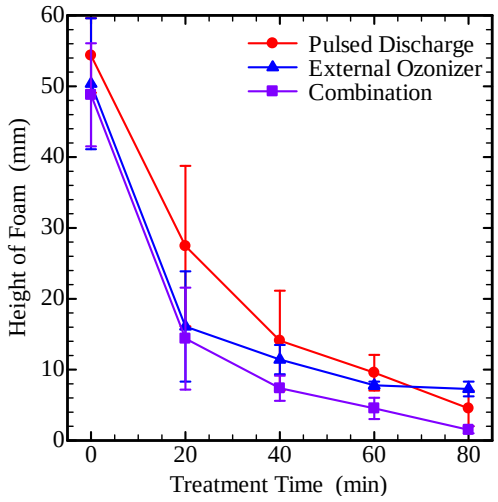

(b) Foaming height

Fig. 7-11. Variation in the foam height using each treatment method.

Fig. 7-12 shows treatment kinetic curves using the decreasing degree of the foaming height in Fig. 7-11(b). Note that the inclination of the line in Fig. 7-12 indicated treatment speed. From Fig. 7-11(a), it was found that the foam on the solution was little. In Fig. 7-11(b), the foaming height with the combination system decreased the fastest of three treatment methods. For 20 minutes from start of pulse application, foaming heights using either the combination system or the ozonizer decreased faster than that using the pulsed power system. From Fig. 7-12, the inclination of the line using the combination system was approximately same as that using the external ozonizer. After 20 minutes' treatment, the inclination of the line using the ozonizer became smaller. It was suggested that surfactant was rarely decomposed by only ozone. On the other hand, because the inclination of the line using the nanosecond pulsed power system was stable during surfactant treatment, it was found that surfactant was treated at a regular speed by using the pulsed power system. In other words, electric discharges would improve surfactant decomposition. After 20 minutes' treatment, treatment speed using the combination system was approximately same as that using the pulsed power system, so that it could be suggested that water treatment at a regular speed was performed by using the pulsed power system or electric discharges.

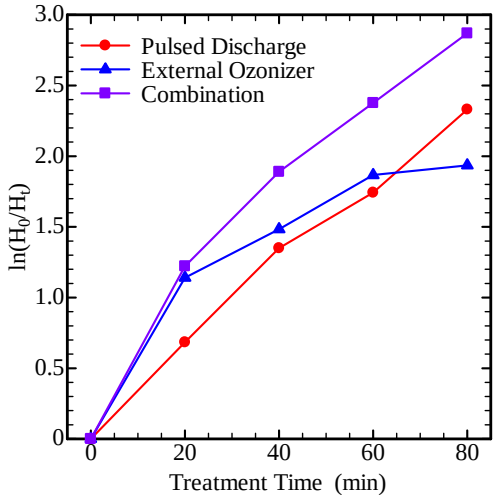

Fig. 7-12. Kinetic curves of foaming height on each treatment.

Fig. 7-13 shows the ozone concentration exhausted from the water treatment device. Fig. 7-14 presents the absorbance at each 20 minutes for surfactant treatment with the combination system. In Fig. 7-13, the ozone concentration using the combination system was between using the ozonizer and the pulsed power system. It was considered that ozone concentration using the ozonizer greatly exceeded ability for ozone production of the discharge plasma in the water treatment device. Namely, the occurrence of ozonolysis with the electric-discharges plasma would be more than that of ozone production, so that ozone concentration using the combination system was lower than that using the ozonizer. The ozone concentration using either the combination system or the ozonizer was higher than that using the pulsed power system. Because of higher ozone concentration, foaming height during 20 minutes' treatment from experiment start would decrease that using the pulsed power

system. Although using the external ozonizer could cause the highest ozone concentration, the decrease of foaming height was the slowest after 80 minutes' treatment. On the other hand, foaming height using the combination system was decreasing during surfactant treatment constantly. It was suggested that surfactant treatment without electric discharges near the target solution was promoted rarely even if high ozone concentration was used as the condition of working gas.

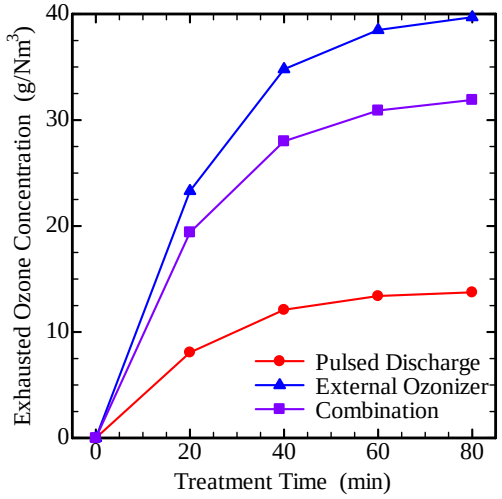

Fig. 7-13. Variation in the ozone concentration exhausted from the water treatment device during surfactant treatment.

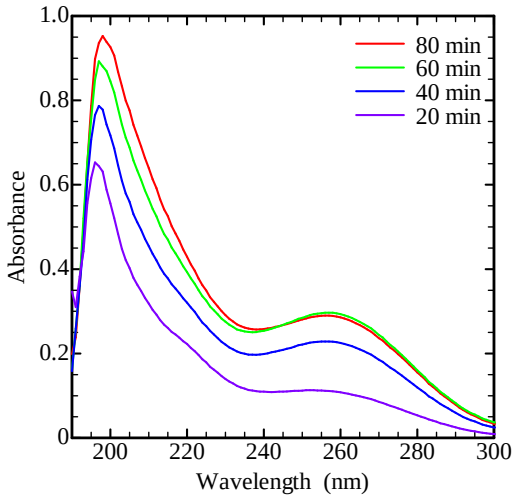

Fig. 7-14. Variation in the absorbance at each 20 minutes for surfactant treatment with the combination system.

Moreover, comparing treatment methods with the electric discharges, the surfactant treatment using the combination system was faster than that using the pulsed power system. It was considered that electric discharges in high ozone concentration generated more OH radical which was able to contribute to surfactant decomposition strongly. As seen in Fig. 7-14, because the absorbance around 200 nm with the combination system was the highest of the three treatment methods, it was also

indicated that more active species were produced in the solution. Using the combination system, electric discharges in more active species and high ozone concentration could promote water treatment. However, because surfactants would not be decomposed completely, a new water treatment device should be developed in the future. Moreover, in order to solve the issue, chemical analysis such as liquid chromatography (LC) will be helpful.

7.5. Conclusion of Surfactant Treatment Using Improved Water Treatment Device

In order to evaluate the performance of the new water treatment device, surfactant treatment using the nanosecond pulsed power system was performed. Especially, the effect of the discharge area and the necessity of electric discharges were investigated. The effect of the discharge area was investigated by changing the number of inner wire electrodes, whereas the necessity of electric discharges was investigated through comparison with using an external ozonizer instead of the nanosecond pulsed power system. As a result, faster surfactant treatment was obtained when the discharge area was larger and when the nanosecond pulsed power system was used. This was attributed to the direct effects of electric discharges, when the nanosecond pulsed power system was used, so than UV rays and ionic wind would promote chemical reactions between active species and target organic compounds. Then, it was suggested that a stronger direct effect of electric discharges was obtained by a larger discharge area. Moreover, surfactant treatment using the nanosecond pulsed power system was faster than that using the external ozonizer although ozone concentration using the ozonizer was higher than that using the nanosecond pulsed power system. This was indicated that the occurrence of the electric discharges nearer the target solution rather than higher ozone concentration should be effective for faster water treatment with oxygen gas. Moreover, when nanosecond pulsed power system or electric discharges were used for water treatment, it was found that electric discharges generated under higher ozone concentration could contribute to decomposition of target organic compounds more strongly and faster.

References-7

[7.1] M. Morimoto, K. Shimizu, K. Teranishi, and N. Shimomura, “Effect of the Number of Inner Wire Electrodes on Surfactant Treatment Using Nanosecond Pulsed Powers,” IEEE International Power Modulators and High Voltage Conference (IPMHVC2016), July, 2016.

[7.2] T. Sato, “Biological Interference Mechanism of an Atmospheric Plasma Flow,” Institute of Fluid Science, Tohoku University, pp. 61-65, February, 2012. (in Japanese)

[7.3] Y. Iwasawa, “Chemical Handbook Fundamentals Revised 5th Edition,” The Chemical Society of Japan, vol. 2, pp. 580-583, February, 2004. (in Japanese)

[7.4] M. Morimoto, K. Shimizu, K. Teranishi, and N. Shimomura, “Effect of Surfactant Treatment with Combination of Nanosecond Pulsed Power and Ozonizer,” Society for Pulsed Power, pp. 7-12, August, 2016. (in Japanese)

[7.5] R. Mabuchi, Y. Nakata, T. Kageyama, K. Teranishi, and N. Shimomura, “Investigation of Ozone Production Using Nanosecond Pulsed Power to Increase Ozone Concentration,” IEEE International Power Modulator and High Voltage Conference (IPMHVC2012), pp. 512-515, 2012.

8. Conclusion

The nanosecond pulsed power system was applied to water treatment. When indigo carmine solution was treated for water treatment evaluation, the decoloration of indigo carmine using oxygen as the working gas was faster than that using nitrogen during pulse application because ozone and active species such as the OH radical were generated by electric discharges in the oxygen gas. Moreover, treatment of surfactants, which are contained in domestic wastewater, with the nanosecond pulsed power system was also investigated. The foam height of the surfactant was reduced after 100 minutes' pulse application. Moreover, the treatment of surfactant in purified water was faster than that of surfactant in tap water because the difference in the pH value and the electric conductivity of the solutions could affect production of active species such as ozone and OH radical. In a word, it could be considered that water quality of target solution was a little influence water treatment. In order to investigate necessity of electric discharges, surfactant treatment using the nanosecond pulsed power system was compared with that using an external ozonizer. Foaming height using the nanosecond pulsed power system decreased more than that using the ozonizer. However, when NaTA solution to evaluate OH radical production was treated, OH radical production using the nanosecond pulsed power system was almost the same as that using the ozonizer. It would be indicated that the surfactant was not decomposed sufficiently by ozone and OH radical. Then, when electric discharges were used for water treatment, the electric discharges would promote chemical reactions between ozone or OH radical and surfactant. In order to promote chemical reaction between more OH radical and target organic compounds effectively, the nanosecond pulsed power system using electric discharges should be applied to water treatment for organic compounds.

In the experiment of indigo carmine treatment, it was suggested that more ozone and more OH radical were needed for faster water treatment. In order to produce ozone efficiently, electric discharges in the coaxial reactor were studied. Then, it was found that spark discharge, which is considered an ozone-decomposition factor, was caused by curving inner wire electrode of the coaxial reactor. Indeed, curving the inner wire electrode resulted in topical electric discharge such as spark discharges, so that volume of streamer discharges decreased. The curving inner wire electrode occurred at high pulse frequency notably. At that time, ozone concentration decreased. As a method of preventing the inner wire electrode from curving, a coaxial reactor that can tense the inner wire electrode was created. When the coaxial reactor with tensing the inner wire electrode, ozone concentration was stable at high pulse frequency without curving the inner wire electrode and producing spark discharges, so that stable ozone-production efficiency was obtained.

As well as the ozone production experiments, removal ratio of NOx which caused air pollution also decreased at high pulse frequency. In NOx treatment, in order to tense inner wire electrode of the coaxial reactor, a spring was used. As a result, a stable and higher NOx removal ratio was also obtained than that using a non-tensed inner wire electrode, so that NOx treatment efficiency increased.

From results of ozone production and NOx treatment, in a new water treatment device, not both ends but the tops of the inner wire electrodes were fixed for preventing curving inner wire electrode. Moreover, in order to increase the treatment volume of the water treatment device, the inner diameter

of a glass pipe used as the outer electrode became larger. In addition, for an aim to increase direct effects of electric discharges such as UV rays and ion wind, the number of inner wire electrode increased. In order to evaluate the influence of the discharge area size on the surfactant treatment, the number of stainless steel wires was changed. Faster surfactant treatment was achieved with increasing the number of stainless steel wire in water treatment device. Because of larger discharge area, it was easy for water treatment using the nanosecond pulsed power system to benefit from direct effects of electric discharges which UV rays promoted active species production and ion wind pushed the active species toward target solution. In addition, in order to investigate necessity of electric discharges, surfactant treatment using the nanosecond pulsed power system was compared with water treatment using an external ozonizer. The foam height using the ozonizer decrease slower than that using the nanosecond pulsed power system even when ozone concentration using the ozonizer was higher than that using the nanosecond pulsed power system. It was found that, even when ozone concentration was low, electric discharges could promote chemical reactions between OH radical and surfactant, so that water treatment with the pulsed power system was faster than that with high ozone concentration without using electric discharges. As improvement of surfactant treatment, surfactant treatment with a combination system using electric discharges in high ozone concentration was performed. The surfactant treatment using the combination system was faster than that using the pulsed power system. Because more active species were generated by the combination system than only pulsed power system, it could be suggested that more active species and electric discharges contribute to surfactant decomposition. However, in the future, in order to develop water treatment with the nanosecond pulsed power system, chemical analysis such as liquid chromatography (LC) should be carried out. Then, based on the LC results, new water treatment device would be developed.

Consequently, streamer discharges generated uniformly inside of the treatment device using the nanosecond pulsed power system should be applied for water treatment because the direct effect of the streamer discharges such as UV rays and ion wind could push the active species toward target solution, so that faster water treatment could be obtained.

9. Future Plans

In order to analyze water treatment chemically, a target solution before or after the treatment should be investigated by liquid chromatography (LC). Then, by-products after the water treatment helps to predict chemical reactions during the water treatment. Moreover, in order to practicalize water treatment with the nanosecond pulsed power system, increase of the treatment volume with the water treatment device using a horizontal reactor and improvement of water circulating method are needed.

Acknowledgments

I pay my heartfelt respects and gratitude to those who worked so hard for me. Especially, I would like to show my greatest appreciation to Professor Shimomura and Associate Professor Teranishi. Mr. Shimizu and Mr. Shimomura made enormous contribution to do experiments of water treatment with me. Moreover, Mr. Ikemoto and Mr. Omatsu helped me to carry out experiments of ozone production and NOx treatment for my graduation of a doctoral course. In addition, I convey a sense of gratitude to the relevant parties of Tokushima University. Thank you again for the present.